UNIVERSITÀ DEGLI STUDI DELL'AQUILA

Department of Civil, Construction-Architectural and Environmental Engineering

Doctoral Thesis

The use of subspace-based methods for Damage Detection in civil structures: a Machine Learning approach

Ph.D Course in Civil, Construction-Architectural and Environmental Engineering

XXXIV cycle

Candidate

Riccardo Cirella

SSD

ICAR/08

Course Coordinator

Prof. Marcello Di Risio

Thesis Tutor

Prof. Rocco Alaggio

The use of subspace-based methods for Damage Detection in civil structures: a Machine Learning approach

Riccardo Cirella

Prof. Rocco Alaggio

Reviewers:

Prof.ssa Maria Pina Limongelli *Poilitecnico di Milano*
Prof. Giuseppe Carlo Marano *Politecnico di Torino*

The use of subspace-based methods for Damage Detection in civil structures: a Machine Learning approach

Riccardo Cirella
Candidate ID number: 261142

Department of Civil, Construction-Architectural and Environmental Engineering-DICEAA
University of L'Aquila

Website: http://diceaa.univaq.it/

To my family.

[Blank page]

Acknowledgements

This thesis is not only the result of my work and my passion, but also of those who have been close to me and encouraged me all these years.
Special thanks to Professor Rocco Alaggio, who once again guided me along this path. I warmly thank him for his availability, his support, his mentorship, but above all for the great passion he shows for this activity, which he has been able to pass down to me.
I also wish to thank my family for their patience, love and endless moral support: other words are unnecessary.
I would like to thank my colleagues and friends, especially Ilaria and Angelo, for sharing unforgettable moments in all the activities carried out and in the moments of leisure: I wish them all the best that the future may reserve.
A deep appreciation goes to all my friends who have accompanied and encouraged me during this last three years, as they have done all my life.
I would like to thank myself for getting into this challenge three years ago and for being able to bring it to conclusion, not without difficulties. I hope that this experience will give me the awareness of my means and the maturity to make the right choices in the future.
I want to leave the last lines for the most important thanks: I want to do it with all my heart to Giulia, that I am lucky to have with me and who in this years has been the strength for getting to the end of this journey.
I heartily thank you for all the things you are giving me.

[Blank page]

Abstract

Events in recent years have shown how important it is to monitor the structural health of existing civil works. Structural Health Monitoring systems are a useful tool to provide an objective and automatic evaluation of the state of health of a structure, in order to detect the emergence of anomalies in its behavior. They are also an auxiliary tool in the decision-making phase for maintenance work or after extraordinary events. The Thesis work explores the topic of damage detection based on the analysis of subspaces of dynamical systems matrices.
The aim of the research was to investigate a method for the development of levels in the damage diagnosis scale, ranging from the identification of the anomaly to the localization and subsequent assessment of the entity of the damage occurred.
The study is carried out following two approaches: in the first, damage indices present in the literature are considered, and a newly developed one is presented. In the second approach, the identification issue is addressed by introducing the most recent Machine Learning tools: the goals are achieved through the supervised training of a classifier, with the task of localizing and quantifying the damage.
In both cases, the methods used are *model-driven* type, based on simulations of the damage scenarios through Finite Element modeling. The thesis work therefore aimed to evaluate the effectiveness of the same *subspace-based* indices as objective functions in the optimization process related to the *model updating* process of the FE model, such that the simulated response in subsequent analyses would be as close as possible to the real one. The findings of the tests, both numerical and experimental, confirm the effectiveness of both proposed methods, highlighting their shortcomings and strengths.
The concepts developed were subsequently applied to a case study, represented by the Basilica of Santa Maria di Collemaggio, in L'Aquila.
In the first stage, the dynamic behavior of the Basilica was investigated, over the years of monitoring. Subsequently, traditional and Machine Learning algorithms have been implemented for the purpose of anomaly detection: the procedure has been performed considering as damaged a case, one produced after a structural intervention subsequent to the installation of the monitoring system. The studies on the Basilica showed a complex dynamic behavior, strongly influenced by environmental factors: nevertheless, the implemented algorithms proved to be effective for the defined purpose.

[Blank page]

Sommario

Gli eventi accaduti negli ultimi anni hanno mostrato quanto sia importante monitorare la salute strutturale delle opere civili esistenti. Un sistema adibito allo *Structural Health Monitoring* è uno strumento utile per avere un giudizio obiettivo ed automatico sullo stato di salute di una struttura, al fine di rilevare l'insorgere di anomalie nel suo comportamento. Esso rappresenta anche uno strumento ausiliare nella fase di decision-making di interventi di manutenzione o a seguito di eventi straordinari. Il lavoro di tesi approfondisce il tema dell'identificazione del danno basata sull'analisi dei sottospazi delle matrici dei sistemi dinamici.
Lo scopo della ricerca è stato quello di analizzare un metodo per lo sviluppo dei livelli nella scala della diagnosi del danno, che vanno dall'identificazione dell'anomalia fino alla localizzazione e successiva valutazione dell'entità del danno verificatosi.
Lo studio è stato svolto seguendo due approcci: nel primo, sono stati considerati indici di danno presenti in letteratura, ed uno di nuova concezione è stato presentato. Nel secondo approccio, il tema dell'identificazione viene affrontato introducendo i più recenti strumenti del Machine Learning: gli scopi vengono raggiunti tramite l'addestarmento supervisionato di un classificatore, con il compito di localizzare e quantificare il danno.
In entrambi i casi, i metodi utilizzati sono di tipo *model-driven*, basati su simulazioni degli scenari di danno tramite modellazione agli Elementi Finiti. Il lavoro di tesi ha dunque voluto valutare l'efficacia degli stessi indici *subspace-based* come funzioni obiettivo nel processo di ottimizzazione legato al processo di *model updating* del modello FE, in modo che la risposta simulata nelle successive analisi fosse il più possibile attinente a quella reale. Quanto emerso dai test, sia numerici che sperimentali, conferma l'efficacia di entrambi i metodi proposti, evidenziandone carenze e punti di forza.
I concetti sviluppati sono stati successivamente applicati ad un caso di studio, la Basilica di Santa Maria di Collemaggio, a L'Aquila.
In prima fase, si è determinato il comportamento dinamico della Basilica nel corso degli anni in cui è stata oggetto di monitoraggio. Successivamente, sono stati implementati algoritmi tradizionali e di Machine Learning per scopi di *anomaly detection*: la procedura è stata eseguita considerando come danneggiato un caso, prodotto a seguito di un intervento strutturale successivo all'installazione del sistema di monitoraggio.
Gli studi sulla Basilica hanno evidenziato un comportamento dinamico complesso, influenzato fortemente dai fattori ambientali: ciononostante, gli algoritmi implementati si sono dimostrati efficaci allo scopo definito.

[Blank page]

Contents

List of Figures

List of Tables

Introduction

Chapter abstract

This chapter is an introduction of the context in which the research activity has been developed.
In this chapter, the reasons that lead to the application of a monitoring system on civil structures are explained, as well as all the problems related to the procedure.
The role of Damage Detection within the structural monitoring process is investigated and its fundamental characters are described. Field-specific terminology is introduced.
Finally, the motivations that led to the development of the thesis topic are described and its structure is presented.

1.1 Introduction

Civil structure are designed to maintain their efficiency in a service life which is often of 50 or 100 years, depending on the importance of the structure itself. During this time, they are expected to preserve structural integrity, if no extreme event occurs.
It has been noticed that, after the period of service or even during their service life, structures inevitably begin to experience drops in performance, for example due to:

- degradation phenomena related to exposure to atmospheric agents;
- long-term effects like creep, shrinkage or fatigue;
- unexpected local damages caused by accidents

These hazards may be the causes of structural damages or even collapse.
The collapse of a structure can have catastrophic effects, not only in terms of economic or human lives losses, but also for the related social and psychological consequences.
In particular, civil structures like bridges are of strategic importance for the transport network, allowing the distribution of goods and people even in more remote areas. Structures like these are exposed to excitation of both environmental and anthropological nature, as well as to phenomena of degradation.
Nowadays, situation sees a growing traffic demand, while on the other hand, the infrastructures are becoming dated, increasing their risk of failure. The consequences of failure phenomena have repercussions on the urban, social, and economic network of the area and, depending on the importance of the work, also on the economy of the neighbouring areas. Inconveniences affect both the community that directly inhabit the area, and those who use the network for the transit of goods and services.
In February 2019, in a study conducted by the Italian "*Osservatorio statistico dei consulenti del lavoro*" entitled "*Gli effetti del crollo del ponte Morandi su economia, occupazione e integrazione sociale*" reporting the results of the main surveys published in the previous months, it was highlighted that in the two months after the collapse of the Ponte Morandi in Genova, the

economic damage to the transport in transit for the Genoa hub exceeded 116 million euros (the study is available at the site https://www.consulentidellavoro.it/index.php/component/k2/item/10864). The lack of a direct connection between eastern and western areas of the city led to an extension of over 100 km to cross the city, increasing average travel times of about an hour due to traffic congestion, and creating delays for heavy vehicles entering and leaving the port of the city (estimated about 2 million euros per day). In the same period, there was an overall value of the losses reported by the companies of 422 million euros, with about 85% concerning indirect damages related to the interruption of activities.
From a social point of view, the study instead pointed out that the collapse of the bridge had led, within the municipal area of Genova, to a contraction in the demand for labour of 22,5% in the period August-December 2018, with a clear change in the trend compared to the months preceding the event, which had instead recorded an increase.
In a more general discourse, the consequences of an event such as the collapse of a bridge on an economic network is related to direct or indirect losses, including:

- costs of repair or demolition/reconstruction of a bridge, with cost of material, cost of labour;
- costs due to the taking of temporary measures for emergency management;
- loss of equipment;
- losses incurred by the users, linked to the inevitable delays that are created, combined with additional costs due to maintenance, travel times or accidents

A structural monitoring system therefore represents an auxiliary tool in assessing the health of structure, helping to detect damage in its early state and avoiding economic losses far more serious than the cost of installing the system itself.
Furthermore, the information coming from a system is helpful in the decision-making and prioritization phase of any structural interventions.

For this reason, Structural Health Monitoring (SHM) and damage detection received considerable attention as research topic in the last decades.

1.2 Damage detection methods

In the most general terms, damage can be defined as a change introduced into a system that adversely affects its current or future performance (Farrar and Worden (2007)).

Damage is something that initially appears at a microscopic level and then branches out in the surrounding area, until can be visible to sight. If no measure is taken in this early state, damage accumulate and a local collapse can be reached.

The time interval in which the performance decays depends on the type of phenomena encountered: for example, fatigue or corrosion have consequences that take place in a long time-frame (years), while extraordinary events can cause a sudden collapse. Considering only degradation phenomena, it is clear that these are sometimes not visually identifiable, if not when they are in an advanced form. Furthermore, some areas of the structure subject to damage could not be accessible to visual inspections.

In addition to the difficulty of identifying the area in which the damage occurs, visual inspections defect is that often they are subjective tools: the assessments of the structural health are at the discretion of the technician who carries them out.

In general, it would therefore be preferable to identify the damage combining an automatic tool with visual inspections, in order to require less manpower and more easiness in carrying out tests in risky or difficult to access environments. This, combined with the need of having an objective evaluation tool, has therefore pushed research towards the development of monitoring systems and fault detection techniques.

Structural Health Monitoring (SHM) is an interdisciplinary subject that incorporates knowledge and experience coming from civil, mechanical, control and computer engineering. The aim of SHM is the monitoring of the health of a structure, in order to be able to highlight any deficiencies formed over time or to report sudden changes in structural behavior after an unusual event (i.e. post-earthquake damage assessment).

A system installed in a structure gives information on the state of the same after an event, helping in the decision-making phase: it could be able to guarantee a prompt reoccupation of a building or an immediate use of an infrastructure, which would mitigate the enormous losses caused by the event.

A monitoring system is able to give both information relating to particular areas of the structure and on its overall behavior.

Two types can be distinguished: static and dynamic monitoring. Static monitoring is concerned with quantities mainly related to static, such as tensions or deformations, which give information limited to the area of application of the single sensor; dynamic monitoring, also called vibration-based monitoring, provides information on the dynamic response of the structure.

This response is generally transmitted by series of connected sensors, through which it is possible to have an estimate of the response at a global level. The quantities analyzed can be the modal parameters obtained from the time histories or the time series themselves.

Although only techniques of the first type actually foresee modal identification, the techniques and processes mentioned are all associated with the field of Operational Modal Analysis (OMA), indicating the approach of experimental knowledge towards the existing building.

A damage identification system consists of a hardware part and a software part. The hardware part is represented by the sensors and the acquisition control unit. Sensors are transducers, they transform physical quantity into electrical quantity (typically a voltage); they can include accelerometers, velocimeters, stain-gauges or optical fibres. An accurate choice of the position of the sensors along the structure is essential to determine with precision the behavior of the structure itself.

The acquisition control unit is an analog-to-digital converter: the voltage signal coming from the transducers is transformed into a digital sequence of numbers to be subsequently read by the machine.

Once generated and digitalised, the signal is read by the software component of the system, which can be divided into two parts. The first is the acquisition software, in which the signal acquisition and possible data pre-

processing actions are carried out, the second is the part strictly linked to data processing.

One of the SHM axioms states that the identification of the damage must be extrapolated from the comparison between two different states of the system, in which the first represents the initial state in which the structure is concerned, generally considered undamaged.

The quantities through which the comparison between two states is made are called features. The features must be chosen among the quantities capable of discriminating system changes: for civil applications, generally the most examined are the modal parameters (natural pulsations, modal forms or damping) or indicators extracted from the time series.

Within the field of SHM, a large part of the literature has focused on the study of features and the development of statistical models for damage detection.

Depending on the chosen features, techniques can be divided in applied in the frequency domain, in the time domain, or mixed frequency-time.

In recent decades, technological advancement and the relative increase in computational power have led to the development of a new science: computer science, linked to Artificial Intelligence (AI). Within the vast area of AI, the Machine Learning (ML) is the science of developing intelligent algorithms capable of acquiring knowledge automatically from the available data (Alpaydin (2020)).

Artificial intelligence is a generic term and refers to systems or machines that mimic human intelligence: ML is a subset of AI, that is concerned with creating systems that learn or improve performance based on the data they use.

Over time different ML tools have been utilized to develop a wide array of parametric and non-parametric vibration-based damage detection algorithm for civil structures, including Artificial Neural Networks (ANN), Convolutional Neural Networks (CNN) and more (Avci et al. (2021)).

As previously said, the purpose of ML is to make the AI learn the possible relationships between the features extracted from the data and the state of the structure.

If such a relationship exists, but is unknown, the learning problem is to estimate the function that describes this relationship using data acquired from the test structure, called training data. (Farrar and Worden (2012)). These algorithms are therefore divided on the basis of the data given as input during the learning process: if the data are already associated with a certain state - each state represents a class with its own label - we speak of supervised learning. If the data has no label, the purpose of learning can be to try identifying intrinsic relationships between them: in this case the learning is unsupervised. Usually, through unsupervised learning it is not possible to discriminate between classes, but it is possible to build a model representing a single class and then test if new data belongs to it. Algorithms of this type operate the novelty - or anomaly - detection:through them it is possible to detect the occurrence of a damage.

1.3 Aims and motivations

The thesis aims to deepen the theme relating to damage detection. After examining the techniques described in the literature, the work focuses in particular on the use of subspace-based damage indicators as damage features.

These types of indicators are extracted directly from the acquired time history - time domain techniques - and have been used as features for the identification, localization and quantification of damage in numerous works. The choice of non-parametric indicators is dictated by the need to go beyond the step of modal identification, creating a link as direct as possible between the acquired data and the purpose of monitoring. Although the transition to the frequency domain allows a considerable reduction in the size of the data to be stored, modal identification is very often a step that is difficult to implement automatically, especially when interpreting the processed data.

The choice of non-parametric techniques therefore allows an easier implementation of the process, especially if applied to structures of a certain complexity.

Using damage indices often means estimating the state of a structure referring to a scalar quantity: one of the purposes of the thesis work is to

introduce a multidimensional damage indicator - a matrix or array - which can more accurately describe the state of a structure and better distinguish different damaged states.

Damage indices represent an efficient tool for identifying damage; however, from the bibliographic research it has been noted that, to date, the research has not yet pushed itself towards the implementation of ML algorithms that foresee them as discriminating features.

The aim of the work was therefore to use them in the development of ML algorithms, with applications that concern both unsupervised and supervised learning.

The thesis work is structured as follows:

- Chapter 2 provides an overview of the state of the art, useful for placing the work within the vast theme of damage detection;
- Chapter 3 and 4 present the results of the activities carried out for testing the assumed damage indices and the developed ML algorithms. The tests were carried out with a model-driven approach, and a steel beam was used as test-structure.

  The purpose of Ch.3 was that of calibrate the parameters of the FE model used for simulation, in order to simulate the dynamic behavior of the real test-structure in the best possible way.

  In Ch.4, numerical and experimental tests were performed to assess the performance of the selected subspace-based indices as damage features to be used in damage localization and quantification;
- Ch.5 and Ch.6 show the application of the developed methods to a monitoring system installed in the Basilica of Santa Maria di Collemaggio in L'Aquila, Italy.

  In Ch.5, results from the three-years monitoring data from 2018 to 2021 are discussed in terms of long-term monitoring.

  Ch.6 introduces an anomaly detection technique, based on the use of the subspace matrices as damage feature. Anomaly detection tests are carried out following traditional methods and a Auto-associative neural network algorithm;
- The concluding Chapter summarizes in a critical way what is reported

in the work and opens to future developments.

State of the art

Chapter abstract

Several methodologies have been developed for structural monitoring and damage detection tasks in the last decades. The aim has been to identify the onset of degradation or damage phenomena in civil works. Among the studied approaches, the vibration-based ones have attracted much interest: these approaches allow to understand the global behavior of the structure, and identify any unexpected changes, in a non-invasive way.

Literature approaches allowed the study of different levels of deepening of damage detection process, from the anomaly detection up to the estimation of the residual life of a structure: from these studies, several damage sensitive parameters have emerged. Meanwhile, the field of Artificial Intelligence has been increasingly growing, also in the field of civil engineering. Machine Learning algorithms seem to represent a useful tool to deal with typical Structural Health Monitoring problems, for all stages of damage detection.

In this chapter, the state of the art regarding the issues explored in the thesis work is presented: the highlights of traditional methods are described and those related to Machine Learning are provided. Particular attention is given to vibration-based methods.

2.1 Introduction

The theme of Damage Detection (DD) has fascinated research in recent decades. The need that has pushed in this direction is due to the awareness that the structures, during their life, are subject to aging or degradation phenomena. These phenomena could be the cause of the loss of structural performance, and lead to the inadequacy of the structure itself to perform the required service functions.

Over time, structural health diagnosis has been increasingly carried out by preferring non-destructive tests, in order not to compromise the integrity of the work.

The first attempts to diagnose structural health can be labeled as local methods, because they were in search of anomalies focusing just on restricted areas of the entire structure under analysis. An example of this techniques are X-Rays tests, Ultrasonic tests, Laser testing methods, Infrared termography, ground penetrating radar, acoustic emissions and other numerous methods (Rens et al. (1997), McCann and Forde (2001) and Dwivedi et al. (2018)).

In any case, non-destructive local techniques require that the damaged area is known or that the possible damage area can be assumed a priori, which is a condition that hardly occurs if you are analyzing particularly large or complex structures.

Moreover, another discriminating factor is represented by the difficulty that sometimes occurs in reaching the point of the test: this, together with the aforementioned problems, makes non-destructive tests unsuitable for characterizing the behavior of the entire structure, but only of a limited portion of it.

The need to have a tool for controlling the global behavior of the system has pushed research towards so-called vibration-based (VB) methods.

Through a network of sensors suitably arranged throughout the structure, it is possible to establish its behavior by analyzing parameters considered significant, related to the physical characteristics of the structure, such as stiffness, mass and damping. When damage occurs, the structural parameters change, and the response of the structure with them.

Based on this assumption, VB damage recognition techniques can be articulated according to the levels of damage diagnosis process introduced in Rytter (1993) and consolidated over time:

1. Detection: the method gives a qualitative indication that damage might be present in the structure;
2. Localization: the method gives information about the probable location of the damage too;
3. Assessment: the method gives information about the size of the damage;
4. Prognosis: the method gives information about the actual safety of the structure given a certain damage state. In other works, this phase is also called prognosis.

Modern times and technologies led to the addition of another level (Park et al. (2001)):

5. Healing: smart structures, able of self-monitoring and self-healing.

Following these levels, many VB techniques have been developed over time. For them, the literature presents interesting reviews: in Doebling et al. (1998) a list of works up to the 2000s is presented. Sohn et al. (2003) and Carden and Fanning (2004) have updated the list for subsequent years, while in Yan et al. (2007) we find an introduction to works that use modern signal processing techniques, with application to artificial intelligence. There are also two more recent review works, Kong et al. (2017) and Avci et al. (2021): in these, different aspects are analyzed in depth with respect to the previous works.

In particular Kong et al. (2017), after examining the techniques that identify the levels from one to three of the Rytter's scale, focuses more on the techniques that have studied level 4, the one linked to the estimate of the remaining service life of the structures and on decision making for maintenance, that is the ultimate goal of a SHM system.

The second work, by Avci et al. (2021), represents instead a useful tool for those who approach the DD problem, since, in addition to investigating traditional techniques, it focuses on those involving the use of Machine

Learning.
This Chapter shows some VB techniques, from the well-established ones to the more recent ML algorithms.

2.2 Vibration-based damage detection methods

Vibration-based methods (VB) represent the techniques through which the global behavior of the structure is estimated.
As already mentioned in the introduction, these methods are preferred to local ones when focusing on the knowledge of the structural behavior at the global level., with the aim of investigating the cause of a possible change in structural behavior.
If some variation sare recorded, the causes can be investigated both by local methods and by applying techniques that deepen levels 2 and 3 of Rytter's scale.
Based on the information extracted from the monitoring system and processed in the post-processing phase, the VB methods can be divided into parametric and non-parametric: it is considered appropriate to deepen this difference in order to illustrate the positioning of the thesis work in the literature sector.

2.2.1 Parametric methods

Parametric techniques are those in which the damage features are extracted from the analysis of the parameters of the structure. These parameters are essentially the mass, stiffness and modal parameters - frequencies, shapes and modal damping - whose changes are associated to the change in the state of the structure.
In this perspective, and according to what is supported by one of the fundamental axioms of the SHM - for further information, see Worden et al. (2007) - the changes found between two states, the reference and the current one, can be interpreted as indicators of a possible structural damage.
In this section, only output-only techinques has been investigated, due to the difficulties of carrying out input-output tests on large structures such as those usually monitored.

The literature is rich in output-only techniques used for damage detection: from pick-piking of natural frequencies to auto and cross-spectral densities, up to the Stochastic Subspace Identification (SSI) technique (Deraemaeker et al. (2008)) or the NExT-ERA algorithm, Eigensystem Realization Algorithm (ERA), when applied with the natural excitation technique (NExT). The extracted modal parameters are subsequently used for the DD. While the first studies focused directly on these parameters, subsequent researches looked for features deriving from them, demonstrating of having more sensitivity with respect to changes due to damage.

An example is the analysis of possible changes in the modal shape curvature, proposed by Pandey et al. (1991), particularly suitable for structures that exhibit a flexural behavior, as shown in Wahab and De Roeck (1999) and in Dilena and Morassi (2011).

Modal shapes, togheter with natural frequencies, have been used in Toksoy and Aktan (1994) and Catbas et al. (2006) to reconstruct the flexibility matrix of a bridge.

The Interpolation Damage Detection Method (IDDM) for damage localization proposed by Limongelli (2010), has the quality of being able to exploit the information coming from the entire frequency range considered, for the purpose of damage location.

In the end, mention is made of the study of Modal Strain Energy as a discriminating feature of damage (Stubbs et al. (1995)), or the possibility of using Operational Modal Shapes (Schwarz and Richardson (1999)).

2.2.2 Non-parametric methods

Although in some cases the features derived from parametric techniques have been widely used, their effectiveness is often limited to particular applications.

For this reason, after initially focusing on modal features, over time the research has shifted its attention to methods defined as non-parametric. Unlike the previous ones, they directly analyze time data to extract features not strictly related to physical properties of the structure.

In time series-based methods typically data recorded are fitted using regression models, through which parameters sensitive to behavioral changes

due to damage (and preferably insensitive to environmental or operational variations) are subsequently extracted.

Approaches of this type generally make use of Autoregressive (AR) models or their variants, e.g. ARX and ARMA models. Usually, these types of models take into account the uncertainties by considering an error variable within the model equations, assumed to have a zero-mean normal distribution.

As reported in Hou and Xia (2021) - to which refer for an in-depth analysis of the non-parametric techniques developed in the last decade - statistical time series methods are therefore characterized by three steps: random excitation and/or response signals, statistical time series model building and statistical decision making for damage diagnosis.

The decision making is performed by comparing the variation of the chosen damage features with respect to a threshold value representing the reference - undamaged - state. Often, this comparison is made with the use of tools typical of the statistic science: for example, in many works Mahalanobis squared distance has been applied (Mahalanobis (1936)).

Since the beginning of the 2000s, some scholars have studied the damage detection problem by formulating indices based on the analysis of subspaces matrices of the dynamic system.

In Basseville et al. (2000) the authors showed how suspace-based methods used for modal identification in SSI techniques could also be used as damage detection methods, introducing the so called Local approach (Le Cam (1956).

Other scholars have developed subspace-based damage indices (Yan and Golinval (2006)) and investigated the variability of these with varying environmental effects (Döhler et al. (2014)). In this last approach, a χ^2-test is performed on a residual function addressed as robust to environmental effect.

In a recent work by Gres et al. (2017a), the Squared Mahalanobis distance calculated between the indices derived from the subspace analysis is used to preform anomaly detection on a real infrastructure.

The SSI technique and the subspace-based damage detection will be explored in Ch.3, since the topics covered in this thesis work is based on them.

2.3 Machine learning applications for vibration-based damage detection

Structural damage identification can be treated as a Pattern Recognition problem (Farrar and Worden (2012)).

The idea behind Pattern Recognition is the development of algorithms capable of recognizing between the different states of a system.

In PR problems, attributable to classification, the data within a set are sorted according to a scheme Class-Label; the objective is to learn a law that predicts the label once assigned the values present in the class.

In particular, the class represents a group of information, commonly called attributes (in our case in particular, they could be the type, location or extent of damage) that characterize a data set. The label is a value, usually numeric, which identifies the class, distinguishing it from the others and allowing the classification.

When a damage occurs, the validity of a technique based on PR lies in its capacity to recognize the correct class label to which that damage belongs. Focusing on this process, it appears clear that the algorithm must have a priori knowledge of which data come from one state rather than another, in order to be able to associate them in a correct and univocal way: in other words, systems of this type need a diagnostic training phase before being tested.

The training phase is the first step of developing an ML algorithm, and is critical to the success of the process. The modalities by which the training phase is carried out lead to a distinction between the two great training classes typical of ML: supervised learning and unsupervised learning.

In supervised learning a neural network (NN) is allowed to learn through examples. During the training phase, the network is supplied with already-classified data, in such a quantity as to allow the recognition of the classes in the subsequent testing and operative phases: algorithms of this type allow to approach all levels of damage detection scale.

On the other hand, when DD is pursued according to this method, there is

the need for a considerable amount of data and, most of all, of an a priori knowledge of all possible damage scenarios.

Data relating to the damaged states can be obtained through experimental activities or from numerical simulations. The latter case is certainly the representative one of civil engineering applications, since it is impossible to standard reproduction of a structure in order to perform experimental tests procuring damage.

Civil structures are characterized by a strong uniqueness, complexity and extension: if performing supervised learning, damage scenarios must be simulated from numerical models. In this case, the approach to model detection is said to be model-driven.

In the case of supervised learning based on simulated data, the numerical model must necessarily be as pertinent as possible to the behavior of the real structure.

For complex structures, it is difficult to achieve this goal, and it is even more difficult to be able to simulate the damage adequately: this fact is reflected in the difficulty of characterizing the damaged states for Pattern Recognition.

Algorithms that are part of unsupervised learning do not require the introduction of already-labeled classes in the training phase, but they are able to independently establish relationships between data: it makes them more inclined to the study of complex structures through data-driven approaches.

On the other hand, they only allow to reach the first levels of damage detection - identification and, sometimes, localization - just because the trained network is not given useful information about the classification itself. For this reason, the techniques are often referred to as novelty or anomaly detection techniques (Bishop (1994)).

It is worth noticing that both supervised and unsupervised learning algorithms can be applied to both parametric and non-parametric damage detection methods.

2.3.1 Supervised learning alghoritms

The concept of supervised learning developed at the same time as the birth of the neural networks themselves, around the 1980s (Adeli and Yeh (1989)). The purpose was to create a model that would interpret input and output data, managing to grasp relationships and dependencies, even of a non-linear nature and difficult to estimate otherwise.

Over time, many algorithms have spread, each developed to perform different functions. These functions can be summarized in two broad fields: classification and regression.

In the classification problem, the network processes the input data and outputs a discrete number of class labels. Essentially, classification algorithms address the Pattern Recognition problem, and are the most common in damage detection: they can be useful to give a probability of belonging to a given class, and allow to reach up to level 3 of the damage classification scale by Rytter.

In regression algorithms, the model outputs are continuous variables. Algorithms are trained to understand the relationship between independent variables and an outcome or dependent variable. The model can then be leveraged to predict the outcome of new and unseen input data, or to fill a gap in missing data.

The use of regression algorithms becomes fundamental when analyzing level 4 of the damage detection scale, the one referred to prognosis. Although the aforementioned autoregressive models and variants are also used for the regression, it must be noticed that they perform a linear regression on the vibrational data, while very often data comes from systems characterized by non-linearity. The architectures of a neural network are by their nature built on non-linear bonds, and this makes them particularly suitable for approaching regression problems, which are also generally non-linear in nature.

In the thesis work, it has been preferred to investigate only the techniques belonging to the first category, since the prognosis phase was not addressed. For classification purpose, the most common algorithms are Artificial Neural Networks (ANNs), Support Vector Machine (SVM) and Random Forest (RF) based algorithms.

Research in the field of SHM has placed a great attention on ANNs, due to their ability in creating models that represent the relationships between the features extracted from the vibrational data and the parameters of the structural system.

Algorithms such as Multilayer Perceptron (MLP), FeedForward, Recurrent or Cellular Networks extract parametric or non-parametric features and estimate structural integrity. Examples of the use of ANNs for damage detection can be found in Pawar et al. (2007), Mehrjoo et al. (2008), Dackermann et al. (2013), while examples of ANN applied to nonparametric methods are in de Lautour and Omenzetter (2010) or in Figueiredo et al. (2011).

It is worth underlining that on the basis of ANN algorithms, more recently Deep Learning algorithms have been developed, such as Convolutional Neural Networks (CNNs): they are applied to automatically process any type of data, but particularly preferred for working with images.

These networks were used, for example, in Abdeljaber et al. (2017), in which they are trained to learn directly from accelerometric data produced by random excitations. In Bao et al. (2019), the recorded time series are transformed into images and anomalies in the data series from different sensors positioned on a bridge are investigated.

Pathirage et al. (2018) have studied the use of Autoencoders in order to identify structural damage from vibrations.

An interesting review work, which deepens the application of Deep Learning alghorithms to damage detection problem, can be found in Ye et al. (2019).

2.3.2 Unsupervised learning alghoritms

As mentioned in the introduction, unsupervised learning techniques require the networks to be trained just from the reference state of the structure, without providing the class labels for the diagnosis of damage; for this reason they are particularly used for the first level of damage detection, the novelty - or anomaly - detection.

The trained predictive model is used to evaluate the structural conditions when a new registration is made. If the difference between the features

extracted from the current data and those predicted by the model exceed a threshold, the state is considered as a deviation from the distribution of the usual condition of the structure; an anomaly that could be symptom of damage.

Among the most used unsupervised learning techniques are the Self Organizing Map, Restricted and Deep Boltzmann machine, and deep convolutional neural networks.

Avci and Abdeljaber (2016) proposed an unsupervised damage detection algorithm based on self-organizing maps (SOM) for global structural damage detection. In the proposed algorithm, SOMs are used to extract damage indices from the random acceleration response of the monitored structure in the time domain.

Rafiei and Adeli (2018) used an unsupervised deep Boltzmann machine to extract features from the frequency domain of the ambient vibration signals. A probability density function is used to create a structural health index (SHI) to verify the insurgence of damage both globally and locally.

In Cha et al. (2017), a CNN Deep Learning network for detecting cracks in concrete in one artifact was used. By providing the network with a sample of about 40k images without calculating the defect features, the vision-based algorithm is able to discriminate the injured states.

2.4 Conclusions

This Chapter briefed on the techniques developed for the vibration-based damage detection problem.

Always taking into account the definition of the four levels of the damage characterization process introduced by Rytter, first of all parametric and non-parametric techniques have been distinguished. In parametric techniques, the damage features are extracted from quantities attributable to the physical characteristics of the structure, such as modal parameters.

First approaches to the problem attempted to correlate the damage directly to the variation of the modal parameters themselves, while over time, features more complex and more sensitive to damage have been derived from them.

The features extraction process in the case of non-parametric techniques,

on the other hand, requires the acquired time series to be directly interpreted: this is generally done by implementing autoregressive models, and evaluating the change in the coefficients as a function of the damage caused. With the technological advancement of the last decades, Machine Learning algorithms have become accessible to all users, promoting their development even in areas not directly involved in the field of information technology, such as SHM. Algorithms based on Machine Learning before, and on Deep Learning for about ten years, allow to achieve good results in damage detection and characterization. This is due to the fact that through a neural network it is possible to create models with non-linear relationships, which is well suited to the trends over time of the typical parameters of structural problems.

The most common algorithms were therefore introduced, ranging from the field of Supervised Learning, in which the model is trained with data already classified in classes, to that of Unsupervised Learning, in which unlabeled data are delivered to the network.

System identification with subspace-based indicators

Chapter abstract

Damage detection methods present in literature can be distinguished in two categories: data-driven methods and model-driven methods. The latter are based on the implementation of a numerical model through which damage scenarios are simulated: in this way, they allow to study damage detection levels 2 and 3 in Rytter's scale, related to the localization and quantification of the damage, respectively.

However, it is necessary for the numerical model to simulate a response as much pertinent as possible to that produced from the real structure: this is the reason why the methods that use this type of approach often involve the calibration of the parameters of the numerical model as a preliminary phase of the process. This procedure is also called model updating, or system identification procedure.

In this chapter, indices based on the analysis of subspaces of a dynamical system are presented. They are tested as objective functions in a model updating process aimed at determining the physical parameters to associate to an FE model of a laboratory test structure. Both simulated and measured vibration data are used to validate the effectiveness and the accuracy of the approach.

The tests showed that the selected damage indices are well suited to be used as objective functions for the model updating task. They also showed higher sensitivity than other parameters, such as modal parameters.

3.1 Introduction

The objective of this thesis work is to develop a damage detection method for diagnosis of the health status of a structure, identifying, locating and giving an estimate of the extent of damage.
As said before, data-driven approaches often allow to perform only the novelty detection level; for this reason, many methods are based on the model-driven approach.
Developing a numerical model it is possible to simulate the damage scenarios that may occur in a structure, which is impossible to do experimentally, given the non-reproducibility of civil structures.
In this work, numerical analyses have been carried out on an Finite Elements model, to simulate the damage scenarios to be compared with the one subsequently produced at experimental level.
The comparison between simulated and experimental data, in terms of subspace indicators, has led to assess the effectiveness of the proposed method.
Reasoning with a model-driven method, a preliminary step to the real damage detection phase is necessary: that of model updating.
The FE model must be calibrated, so that the simulated response is as close as possible to the real one with which it will be compared.
The model updating generally is based on the definition of an objective function to be minimized. It is therefore a process of optimization, in which the cost function varies depending on the parameters - generally physical quantities - related to the structural behavior.
In the thesis work, the effectiveness of damage indicators as cost functions to be minimized has been evaluated. In this case, the damage is fictitious, it is coinceved as the difference between the dynamic behavior of the real structure an the one simulated numerically. Therefore, the index tends to zero if there is resemblance between the two behaviors.
The parameters for which the minimal value of the function is reached, is considered to represent the real ones: this type of problem is also referred as a system identification problem.

3.2 Sub-spaced based methods theoretical background

Under the main assumption that a structure can be studied as a linear time-invariant dynamical system, it is possible to write the equations that govern its behavior:

$$M\ddot{z}(t) + C\dot{z}(t) + Kz(t) = v(t) \tag{3.1}$$

with $M, C, K \in \mathbb{R}^{mxm}$ being the mass, damping and stiffness matrices, respectively; $z(t) \in \mathbb{R}^m$ is the vector representing the displacement of each DOFs, and $v(t) \in \mathbb{R}^m$ is the vector of the external excitation, with m being the number of degrees of freedom of the system.
Taking into account that experimental tests are carried out with sensors acquiring at discrete time instants $t = k\tau$ ($1/\tau$ is the sampling rate), the dynamics of the system can be written also by its discrete-time state-space:

$$\begin{aligned} x_{k+1} &= Ax_k + Bu_k + v_k \\ y_k &= Cx_k + Du_k + w_k \end{aligned} \tag{3.2}$$

with the states $x_k = [z(k\tau)\ \dot{z}(k\tau)] \in \mathbb{R}^m$, the observed inputs $u_k \in \mathbb{R}^m$, the outputs $y_k \in \mathbb{R}^r$, and the unobserved input and output disturbances v_k and w_k.
Matrix

$$A = exp\left(\begin{bmatrix} 0 & I \\ -M^{-1}K & -M^{-1}C \end{bmatrix}\tau\right) \in \mathbb{R}^{nxn} \tag{3.3}$$

is the state transition matrix, and

$$C = \begin{bmatrix} L_d - L_a M^{-1}K & L_v - M^{-1}C \end{bmatrix} \in \mathbb{R}^{rxn}$$

is the observability matrix. In the equations, r represents the number of DOFs acquired by sensors, $n = 2m$ is the system order, matrices L_d, L_v, $L_a \in [0,1]^{rxm}$ are the output location matrices for displacements, velocities and accelerations, respectively.
Often, in the context of Operational Modal Analysis, the input excitation

is unknown. For this reason, the assumption is made that the response of the structure is due only to the two stochastic processes v_k and w_k. Eq.3.2 is simplified:

$$\begin{aligned} x_{k+1} &= Ax_k + v_k \\ y_k &= Cx_k + w_k \end{aligned} \tag{3.4}$$

Both the noises are immeasurable, but they are assumed to be zero mean, stationary white noises, with constant covariance matrix $Q = \boldsymbol{E}(v_k v_k^T) \stackrel{\text{def}}{=} Q\delta(k-k')$, where $\boldsymbol{E}(\cdot)$ denotes the expectation operator. The assumption of white noise is a fundamental base for the SSI process (Van Overschee and De Moor (1996)).

Most of all the Stochastic subspace-based identification algorithms - see for example Peeters and De Roeck (1999) - deals with the identification of matrices A and C after processing a matrix H, called subspace matrix, built from the output data: from matrix A the modal parameters are then obtained.

The two most applied algorithms for evaluating subspace matrix H are known as Covariance-Driven SSI (SSI-Cov) and Data-Driven SSI (SSI-Data).

In the first method, the subspace matrix is built evaluating the output correlations matrices $\Lambda_i \stackrel{\text{def}}{=} \boldsymbol{E}(y_k y_{k-i}^T)$ between the output data (the notation is taken from Yan and Golinval (2006))

$$H_{p,q} \stackrel{\text{def}}{=} \begin{bmatrix} \Lambda_1 & \Lambda_2 & \dots & \Lambda_q \\ \Lambda_2 & \Lambda_3 & \dots & \Lambda_{q+1} \\ \vdots & \vdots & \ddots & \vdots \\ \Lambda_{p+1} & \Lambda_{p+2} & \dots & \Lambda_{p+q} \end{bmatrix} \stackrel{\text{def}}{=} Hank(\Lambda_i) \tag{3.5}$$

with $q \geq p$ user-defined parameters. Using measured data $(y_k)_{k=1,\dots,n}$ a consistent estimate of $\hat{H}_{p,q}$ is obtained from empirical output covariances estimated from a set of N outputs samples

$$\Lambda_i = \boldsymbol{E}(y_k y_{k-i}^T) = \frac{1}{N-i} \sum_{k=i+1}^{N} y_k y_{k-i}^T$$

In the SSI-Data algorithm the Hankel matrix is constructed directly from the measured data.

$$Y_{1,2i} \stackrel{\text{def}}{=} \begin{bmatrix} y_1 & y_2 & \cdots & y_j \\ \cdots & \cdots & \cdots & \cdots \\ y_i & y_{i+1} & \cdots & y_{i+j-1} \\ y_{i+1} & y_{i+2} & \cdots & y_{i+j} \\ \cdots & \cdots & \cdots & \cdots \\ y_{2i} & y_{2i+1} & \cdots & y_{2i+j-1} \end{bmatrix} = \begin{pmatrix} Y_p \\ Y_f \end{pmatrix} \tag{3.6}$$

where $2i$ is a user-defined number of rows, i is often called *time lag* and j the number of column, which in practice is taken equal to $j = N - 2i + 1$. The Hankel matrix is split into a "past" and a "future" matrix, each one having i rows.

Then, it is possible to obtain the subspace matrix $\hat{H}_{1,2i}$ from the product (Benveniste and Mevel (2007))

$$\hat{H}_{1,2i} = \frac{1}{j} Y_f Y_p^T \tag{3.7}$$

Once defined $\hat{H}_{p,q}$,the state matrix A can be traced following various approaches: the one described here is the one implemented in the analyses presented in Ch.5. It involves solving the problem by exploiting the shift invariance property of the observability matrix.

Given $H_{p,q}$, factorization can be made

$$H_{p,q} = W O_p Z_q \tag{3.8}$$

allowing to extrapolate the observability matrix

$$O_p \stackrel{\text{def}}{=} \begin{bmatrix} C \\ CA \\ \vdots \\ CA^p \end{bmatrix} \in \mathbb{R}^{pr \times n} \tag{3.9}$$

The matrix W is the weight matrix, which depends on the chosen algorithm: it is usually taken equal to the identity matrix.

The observation matrix C is therefore computed from the first block-row

of the observability matrix, while the matrix A is estimated by exploiting the shift structure of the observability matrix.

$$O_p^{\uparrow} A = O_p^{\downarrow} \tag{3.10}$$

where the terms

$$O_p^{\uparrow} \stackrel{\text{def}}{=} \begin{bmatrix} C \\ CA \\ \vdots \\ CA^p \end{bmatrix} \quad , \quad O_p^{\downarrow} \stackrel{\text{def}}{=} \begin{bmatrix} CA \\ CA^2 \\ \vdots \\ CA^{p+1} \end{bmatrix}$$

are obtained from O_p by removing the last and first block-row, respectively. Inverting Eq.3.10, matrix A is obtained:

$$A = O_p^{\uparrow +} O_p^{\downarrow} \tag{3.11}$$

Usually, is practice to reach an estimate of the observability matrix by first doing a truncation at the model order n, performing a Singular Values Decomposition of the subspace matrix.

$$\hat{H}_{p,q} = \begin{bmatrix} \hat{U}_1 & U_0 \end{bmatrix} \begin{bmatrix} \hat{\Delta}_1 & 0 \\ 0 & \hat{\Delta}_0 \end{bmatrix} \begin{bmatrix} \hat{V}_1^T \\ \hat{V}_0^T \end{bmatrix} \tag{3.12}$$

Comparing also with Eq.3.8, considering the first non-zero singular values contained in $\hat{\Delta}_1$ an estimate of the observability matrix can be obtained

$$\hat{O}_p = \hat{W}^{-1} \hat{U}_1 \hat{\Delta}_1^{1/2} \tag{3.13}$$

progressively tracing back to A and C.

3.3 Damage detection

It has been described how to find the observation and state matrices implementing SSI algorithms. Instead, the damage detection techniques studies take place directly from the definition of the subspace matrix, and this is why they are called subspace-based damage detection methods.
The concept behind damage detection is that any damage corresponds to

a change in the matrices that govern the dynamic behavior of Eq. 3.1.

All the matrices described in the previous paragraph implicitly depend, among other things, also on the above mentioned matrices: therefore the change of behaviour following damage can be studied through the elaboration of the data acquired by the sensors.

Thus, the methods investigated involve a comparison between data acquired from a state considered undamaged - called *reference* - and data recorded in the current state, or *actual*.

Any damage diagnosis method requires the extraction of damage-sensitive features from measured data of the monitored system (Döhler and Mevel (2012)): the comparison between the features of the reference and of the actual state leads to residuals, which are usually evaluated with statistical methods (Allahdadian et al. (2019)).

Many residuals have been used in the literature: the subspace residual, the transfer matrix-based residual (Bhuyan et al. (2017)), residuals built on a null-space based comparison of data Hankel matrices (Yan and Golinval (2006)), on the difference of output covariance Hankel matrices (Gres et al. (2017b)) or directly on the modal parameter differences (Parloo et al. (2003)).

In the thesis work, an indicator coming from the comparison between output covariance matrices is tested, even if tests using the subspace residual proposed by Yan and Golinval (2006) is also reported.

3.4 Tested and proposed damage indicators

In this section, a theoretical background is made to the subspace-based indices already found in literature and used in the tests. The new proposed index is also introduced.

3.4.1 Derivation of the matrix of residuals

In Basseville et al. (2000, 2004) a residual function was proposed to detect changes in the eigenstructure of the system from measurements y_k without actually identifying the eigenstructure in the possibly damaged state. The considered residual is associated with a covariance-driven output-only sub-

space identification algorithm. The residual function originally proposed compares the undamaged system state with the current one. The considered residual can be written as

$$R_c = \hat{S}_0^T \hat{H}_{p+1,q} \tag{3.14}$$

where $\hat{S}_0^T$ is the left null space of the block Hankel matrix $\hat{H}_{p,q}^{ref}$ in the reference state, while $\hat{H}_{p+1,q}$ is the subspace-based matrix of the actual state. In practice, the excitation covariance Q may change between different measurement sessions of the system due to different environmental factors, while the excitation is still assumed to be stationary during one measurement. A change in the excitation covariance Q leads to a change in the cross-covariance between states and outputs G and thus in the Hankel matrix.

This is the reason why other metrics tends to be preferred to conventional residuals: for example, some researchers (Döhler et al. (2014); Yan and Golinval (2006)) proposed new residuals, which are robust, less sensitive to changing excitation. Let $\hat{U}_1$ be the estimated matrix of the left singular vectors obtained from an SVD of $\hat{H}_{p,q}$, as in Eq.3.12. U_1 is a matrix with orthonormal columns and can be regarded as independent from the excitation covariance.

This property qualifies its use to build a residual function that is robust to changes in the excitation covariance: the robust residual can be written as

$$R_r = \hat{S}_0^T \hat{U}_1 \tag{3.15}$$

A subspace-based damage indicator may be defined as an arbitrary scalar function of the residual matrix.

$$I_d = f(R) \tag{3.16}$$

where I_d is a damage indicator, $f(.)$ an arbitrary scalar function and R the residual matrix.

The first indicator, I_y is the one present by Yan and Golinval (2006) and

built on the robust residuals.

$$I_{y,r} = norm(R_r) \tag{3.17}$$

where *norm* picks the maximum singular value of a matrix; subscript r stays for *robust*.

3.4.2 Proposed damage index

The second damage indicator tested in this work is the one proposed: it derives from a direct comparison of the subspace matrices of the *reference* and the *actual* states.

Given two matrices $A, B \in \mathbb{R}^{m \times n}$, the 2D-correlation coefficient between the two matrices is defined as:

$$r = corr(A,B) = \frac{\sum_m \sum_n \left(A_{nn} - \bar{A}\right)\left(B_{nn} - \bar{B}\right)}{\sqrt{\left(\sum_m \sum_n \left(A_{mn} - \bar{A}\right)^2\right)\left(\sum_m \sum_n \left(B_{mn} - \bar{B}\right)^2\right)}} \tag{3.18}$$

where the apex $(\bar{\cdot})$ indicates the mean between all the elements of the matrix

This index was initially introduced to measure the similarity between images: one of the most employed applications in image processing is the recognition of a specified object in pictures containing several different objects (template matching). The subspace matrices can be treated as images: the assumption is made that the numerical values within the them are distributed in a similar way, if the compared data belong to two realizations of the same state. If comparing different states, the distribution of the values in the matrices also changes, and the correlation index decrease. In this work, the coefficient is used to evaluate how similar the *actual* state matrix is to the *reference* state matrix.

The value of the index varies from 0 (total dissimilarity) to unity (full correlation between the two matrices).

When any form of damage occurs, a decrease in the 2D-correlation index is expected. In order to introduce a damage index as a value of dissimilarity between two states, the proposed damage index is conceived as the

difference between the unity and the 2D-correlation index.

$$DI_{corr} = 1 - r = 1 - corr(\hat{H}^{ref}_{p,q}, \hat{H}_{p,q}) \tag{3.19}$$

Thus, when two sets both belonging to the *reference* state are compared, the index is close to zero, while it increase in other cases.
This index, like the others, can be used in data-driven approaches for anomaly detection (level 1 in Rytter's scale), but it can also be used as a damage feature in a model-driven approach for localization or quantification purposes, as it will be discussed in next chapters.

3.5 System identification

A system is considered to be an object in which different variables interact at all kinds of time and space scales and that produces observable signals (Keesman (2011)).
According to Ljung (1986), system identification deals with the problem of building mathematical models of dynamical systems based on data observed from the systems themselves.
System identification consists of three elements: the acquired data, the mathematical model of the system, and a loss function, which expresses the discrepancy between measured data, revealing the actual structural behaviour, and the simulated response from the numerical model.
Identification problems are optimization problems, in which the minimization of the objective function leads to the identification of the system parameters.
The parametric identification stands on the following hypothesis: the set of parameters $\bar{x}$ that minimizes a given objective function $\mathcal{C}(x) : \mathcal{D} \subset \mathbb{R}^z \to \mathbb{R}$ in a domain $\mathcal{D}$, which spans the expected ranges of variations of the estimand z parameters, coincides with the actual estimand of interest $\hat{x}$. Then, the parametric identification can be expressed by the following optimization problem

$$\bar{x} \equiv \hat{x} = \underset{x \in \mathbb{R}^z}{\arg\min}\, \mathcal{C}(x) \tag{3.20}$$

The choice of the objective function is conditioned by the measured data: when performing vibration tests on large structures such as civil engineering structures, data collection is subjected to important constraints since it is often unpractical and expensive to use artificial excitation such as shakers or drop weights because of their size, mass and/or power consumption Reynders et al. (2008). This is the reason why output-only methods, that were possible since the introduction of stochastic system identification (SSI) methods, became very popular for testing large structures.
As they are defined, damage indicators are well suited to be used as objective function in an identification procedure.

3.5.1 Introduction to tests

In the previous sections, the role of the damage indicators as possible objective function in the identification of structural parameters has been discussed. With the aim of validating the method and illustrating the performance of these indicators in guessing the actual values of the parameters involved, the following tests are performed:

- A numerical application of the identification method is presented in Section 3.6. Both indicators in Eq.3.17 and Eq.3.19 are used as objective function, and their reliability is tested.

- The procedure is then applied to an experimental steel beam used as test-structure: results are presented in Section 3.7.

In all the tests, the optimization procedure is applied for the identification of the Young modulus E and the mass density ρ of the beam.
Both parameters have been discretly varied within a range of feasible values: this allows to graphically represent the trend of the various objective functions and verify the possible presence of local minima.

3.5.2 Experimental setup

The structure considered in both numerical and experimental tests is a $2.5m$ long steel IPE120 beam, with welded rectangular end plates of 200 mm x 100 mm x 5 mm. The beam is held up by two steel supports using springs. The structure corresponds to an actual experimental setup at the

Dynamic Laboratory of the DICEAA, Università degli Studi dell'Aquila, Italy (Fig.3.1).

The data acquisition system is composed of seven vertical velocimeters,

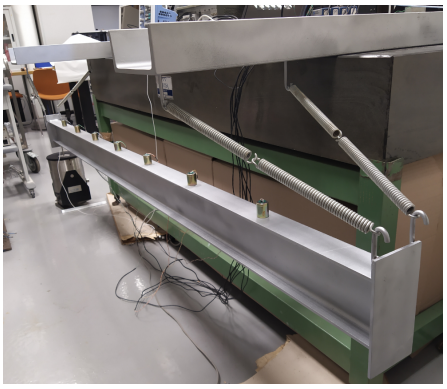

Figure 3.1. Experimental setup.

placed over the beam at equidistant positions and aligned along its longitudinal axis. The input signal is a white noise in the frequency band 0-1000 Hz applied by means of an electrodynamic shaker at the left end of the beam.

3.5.3 Numerical model

In order to perform the analyses required for the identification process, an in-plane FE model of the beam described above has been considered (Fig. 3.2).

The beam has been divided in 8 beam finite elements (Bathe and Wilson (1976)), basing on the disposition of the velocimeters on the real structure. The input signal is simulated with a white noise vertical displacement, assigned to node 1. The output signals obtained from the model are the 7 vertical velocities registered in the nodes in positions corresponding to that of the velocimeters placed over the experimental beam. Damping factors adopted in the numerical model are that obtained in a preliminary modal identification (see Section 3.7.1).

3.6 Numerical tests

In this paragraph, the proposed algorithm is verified through numerical simulations. In order to carry out the analysis, the FE model presented in

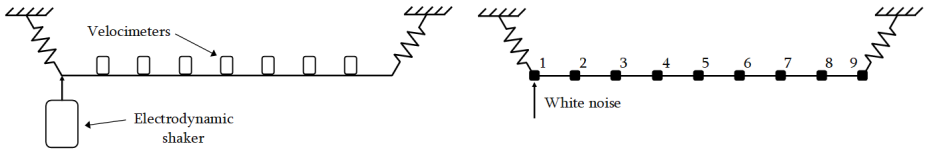

(a) (b)

Figure 3.2. Schematic representation of the setup (a) and finite element model of the steel beam (b).

Par.3.5.3 has been considered: after assigning to the model a chosen value $\bar{E}$ to the Young modulus and $\bar{\rho}$ to the mass density as the target values to be identified, its dynamic response has been simulated. This response is considered as the *reference* state in the identification procedure. The *actual* states are produced by varying E and ρ in a discrete range of values; the different objective functions are then estimated comparing each damaged state to the reference.

Referring to Eq.3.17 and Eq.3.18, the two matrices A and B used are therefore the one relating to the chosen target case and that from the actual ones, respectively. They were used to compute both of the considered indices.

The test was repeated for N=2000 times varying the white noise and its amplitude, in order to produce a significant statistical population.

Fig.3.3 shows that both robust indicators present a trend in which min-

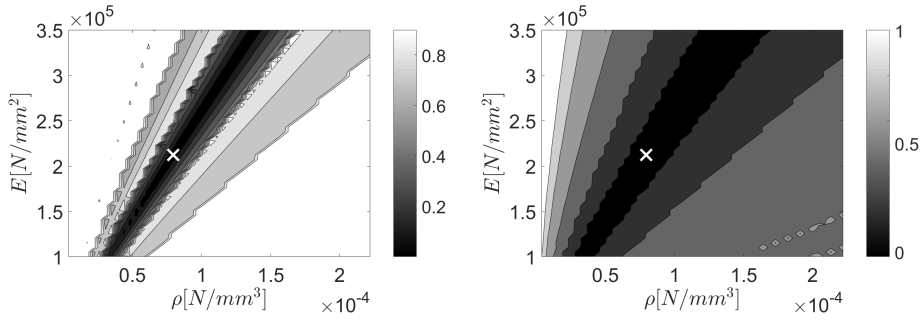

(a) $I_{y,r}$ indicator. (b) DI_{corr} indicator.

Figure 3.3. Variation of the objective function over the selected range of values for parameters E and ρ: numerical tests. The white cross indicates the absolute minimum identified.

ima are arranged along a straight line, whose direction is that given by constant ratio between E and ρ. The sections of the surface along this

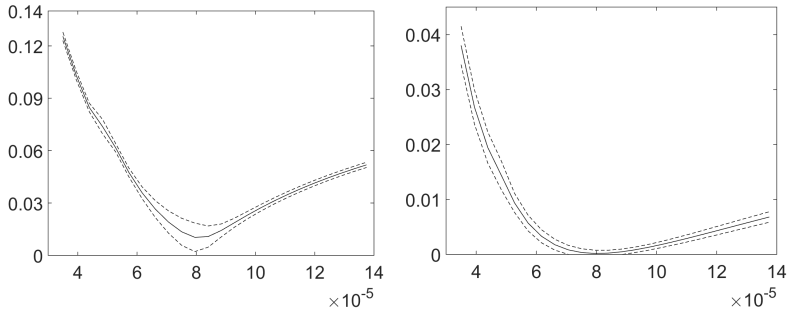

(a) $I_{y,r}$ optimal point. (b) DI_{corr} optimal point.

Figure 3.4. Mean values of the objective functions along the direction of lower values.

direction (Fig.3.4) highlight the presence of an absolute minimum, right in correspondence of the chosen pair ($\bar{\rho}$, $\bar{E}$): in the best point, the mean value of indicators is close to zero. Furthermore, the objective function $I_{y,r}$ seems to be more sensitive to changes in the system parameters than indicator DI_{corr}, since its trend around the point of minimum has a higher slope.

Tab.3.1 shows the values of the mean indexes and the variance obtained from repeating the identification procedure N times. What can be noticed

Table 3.1. Numerical test: mean values μ_{I_i} and variances $\sigma^2_{I_i}$ of the indexes, evaluated repeating the identification procedure for N times.

	μ_{I_i}	$\sigma^2_{I_i}$
$I_{y,r}$	0.0084	$2.02 \cdot 10^{-5}$
DI_{corr}	$1.01 \cdot 10^{-4}$	$8.65 \cdot 10^{-7}$

is that the numerical studies demonstrate the efficiency of assuming the damage index as loss function to minimize, and demonstrate the robustness of the latter tho changing in noise excitation.

3.7 Experimental validation

The same data processing methodology tested in the numerical case of Sec.3.6 has been applied to identify the Modulus E and the mass density ρ of the experimental steel beam described in Section 3.5.2.

In the optimization process, experimental data is used as *reference* state, while simulated data refers to the *actual* states produced using attempt parameters.

The identified parameters $\hat{E}$ and $\hat{\rho}$ are then compared with the pair $E_{exp} = 210000\ MPa$ and $\rho_{exp} = 7.95 \cdot 10^{-5}\ N/mm^3$, which are respectively the declared value of the Young modulus adopted for the steel, and the assumed mass density of the beam.

3.7.1 Modal identification results

Vibration data acquired during the experimental tests has been processed according to the SSI algorithm, in order to detect the natural frequencies, the damping factors, and the mode shapes of the steel beam.
An automatic modal identification algorithm was implemented, following what presented in Cabboi et al. (2017).
Fig.3.5 shows the stabilization diagram resulting from the application of the SSI algorithm. In the frequency band 0-1000 Hz, the first three modes are rigid body ones (with frequencies lower than 12 Hz) followed by four flexural in-plane modes, described in Table 3.2 and Fig.3.6.

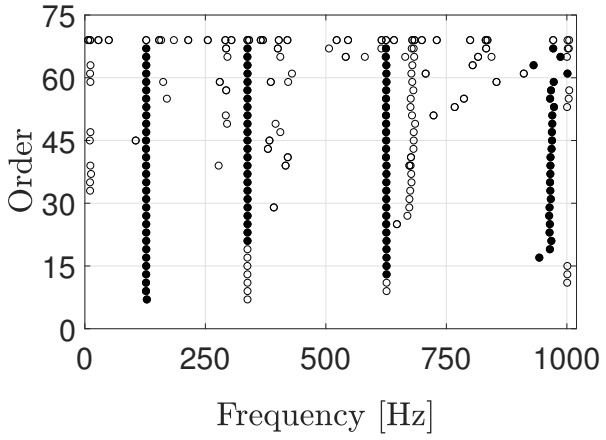

Figure 3.5. Stabilization diagram of the SSI-COV driven algorithm (Peeters and De Roeck (1999)). Filled black dots represent the poles considered as stable by the automated identification algorithm.

Table 3.2. Beam parameters, frequencies and damping ratios of the first four flexural modes from modal identification, with their uncertainty bounds.

$f_{exp,1}$ (Hz)	$f_{exp,2}$ (%)	$f_{exp,3}$ (Hz)	$f_{exp,4}$ (Hz)	$\xi_{exp,1}$ (Hz)	$\xi_{exp,2}$ (%)	$\xi_{exp,3}$ (%)	$\xi_{exp,4}$ (%)
127.4±0.27	337.5±0.149	625.5±0.312	969.1±2.0013	2.06±0.29	1.10±0.069	0.553±0.022	0.211±0.07

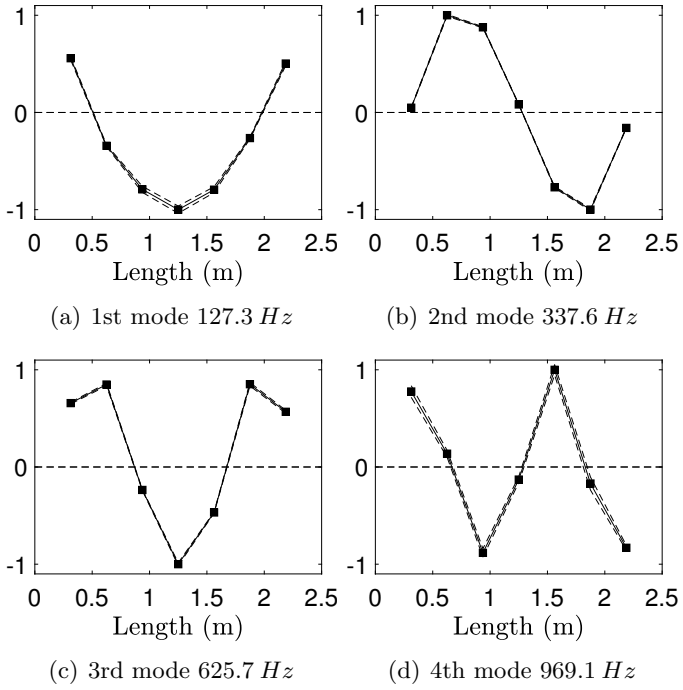

(a) 1st mode 127.3 Hz (b) 2nd mode 337.6 Hz

(c) 3rd mode 625.7 Hz (d) 4th mode 969.1 Hz

Figure 3.6. First four flexural in-plane mode shapes of the steel beam in the frequency range (0-1000 Hz). Full line: mean mode shapes, dashed line: estimated standard deviations.

Results coming from experimental modal identification will be compared with that from numerical simulation of the optimum model, in order to have an opinion on the effectiveness of the presented method.

3.7.2 Parametric identification results

Fig.3.7 shows the trend of the mean value for both the indicators: both the objective functions have trends similar to that obtained in numerical tests.

Table 3.3 presents the pair of minimum $(\hat{E}, \hat{\rho})$ obtained from the identification procedure for both the indicators adopted and makes a comparison with the nominal one. From results in Table 3.3 it can be noted that there

Table 3.3. Experimental case: identified parameters and discrepancies with measured/declared values.

Ind	$\hat{E}$ (MPa)	$\hat{\rho}$ (N/mm^3)	$\hat{I}_d$	E_{exp} (MPa)	ρ_{exp} $\cdot 10^{-5}$ (N/mm^3)	ΔE (%)	$\Delta\rho$ (%)
$I_{y,r}$	$2.21 \cdot 10^5$	$7.70 \cdot 10^{-5}$	0.0745	$2.10 \cdot 10^5$	$7.925 \cdot 10^{-5}$	5.24	-2.84
DI_{corr}	$2.30 \cdot 10^5$	$8.02 \cdot 10^{-5}$	0.0185	$2.10 \cdot 10^5$	$7.925 \cdot 10^{-5}$	9.52	1.19

are differences between the couple (E_{exp},ρ_{exp}) and identified ($\hat{E}$,$\hat{\rho}$) param-

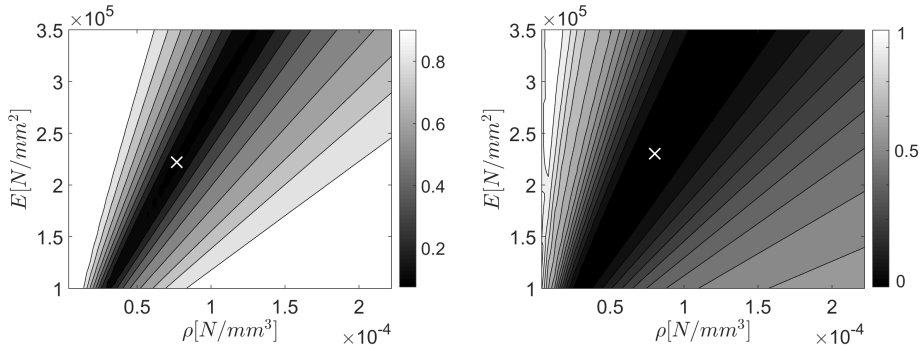

(a) $I_{y,r}$ indicator. (b) DI_{corr} indicator.

Figure 3.7. Variation of the objective function over the selected range of values for parameters E and ρ: experimental tests. Figures (a) and (b) show results obtained with the indicators $I_{y,r}$ and DI_{corr}, respectively. The white cross indicates the absolute minimum identified.

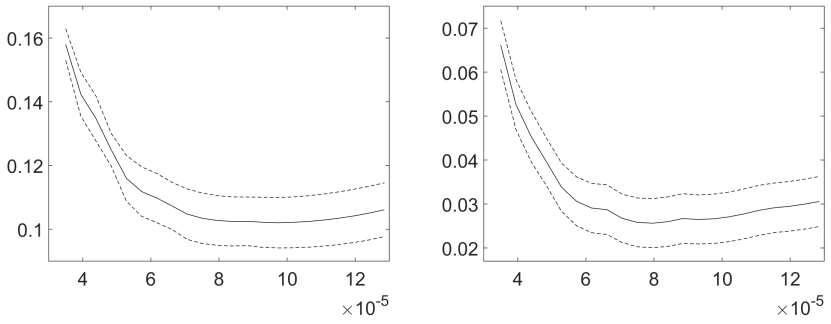

Figure 3.8. Experimental tests: mean values of the robust indicators along the direction of lower values and their σ bounds.

eters less than 10%: unlike the numerical case, the value of the objective functions in the minimum point are not so close to zero (Fig. 3.8).
This discrepancy can be justified by thinking about the uncertainties that characterize the whole process, mainly related to:

- Bias of the model;
- Computational uncertainty due to the chosen discretization of the parameters state $\mathcal{D}$;
- Uncertainty due to experimental measures, i.e. number of sensors used in vibrational data acquisition, sample frequency, noise presence.

The value of indicators in the optimal point can be seen as a measure of the general inaccuracy.

Table 3.4. Numerical frequencies obtained after the identification procedure and comparison with the experimental ones - part 1.

Ind	f_1 (Hz)	$f_{exp,1}$ (Hz)	Δf_1 (%)	f_2 (Hz)	$f_{exp,2}$ (Hz)	Δf_2 (%)
$I_{y,r}$	127.0	127.4	-0.31	337.04	337.5	-0.14
DI_{corr}	127.1	127.4	-0.24	336.9	337.5	-0.18

Table 3.5. Numerical frequencies obtained after the identification procedure and comparison with the experimental ones - part 2.

Ind	f_3 (Hz)	$f_{exp,3}$ (Hz)	Δf_3 (%)	f_4 (Hz)	$f_{exp,4}$ (Hz)	Δf_4 (%)
$I_{y,r}$	627.07	625.5	0.25	964.7	969.1	-0.45
DI_{corr}	626.34	625.5	0.13	962.96	969.1	-0.63

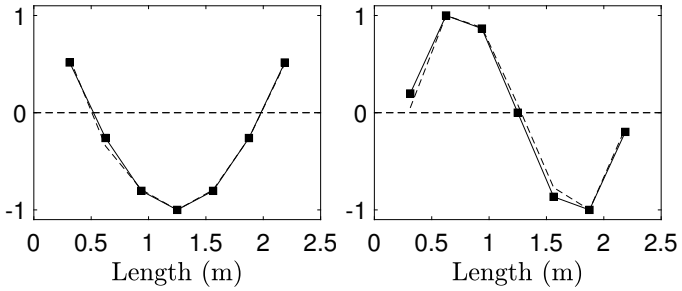

(a) 1st mode 127.0 Hz (b) 2nd mode 337.0 Hz

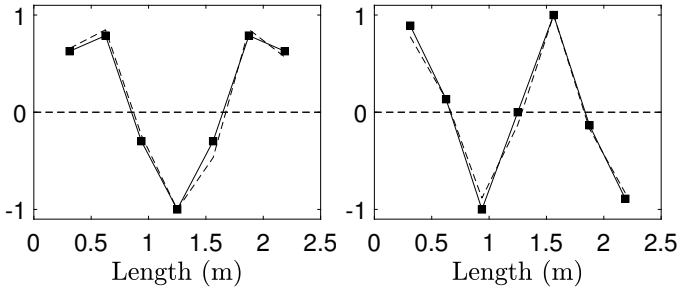

(c) 3rd mode 627.1 Hz (d) 4th mode 964.7 Hz

Figure 3.9. Mode shapes obtained from the finite element model updated using $I_{y,r}$ as objective function. The dotted line indicates the experimental shape.

Table 3.6. MAC matrix, calculated between numerical and experimental modes: $I_{y,r}$ indicator.

MAC	I_{num}	II_{num}	III_{num}	IV_{num}
I_{exp}	**0.9971**	4.051e-04	0.2858	1.108 e-04
II_{exp}	0.005	**0.9894**	0.03	0.1156
III_{exp}	0.2997	0.0037	**0.9882**	0.0019
IV_{exp}	6.76e-06	0.0957	1.298e-04	**0.9910**

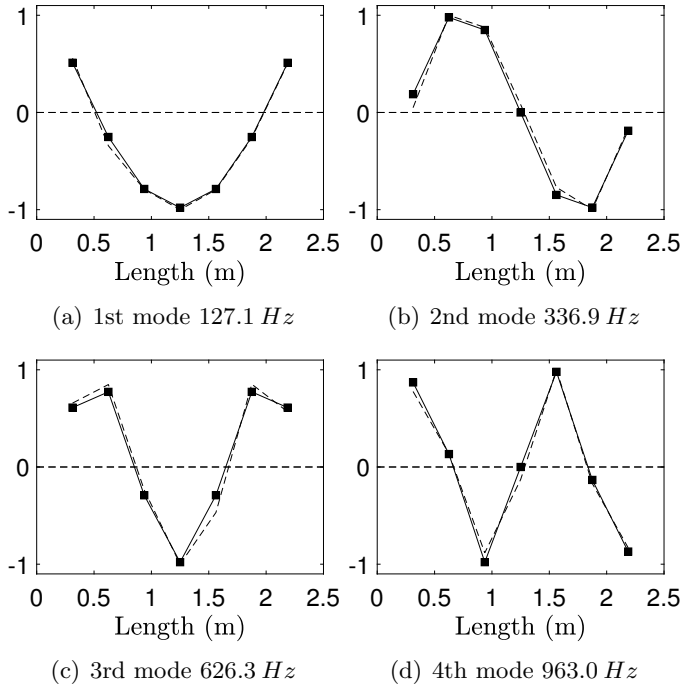

(a) 1st mode 127.1 Hz (b) 2nd mode 336.9 Hz

(c) 3rd mode 626.3 Hz (d) 4th mode 963.0 Hz

Figure 3.10. Mode shapes obtained from the finite element model updated using DI_{corr} as objective function. The dotted line indicates the experimental shape.

Table 3.7. MAC matrix, calculated between numerical and experimental modes: DI_{corr} indicator.

MAC	I_{num}	II_{num}	III_{num}	IV_{num}
I_{exp}	**0.9970**	4.084e-04	0.2844	1.094 e-04
II_{exp}	0.005	**0.9899**	0.003	0.1152
III_{exp}	0.3028	0.0037	**0.9883**	0.0019
IV_{exp}	6.2629e-06	0.0977	1.325e-04	**0.9911**

Tab.3.4-3.6, Fig.3.9-3.10 compare experimental modal parameters and that obtained from numerical model with identified parameters: despite the discrepancy between identified and measured physical parameters, a very small difference between the numerical and experimental frequencies and modal shapes can be observed.

It's worth noticing that, while modal shapes and frequencies are almost perfectly matching, the index could be further minimized, working on the inaccuracies: this suggests that objective function based on indicators could contain more information about the system dynamics than ones based only on modal properties.

Table 3.8. Experimental test: values and variances of the indexes, evaluated repeating the identification procedure for N times (left) and from a single test (right). μ_{I_i} and $\sigma^2_{I_i}$: mean values and variances over N times simulations. I_i and $\hat{\sigma}^2_{I_i}$: indicators and their variances estimated from a single test.

	Empirical evaluation	
	μ_{I_i}	$\sigma^2_{I_i}$
$I_{y,r}$	0.0746	$2.89 \cdot 10^{-6}$
DI_{corr}	$1.85 \cdot 10^{-2}$	$5.77 \cdot 10^{-7}$

3.8 Conclusions

This chapter presented a novel technique for the identification of the parameters of a dynamical system, assuming two residual indicators as objective function in a optimization algorithm.

In the first step, the proposed method has been assessed with numerical tests on a FE beam model. Secondly, the method has been validated through an experimental test, carried out to identify the mass density and the elastic modulus of a real steel beam.

The proposed method gives promising results and seems to be more sensitive to the variation of dynamic system properties than techniques which uses objective functions based only on modal parameters.

The results of the model updating led to the definition of a calibrated model: this FE model has been subsequently used for damage detection tests.

Damage Detection tests

Chapter abstract

Damage localization and quantification represent level 2 and 3 of Rytter's scale in the damage detection procedure. Algorithms of this type allow to estimate the presence of a damage, the position in which it occurs and the extent of the damage. This is done by comparing the actual recorded state with data coming from a reference state, considered undamaged, by means of damage-sensitive features. The presence of damage is assumed when there is a noticeable change in features.

In this chapter, subspace matrices are proposed as features for damage detection. The proposed method approaches the localization and quantification problem first with a traditional approach: a damage index is proposed based on the calculation of the 2D-correlation coefficient between the two matrices of the undamaged and actual states.

Subsequently, the effectiveness of the subspace matrices taken as damage features is tested by training an artificial neural network, with the aim of correctly classifying the produced damage scenarios.

Both methods are tested numerically and experimentally on a laboratory steel beam: the damage is produced by adding a point mass on the beam. The results, evaluated with the variation of the position of the mass along the beam and of its entity, show that the proposed indices and the analyzed algorithms are promising for the damage detection task.

4.1 Introduction

In the previous chapter, the features of the proposed damage detection method have been presented. In this chapter, the proposed method is assessed with tests performed in the laboratory. As already mentioned, the 2D-correlation coefficient is very often used to search for the similarity between two images, in the field of Image Processing. Given the close resemblance of matrices to images (the latter are basically matrices, where each pixel represents a component), it seems logical to relate the process of calculating the index as a difference between matrices, to the process of Pattern Recognition typical of Image Processing.

This evidence led to the development of an algorithm for damage detection based on the use of an artificial neural network for classification. The following chapter shows the results of the laboratory tests. The aim of the tests is to assess the performance of both the 2D-correlation index and the neural network, in covering the two steps of localization and quantification of damage. A steel beam has benen cosidered as test-structure, and the damage has been produced placing a punctual mass along the beam: the unknown variables of the investigated problem have been therefore the position of the mass (that can be traced back to the localization problem) and its entity (that can be associated to a problem of identification of the gravity of the damage).

Machine Learning is one of the most used tools in Artificial Intelligence, although it represents only a branch of it. Over years, the application of ML has led to significant advances in areas such as speech recognition, outlier detection, image recognition and many other numerous fields.

The role of AI, and Machine Learning in particular, in damage detection has already been discussed in Ch.2 , in which some works that applied these concepts were presented. However, many works have focused on the use of modal parameters or coefficients from autoregressive models as features; in none of them the ML approach has been applied to subspace-based features.

Before reporting the results of the damage detection test, it is necessary to make a brief introduction to neural networks, in order to clarify some

concepts that will recur within the chapter.

4.2 Introduction to Artificial Neural Networks

An artificial neural network (ANN) can be thought exactly like the network of neurons present in the human brain: in this system, each neuron receives one or more signals - of electrical nature - from the outside, synthesizes its content and transmits it to other neurons. In this way, the human body succeeds in the basic functions of perception coming from the senses, of transmitting orders for motor skills and many more functions.
Man is able to recognize a certain object since the image of the observed object is already classified in his brain: we recognize objects that we already know in our memory from experience.
Our brain is able to classify what comes from sensory experience basing on the electrical impulses transmitted by neurons. When we are faced with a new object, we are unable to classify it, but we compare it to what is known to our memory (we try to give it a classification based on what we know): we recognize it as a new thing - an anomaly - with respect to the baggage of our experience.
This latter is a typical case of anomaly detection, recurrent in unsupervised learning.
ANNs have been designed with the same architecture of human brain: they acquire data from an input layer (in this case they are features, not sensorial stimuli transformed into electrical impulses), process them through specific activation functions and give a response in terms of output layer.

4.2.1 A Neural Network

Exactly as in the human case, ANN need to be trained in order to carry out the functions of recognition and classification: if in the training phase they are furnished also of the class labels, the learning is said supervised, in contrary case, unsupervised.
In order to fully understand the architecture of a neural network, consider first a supervised learning problem.

In this type of problem, training examples $(x^{(i)}, y^{(i)})$ are provided: x and y denote the input vectors and the output class label by which performing the training of the network. Neural networks address the problem by producing in output a function $h_{W,b}(x)$.

The neuron - also called perceptron - represents therefore a computational

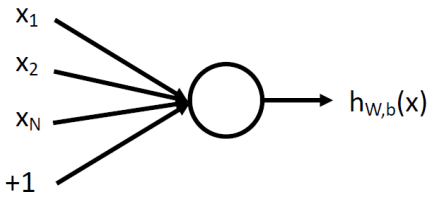

Figure 4.1. Scheme of a simple neuron.

unit that extract outputs from a series of input x^i.

$$h_{W,b}(x) = f(W^T x) = f\left(\sum_{i=1}^{N} W_i x_i + b\right) \tag{4.1}$$

where $f : \mathbb{R} \to \mathbb{R}$ is called activation function: it is represented by the weighted sum of N inputs x_i, with weights W_i ; the term b is a bias.

A neuron is said to be activated - it is "firing" - when the sum of the terms in brackets exceeds a certain threshold, called threshold of activation. In early neural network models, the proposed activation function was a hard threshold function (the first studies date back to McCulloch and Pitts (1943)); over time, it was noted that the training of neural networks would perform better if less rigid activation functions and thresholds were adopted.

Currently, the most used activation functions are the sigmoid function:

$$f(z) = \frac{1}{1 + e^{-z}} \tag{4.2}$$

or the hyperbolic tangent function:

$$f(z) = tanh(z) = \frac{e^z - e^{-z}}{e^z + e^{-z}} \tag{4.3}$$

with $z = \sum_{i=1}^{N} W_i x_i + b$. The peculiarity of these functions is that their valus lie within an interval ([0;1] the sigmoid, [-1;1] the hyperbolic tangent): in this way, they are therefore well suited to describe the binary condition

- on/off - of the neuron.

ANNs are obtained simply by putting several neurons together, so that the output of one neuron becomes the input for another.

Within the network, neurons are organized in layers: for this reason, it also takes the name of multilayer perceptron (MLP).

Every j-th node of a layer is connected to the node i-th of the successive

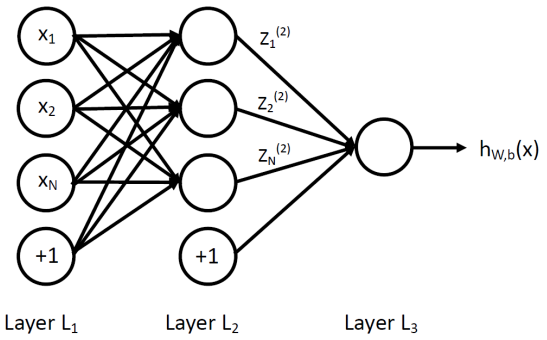

Figure 4.2. Neural network composed by one hidden layer. In this example, the input layer has three nodes, excluding the bias.

layer for means of weights W_{ij}, via the weighted sum of Eq.4.1.

Thus, the signal is transferred from an input layer, is processed in hidden layers and the result emerges from the output layer. In this setting, to calculate the output of the network, all the activations in the second layer, third and so on are calculated in succession. This is an example of a feedforward neural network, since its architecture does not present any loops or cycles.

4.2.2 Backpropagation algorithm

The first step to make a neural network operative is to train it. Training a network consists in calibrating the weights W_{ij} in order for the net to correctly classify the target outputs, given the input.

At each step of the training, an input set is passed to the network and the final outputs are evaluated, comparing them with the target outputs: if the error between the two is acceptable, the weights are not adjusted. If the opposite happens, the weights are adjusted according to the error.

Thus, in the next iterations the error is minimized. The procedure is repeated until the error is small enough to be considered acceptable: the procedure represents an optimization procedure, in which the error is the

objective function to minimize.

Generally, the objective function for a training example (x, y) is is based on the squared-error function:

$$J(W, b; x, y) = \frac{1}{2} \sum_{i=1}^{N} (h_{W,b}(x) - y)^2 \tag{4.4}$$

Given a training set of k examples, the cost function is given by the mean of the Sum of the Squared Error (SSE). Usually, another term is added, according to the equation:

$$\begin{aligned} J(W, b) &= \left(\frac{1}{k} \sum_{i=1}^{k} J(W, b; x^i, y^i) \right) + \frac{\lambda}{2} \sum_{l=1}^{n_l - 1} \sum_{i=1}^{s_l} \sum_{j=1}^{s_{l+1}} \left(W_{ij}^{(l)} \right)^2 \\ &= \left(\frac{1}{k} \sum_{i=1}^{k} \left(h_{W,b}(x^{(i)}) - y^{(i)} \right)^2 \right) + \frac{\lambda}{2} \sum_{l=1}^{n_l - 1} \sum_{i=1}^{s_l} \sum_{j=1}^{s_{l+1}} \left(W_{ij}^{(l)} \right)^2 \end{aligned} \tag{4.5}$$

in which n_l and s_l are the number of layers in the network and the number of nodes in the l-th layer, respectively.

The first term of the sum in Eq.4.5 is the mean of those in Eq.4.4 calculated among all training sets. In situations in which there is a number of weights approximately similar to that of the data points, it can happen that the weights reach high values: in this case, the predictions of the training set are the result of cancellations between large positive and large negative weights (Farrar and Worden (2012)).

The second term, called Regularization (somewhere L_2 regularization term), helps avoiding the over-fitting problem and get a better generalization by controlling the value of the weights. The addition of this term is called *weight decay regularization*, and the term λ is the weight decay parameter. It has been seen that smaller weights result in a smoother network.

The goal is thus to minimize the cost function $J(W, b)$ as a function of the parameters $W_{ij}^{(l)}$ and $b_i^{(l)}$: in the first iteration of the optimization algorithm, the values of these parameters are generally taken from a normal distribution $N(0, \epsilon^2)$ with zero mean and very small variance.

A typical minimization algorithm is based on the computation of the gradient, even if techniques based on global optimization have been developed over time (see, for example, Tran-Ngoc et al. (2019)). The partial deriva-

tives of the function $J(W, b)$ are calculated and then the weights and biases are updated:

$$\begin{aligned} W_{ij}^{(l)} &= W_{ij}^{(l)} - \eta \frac{\partial}{\partial W_{ij}^{(l)}} J(W, b) \\ b_j^{(l)} &= b_i^{(l)} - \eta \frac{\partial}{\partial b_i^{(l)}} J(W, b) \end{aligned} \tag{4.6}$$

the parameter η is called learning coefficient, and indicates the amplitude of the shift of the parameter value in the direction of the gradient.
One way to compute the partial derivatives of Eq.4.6 is given by the backpropagation algorithm (Haykin and Lippmann (1994)).
Essentially, the idea behind the backpropagation algorithm is as follows: given a training set (x, y), in the first iteration, where the parameters are fixed by normal distributions, we compute all network activations, up to the attempt values of the outputs. Next, for each node i in layer l an error term $\delta_i^{(l)}$ is computed. This term measures the error in the output of each node. For the output nodes, the error $\delta_i^{(n_l)}$ is directly measurable as the difference between the attempt value and the true value: given these differences, the error values for the nodes in the previous layers are computed by making weighted averages of the errors from the output nodes, and so on until the first layer is reached. Hence the term backpropagation: weights are adjusted layer by layer, moving backwards from the output layer.

4.3 Intoduction to tests

With the aim of validating the method and illustrating the performance of both the correlation index and of the ANN, a series of experimental tests were performed. In these tests, the structural damage was caused by adding a point mass on the beam-system illustrated in Ch.3 (Fig.3.1). The addition of a mass changes the modal characteristics of the system: when structural damage occurs, the variation in the mechanical or geometric characteristics of the structural elements generates a variation in the modal parameters, more or less marked according to the extent of the damage.
For this reason, the change in behavior produced by the addition of the mass is assumed to be related to that produced by a structural damage.

Various tests were performed, by varying both the entity of the mass and its position, with the aim of evaluating the effectiveness of the method in guessing these latter. In particular, the following tests have been performed:

- A numerical application is performed, in which the algorithm is tested to change in the noise excitation;
- The procedure is then applied to the real test-structure. In particular, known masses are placed over the actual steel beam and virtual ones are placed over the finite element beam model.
  The scope is then finding the correct position of the mass (damage localization) and its value (damage quantification) by comparing the real dynamic behavior with that simulated with the FE model.

In both the tests, the procedure is applied for the following scopes:

- Identification of the position of the mass: the alghorithm is tested with a fixed mass, varying its positsion along the beam;
- Identification of the entity of the mass: fixed a position, the value of the mass placed on the beam is varied.

Both the tests are used to assess the sensitivity of the method to changes in the two parameters.
In tests using the correlation index, the goal is to find the minimum index value among all those coming from the comparison between a damaged state chosen as reference state and all others. The problem translates, as in the case of model updating described in the previous chapter, to an optimization process, in which the loss function is the index DI_{corr} itself. Unlike the model updating procedure, for which the attempt values of elastic modulus and mass density could be varied in a continuous manner, in this case well defined damage scenarios are produced (referable to those that are assumed to occur in a structure). The optimization in this case would be more of a discrete type, or mixed: the position is varied in a discrete range, while the magnitude of the mass could vary in a continuous range. In any case, it has been chosen to discretize both ranges, focusing more on the study of assessing the indices as features, rather than on the optimization techniques, which certainly deserve a discourse apart.

The effectiveness of the algorithm is evaluated by looking at the percentage that it correctly identifies the produced damage scenario - the position or the mass - compared to the times when it falls in missclassification.
Tests based on the neural network instead require the training of a classifier capable of recognizing the damage class of a current state according to the data provided in the training set, following the procedure described in Par.4.2.1.
In both numerical and experimental tests, training is performed based on simulations from the FE model calibrated in the model updating phase, in order to get the maximum match with the real behavior.
In particular, damage scenarios corresponding to all assumed positions and mass entities are simulated, and then the effectiveness of the training is evaluated by feeding a test set to the network, with the goal of recognize it with the right label.
The validity of the algorithm is then assessed by evaluating the confusion matrix, through which it is established with which percentages a given damage state is recognized by the network, compared to the total number of the simulated cases.
The experimental tests simulate the circumstances of what happens in real damage detection cases. The data acquired from the experimental damaged state are compared with the numerical data simulated with the FE model: in the case of the correlation index, an optimization algorithm is carried out, in the case of the network, the classifier itself directly gives the outcome of the prediction.
In any case, a situation arises where there is a large availability of data related to simulated cases, but a small number of data related to the actual experimental damaged state.

4.3.1 Selected damage scenarios

The experimental structure has already been presented in Ch.3.5.2: it is a steel beam of profile IPE120, of length $2.5\,m$: according to the results of the parametric identification of Ch.3, it is estimated to have a mass density $\rho = 8.02 \cdot 10^{-5}\ N/mm^3$ (corresponding to a total weight of about $27\,Kg$) and a young's modulus $E = 2.30 \cdot 10^5 MPa$. The damage scenarios involve

varying the position of the mass and its magnitude: the beam was therefore discretized into 25 positions (graphically shown in Fig.4.3).

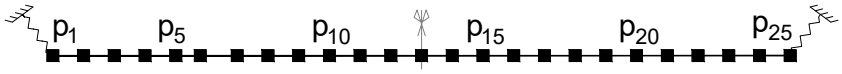

Figure 4.3. Selected mass positions. For numerical values, see Tab.4.1.

Table 4.1. Numerical values of the selected position of the mass along the beam.

POS.	x(mm)	POS.	x(mm)	POS.	x(mm)	POS.	x(mm)	POS.	x(mm)
p1	0	p6	500	p11	1041.7	p16	1562.5	p21	2083.3
p2	104.2	p7	625	p12	1145.8	p17	1666.7	p22	2187.5
p3	208.3	p8	729.2	p13	1250	p18	1770.8	p23	2291.7
p4	312.5	p9	833.3	p14	1354.2	p19	1875	p24	2395.8
p5	416.7	p10	937.5	p15	1458.3	p20	1979.2	p25	2500

The mass varies within the discrete interval presented in Tab.4.2. Considering that the total weight of the beam is about 27 Kg, the range of variation of the mass ranges goes from 1.5% to about 11% of the weight of the beam.

Table 4.2. Numerical values of the selected mass range.

MASS	Kg	MASS	Kg	MASS	Kg	MASS	Kg	MASS	Kg
m1	0.400	m6	0.930	m11	1.46	m16	1.99	m21	2.52
m2	0.506	m7	1.03	m12	1.56	m17	2.09	m22	2.62
m3	0.612	m8	1.14	m13	1.67	m18	2.20	m23	2.67
m4	0.718	m9	1.24	m14	1.78	m19	2.31	m24	2.84
m5	0.824	m10	1.33	m15	1.88	m20	2.41	m25	2.94

4.4 Numerical damage localization tests

In this paragraph, numerical results related to damage localization are presented: in these tests, the mass is kept fixed, and its position varies according to values reported in Tab.4.1. The FE model used for simulations is the one presented in Ch.3.5.3, discretized this time into a number of nodes equal to that of the considered positions.
Following the aforementioned levels of damage diagnosis promoted by Rytter, the initial phase involves evaluating the change in the index DI_{corr} as mass is added to the system and its position is varied, with relation to a statistical population built on the *reference* state alone. This initial phase can be traced back to that of anomaly detection (level 1).

In order to perform the tests, N=200 simulations were conducted for both the undamaged state and the 25 damaged states shown in Tab.4.1, as the excitation noise varied.

As can be seen from Fig.4.4, the insertion of the mass, albeit of low magnitude (0.4 kg compared to about 27 kg of the beam), causes an increase in the damage index.

The index assumes greater values when the mass is placed near the edges of the beam and in its centerline. The figure shows also a marked dependence of the index values on the symmetry of the beam.

What emerges is that the index function is not injective with respect to the position-variable: it is not possible to uniquely relate a precise value of the index function to a given position. This suggests that it is indeed impossible to proceed in level 2 of Rytter's scale, by just performing a data-driven method, justifying the need to proceed via model-driven approach.

It appears from the figure that the damage index, despite the presence of mass, is close to zero in some positions. Nevertheless, still occurs a variation with respect to the population of values relative to the reference state.

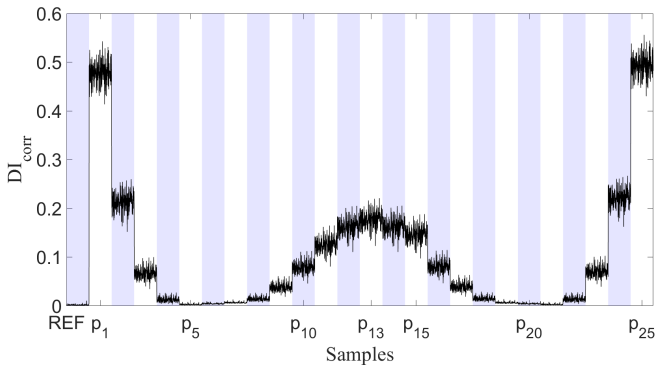

Figure 4.4. Variation of the damage index DI_{corr}, calculated for anomaly detection purposes with respect to the undamaged case, as the position of the fixed mass m10 changes.

4.4.1 Damage localization with the subspace-based index

The damage localization phase is carried out with a model-based approach. Once all plausible damage scenarios are simulated with the FE model, the algorithm is tested by selecting one state from those produced, to be treated

as the target one to be identified. For each state, N_{train}=200 samples were considered for this reference state and N_{test}=80 samples for the actual states to be tested.
For the i-th damaged state to be identified ($i = 1, \ldots, 25$), the test is performed according to the following steps:

- the $H_k^{(i)}$ subspace matrices related to the reference state are computed, for $k = 1, \ldots, N_{train}$. Matrices are evaluated considering a time delay $i = 60$;
- the $H_u^{(j)}$ subspace matrices related to the j-th simulated position, including the selected one, $j = 1, \ldots, 25$ and $u = 1, \ldots, N_{test}$ are computed. Matrices are evaluated considering a time delay $i = 60$;
- damage indices $(DI_{corr})_j^{(i)} = 1 - corr(H_k^{(i)}, H_u^{(j)})$ between the matrices of the state to be identified and the current ones are computed. In this way, each set identifying the j-th attempt position consists of $N_{train} \times N_{test}$ samples;
- for each of the N_{test} sets of indices obtained as the position varies, the minimum is computed;
- the confusion matrix is produced, indicating how many of the simulated cases have been correctly guessed, giving the measure of the accuracy of the method to variation of the noise.

The results of the procedure are summarized in the Tab.4.3 and 4.4.
As can be seen from the tables, producing simulations by varying the excitation noise has generated some uncertainty in the results. However, in the case of localization, this remains limited to small percentages of the samples: almost all of the selected damaged states are correctly identified. What is remarkable is the arrangement of the misclassified cases: in addition to the positions close to the diagonal of the confusion matrix, as could be expected, they are also arranged along its antidiagonal. The main cause of this presence can be addressed to the geometric symmetry of the structure, boundary conditions, and sensor arrangement, as already noted in the anomaly detection phase of Fig.4.4.
The symmetry is probably the cause of the fact that, moving the mass

towards the middle of the beam, the percentage of true positives decreases significantly, while the percentage of surrounding misclassified cases increases. In the position near the midpoint, a percentage of misclassified cases of about 70% is recorded.

The problem concerning the number of misclassified samples is solved by

Table 4.3. Confusion matrix obtained from numerical localization tests - part 1. The columns represent the Target class, the rows contain the predicted output class.

	p1	p2	p3	p4	p5	p6	p7	p8	p9	p10	p11	p12	p13
p1	**100**	0	0	0	0	0	0	0	0	0	0	0	0
p2	0	**99.94**	0.06	0	0	0	0	0	0	0	0	0	0
p3	0	0	**98.89**	1.11	0	0	0	0	0	0	0	0	0
p4	0	0	0.38	**92.31**	7.31	0	0	0	0	0	0	0	0
p5	0	0	0	4.31	**71.94**	23.74	0	0	0	0	0	0	0
p6	0	0	0	0.18	13.62	**84.58**	0.06	0.06	0	0	0	0	0
p7	0	0	0	0	0	1.99	**76.27**	7.98	0	0	0	0	0
p8	0	0	0	0	0	0	13.56	**81.93**	4.42	0	0	0	0
p9	0	0	0	0	0	0	0	7.63	**88.67**	3.68	0	0	0
p10	0	0	0	0	0	0	0	0	7.11	**87.33**	5.57	0	0
p11	0	0	0	0	0	0	0	0	0.01	10.3	**71.41**	6.05	0.4
p12	0	0	0	0	0	0	0	0	0	0.13	14.74	**40.96**	29.46
p13	0	0	0	0	0	0	0	0	0	0.01	3.49	22.06	**61.02**
p14	0	0	0	0	0	0	0	0	0	0.11	8.68	4.41	28.43
p15	0	0	0	0	0	0	0	0	0	0.89	24.74	0.22	5.77
p16	0	0	0	0	0	0	0	0	0.64	0.74	3.13	0	0
p17	0	0	0	0	0	0	0	0.31	0.52	0	0	0	0
p18	0	0	0	0	0	0	0.55	0.78	0	0	0	0	0
p19	0	0	0	0	0	0.04	2.28	0	0	0	0	0	0
p20	0	0	0	0.02	0.64	12.17	0.25	0	0	0	0	0	0
p21	0	0	0	0.77	0	14.93	0	0	0	0	0	0	0
p22	0	0	0	0	0	0	0	0	0.01	0	0	0	0
p23	0	0	0	0	0	0	0	0	0	0	0	0	0
p24	0	0	0	0	0	0	0	0	0	0	0	0	0
p25	0	0	0	0	0	0	0	0	0	0	0	0	0

Table 4.4. Confusion matrix obtained from numerical localization tests - part 2. The columns represent the Target class, the rows contain the predicted output class.

	p14	p15	p16	p17	p18	p19	p20	p21	p22	p23	p24	p25
p1	0	0	0	0	0	0	0	0	0	0	0	0
p2	0	0	0	0	0	0	0	0	0	0	0	0
p3	0	0	0	0	0	0	0	0	0	0	0	0
p4	0	0	0	0	0	0	0	0	0	0	0	0
p5	0	0	0	0	0	0	0.01	0	0	0	0	0
p6	0	0	0	0	0.06	0.23	1.13	0.09	0	0	0	0
p7	0	0	0	0	0.24	0.31	13.21	0	0	0	0	0
p8	0	0	0	0.06	0.03	0	0	0	0	0	0	0
p9	0	0	0.02	0	0	0	0	0	0	0	0	0
p10	0	0	0	0	0	0	0	0	0	0	0	0
p11	0.03	11.81	0	0	0	0	0	0	0	0	0	0
p12	1.98	12.73	0	0	0	0	0	0	0	0	0	0
p13	6.82	6.6	0	0	0	0	0	0	0	0	0	0
p14	**31.5**	26.88	0	0	0	0	0	0	0	0	0	0
p15	21.91	**46.40**	0.08	0	0	0	0	0	0	0	0	0
p16	0	0.06	**89.31**	6.14	0	0	0	0	0	0	0	0
p17	0	0	3.37	**88.43**	7.38	0	0	0	0	0	0	0
p18	0	0	0	4.49	**80.77**	13.41	0.01	0	0	0	0	0
p19	0	0	0	0	8.46	**66.24**	22.98	0	0	0	0	0
p20	0	0	0	0	0.56	12.83	**73.36**	0.18	0	0	0	0
p21	0	0	0	0	0	0	4.36	**76.97**	2.98	0	0	0
p22	0	0	0	0	0	0	0	6.23	**93.53**	0.24	0	0
p23	0	0	0	0	0	0	0	0	0.85	**99.15**	0	0
p24	0	0	0	0	0	0	0	0	0	0.04	**99.96**	0
p25	0	0	0	0	0	0	0	0	0	0	0	**100**

averaging the results obtained for each attempt to localize the i-th state: by computing the means of the $N_{tot} = N_{train} \times N_{test}$ indices $DI^{(i)}_{corr}$, and finding the minimum among the mean values, the target position is found

for every damaged state.

$$\begin{aligned}\overline{DI}_{corr} = [\, & 0.13253\ 0.02335\ 0.03556\ 0.09726\ 0.15141 \\ & 0.16945\ 0.14875\ 0.10291\ 0.05467\ 0.02054 \\ & 0.00492\ 0.00187\ 0.00227\ \mathbf{0.00160}\ 0.00207 \\ & 0.02023\ 0.05412\ 0.10170\ 0.14677\ 0.16748 \\ & 0.14901\ 0.09474\ 0.03418\ 0.02609\ 0.14396\,]\end{aligned} \tag{4.7}$$

As noted in Eq.4.7, when applying the described procedure a correct identification of the target position is achieved, even for the $p14$ case, which was the case with most misclassified samples.

4.4.2 Damage localization tests using the ANN

What emerged in Par.4.4.1 drives further in the direction of using an ANN network. In fact, for its nature, the network tends to mediate the differences due to the noise variationin its training phase. In this phase, calibrating the weights in the neurons connections, it becomes aware of the relationships intercurring between the input data, making the results of the classification as independent as possible from the way in which the data have been produced.

The training, validation and testing phases of the neural network were conducted considering the same number of samples used in the validation of the DI_{corr} index. In particular, the samples used in the training were $N_{train} = 200$, of whom 75% for the actual training and the remaining 25% for the validation set, while in the testing phase $N_{test} = 80$ samples were considered.

Recall that training a classifier falls under supervised learning: during its training, the network is provided not only with the input features, but also with the class labels to which they belong.

The network training and classification algorithm for the purpose of damage localization consists of the following steps:

- Production of input data for network training: for each of the hypothesized damage scenarios, N_{train} subspace matrices H are produced.
- Definition of the network architecture and subsequent training phase:

in order for a network to be trained, it is necessary to define both the parameters directly related to the architecture, i.e. the number of layers constituting it and the number of nodes for each layer, and the nature of the functions that establish the relationships between the nodes. The network used for damage localization is a perceptron that needs one hidden layer, with a number of inner nodes equal to 20.
The used activation function is the sigmoid - see Par.4.2.1. The loss function considered during the training is the cross-entropy loss function. Given the targets vector t and output vector y, the cross-entropy for each pair of output-target elements is calculated as:

$$(cross)_i = -t_i \cdot log(y_i)$$

to which is added the regularization term as in the case of the SSE defined in Eq.4.5.
The function has been preferred to SSE because it returns a value that heavily penalizes outputs that are extremely inaccurate (y near 1-t), with very little penalty for fairly correct classifications (y near t).
The overall performance of the network is evaluated from the mean of the individual value;

- Classification of current data coming from the test set: after the training, classification tests are performed. N_{test} samples for each i-th damaged state are tested to be recognized by the network. The confusion matrix is constructed.

The training and classification results are shown in the following figures. Fig.4.5 shows the trend of the objective function during the training phase: an acceptable optimum value for the loss function is reached after about 300 epochs. Fig.4.6 shows the gradient calculated in the various iterations: the low value of the function symbolize the correct occurrence of the training.
Classification outcomes are read from the confusion matrix in Fig.4.7. As happened with Tab.4.3, the terms on the diagonal indicate how many cases, among those tested, were correctly identified by the network.
As can be seen, all the tested cases fall within the diagonal, whichever

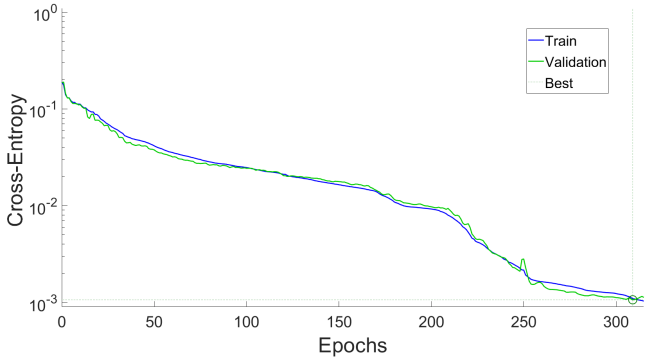

Figure 4.5. Crossentropy parameter evaluated as performance index in the training of network for localization.

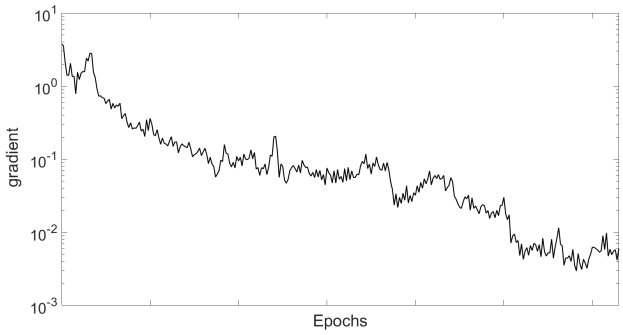

Figure 4.6. Trend of the gradient of the loss function during the training phase of the ANN used for localization.

state has been chosen as damaged: the network, as a result of the training, contains within it all the information needed to correctly discriminate the various damage scenarios. Despite the noise, in this case, the percentage of misclassified cases (elements outside the diagonal) is even zero, in the position near the midpoint.

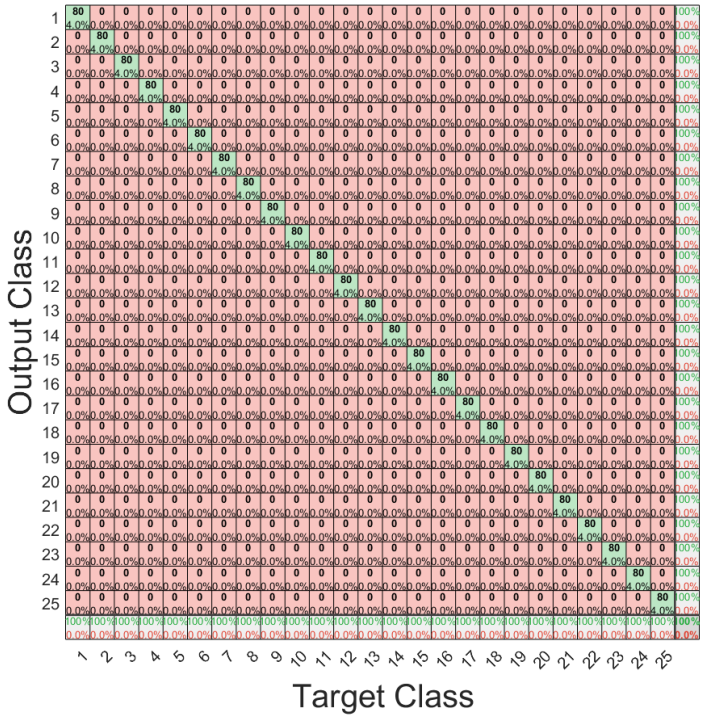

Figure 4.7. Confusion matrix evaluated for the damage localization problem.

4.5 Numerical Damage quantification tests

What described previously for the localization tests is also carried out for the damage quantification tests: therefore, anomaly detection is performed first. For the novelty detection test, the mass position is kept fixed in $p15$ (about 1.5 m from the left edge of the beam), and N=200 simulations are conducted for the *reference* state and for the 25 damaged states shown in Tab. 4.2, as the excitation noise varied.

As can be seen from Fig.4.8, the addition of the mass generates an increase in the value of the index DI_{corr}.

4 Differing from what happened in the localization case, the index takes on larger values as the magnitude of the mass increases. In this case,

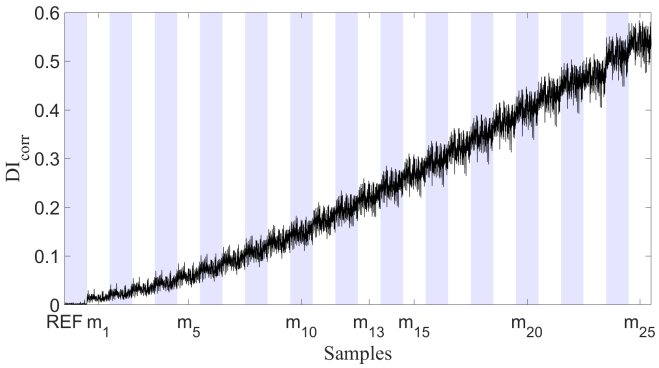

Figure 4.8. Variation of the damage index DI_{corr}, calculated for anomaly detection purposes with respect to the undamaged case, as the magnitude of the mass changes, while position remains fixed in p15.

therefore, given the location of the mass, the increase in the damage index can be correlated with the increase of damage in the structure, allowing to investigate level 3 of the Rytter scale exclusively through data-driven methods. Simulations by means of the FE model are necessary, however, where a specified damage magnitude is actually to be classified in relation to others.

4.5.1 Damage Quantification using the subspace-based index

Once all damage scenarios were simulated, the algorithm was tested by essentially replicating the procedure described for damage localization.
For each state, N_{train}=200 samples were considered for the reference state and N_{test}=80 samples were considered for the states to be checked.
As can be seen from Tab.4.5 and Tab.4.6 ,the production of simulations by varying the excitation noise generated some uncertainty in the classification process.
Compared to the damage localization case, there are basically two differences:

- the misclassification extends among the cases in the surroundings of the elements of the diagonal of the table. There is a certain percentage of misclassified cases exclusively in a band adjacent to the diagonal, in contrast to the localization case, in which the symmetry of the structure caused some misclassified cases to be present even along

the antidiagonal;

- The percentages by which the selected damage state is correctly classified is significantly lower than that in the localization case. Such values, ranging from a maximum of 68% to a minimum of 27%, with an average of about 38%, prove a lower sensitivity of the damage index DI_{corr} to variation in mass - magnitude of damage - rather than in the position in which it is located.

Table 4.5. Confusion matrix obtained from numerical damage quantification tests - part 1. The columns represent the Target class, the rows contain the predicted output class.

	m1	m2	m3	m4	m5	m6	m7	m8	m9	m10	m11	m12	m13
m1	**65.29**	27.2	6.94	0.56	0.01	0	0	0	0	0	0	0	0
m2	26.67	**39.08**	26.91	6.72	0.61	0.01	0	0	0	0	0	0	0
m3	5.12	22.17	**39.29**	26.26	6.49	0.65	0.01	0	0	0	0	0	0
m4	0.38	4.98	22.66	**39.33**	25.41	6.56	0.67	0.02	0	0	0	0	0
m5	0	0.38	5.21	23.18	**39.39**	24.66	6.48	0.69	0.02	0	0	0	0
m6	0	0	0.4	5.46	23.86	**38.88**	24.31	6.39	0.69	0.03	0	0	0
m7	0	0	0	0.4	5.71	24.41	**38.68**	23.66	6.21	0.92	0.02	0	0
m8	0	0	0	0	0.34	6.07	24.93	**38.31**	22.14	7.24	0.95	0.01	0
m9	0	0	0	0	0	0.38	6.29	25.39	**35.21**	24.55	7.44	0.74	0.01
m10	0	0	0	0	0	0.01	0.84	8.99	26.14	**37.14**	21.93	4.54	0.41
m11	0	0	0	0	0	0	0	0.51	5.54	24.43	**40.42**	22.39	6.06
m12	0	0	0	0	0	0	0	0	0.42	5.95	27.38	**37.11**	22.69
m13	0	0	0	0	0	0	0	0	0	0.51	7.14	26.24	**37.57**
m14	0	0	0	0	0	0	0	0	0	0.02	0.74	6.75	26
m15	0	0	0	0	0	0	0	0	0	0	0.02	0.87	7.33
m16	0	0	0	0	0	0	0	0	0	0	0	0.03	0.95
m17	0	0	0	0	0	0	0	0	0	0	0	0	0.04
m18	0	0	0	0	0	0	0	0	0	0	0	0	0
m19	0	0	0	0	0	0	0	0	0	0	0	0	0
m20	0	0	0	0	0	0	0	0	0	0	0	0	0
m21	0	0	0	0	0	0	0	0	0	0	0	0	0
m22	0	0	0	0	0	0	0	0	0	0	0	0	0
m23	0	0	0	0	0	0	0	0	0	0	0	0	0
m24	0	0	0	0	0	0	0	0	0	0	0	0	0
m25	0	0	0	0	0	0	0	0	0	0	0	0	0

Table 4.6. Confusion matrix obtained from numerical damage quantification tests - part 2. The columns represent the Target class, the rows contain the predicted output class.

	m14	m15	m16	m17	m18	m19	m20	m21	m22	m23	m24	m25
m1	0	0	0	0	0	0	0	0	0	0	0	0
m2	0	0	0	0	0	0	0	0	0	0	0	0
m3	0	0	0	0	0	0	0	0	0	0	0	0
m4	0	0	0	0	0	0	0	0	0	0	0	0
m5	0	0	0	0	0	0	0	0	0	0	0	0
m6	0	0	0	0	0	0	0	0	0	0	0	0
m7	0	0	0	0	0	0	0	0	0	0	0	0
m8	0	0	0	0	0	0	0	0	0	0	0	0
m9	0	0	0	0	0	0	0	0	0	0	0	0
m10	0	0	0	0	0	0	0	0	0	0	0	0
m11	0.65	0.01	0	0	0	0	0	0	0	0	0	0
m12	5.87	0.57	0.01	0	0	0	0	0	0	0	0	0
m13	22.22	5.79	0.54	0.01	0	0	0	0	0	0	0	0
m14	**37.26**	22.61	6.02	0.58	0.03	0	0	0	0	0	0	0
m15	26.11	**36.80**	22.59	5.68	0.59	0.03	0	0	0	0	0	0
m16	7.44	25.48	**37.36**	22.39	5.69	0.63	0.03	0	0	0	0	0
m17	1.07	7.13	25.36	**37.59**	22.51	5.58	0.69	0.03	0	0	0	0
m18	0.07	0.99	7.23	25	**37.7**	22.65	5.61	0.73	0.02	0	0	0
m19	0	0.07	1.04	7.19	24.59	**37.95**	22.68	5.69	0.66	0.12	0	0
m20	0	0	0.09	1.05	7.19	24.17	**38.10**	22.84	5.00	1.44	0.13	0
m21	0	0	0	0.09	1.06	7.19	23.96	**37.89**	18.63	9.59	1.56	0.04
m22	0	0	0	0	0.09	1.03	7.23	23.66	**27.33**	**29.18**	10.65	0.83
m23	0	0	0	0	0.01	0.43	3.48	15.18	23.21	**36.09**	19.29	2.32
m24	0	0	0	0	0	0	0.08	1	3.94	17.74	**46.02**	31.23
m25	0	0	0	0	0	0	0	0.07	0.47	4.59	26.23	**68.64**

The problem concerning the number of misclassified samples is solved by averaging the results obtained for each attempt to identify the i-th state: by computing the means of the $N_{tot} = N_{train} \times N_{test}$ indices $DI_{corr}^{(i)}$, and finding the minimum among the mean values, the quantification turns out to be correct in all cases.

$$\begin{aligned}\overline{DI}_{corr} = [\, & 0.33634 \;\; 0.30488 \;\; 0.27477 \;\; 0.24609 \;\; 0.21891 \\ & 0.19328 \;\; 0.16923 \;\; 0.14680 \;\; 0.12600 \;\; 0.11001 \\ & 0.08936 \;\; 0.07351 \;\; 0.05930 \;\; 0.04645 \;\; 0.03575 \\ & 0.02637 \;\; 0.01855 \;\; 0.01225 \;\; 0.00743 \;\; 0.00406 \\ & 0.00208 \;\; \mathbf{0.00146} \;\; 0.00160 \;\; 0.00411 \;\; 0.00730 \,]\end{aligned} \tag{4.8}$$

As noted in Eq.4.8, when applying the described procedure a correct identification of the target mass is achieved even for the $m22$ case, which was previously confused.

4.5.2 Damage quantification tests using the ANN

In the following section, numerical tests are conducted exactly as reported in Par.4.4.2. The training, validation and testing phases of the neural network were conducted considering a total of 347 samples for each simulated state. of samples . Specifically, the number of samples used in the training were $N_{train} = 200$, the same as used in the validation of the DI_{corr} index. Of these samples, 75% was used for the actual training and the remaining 25% for the validation phase. The remaining $N_{test} = 147$ samples were used in the testing phase.

Fig.4.9 and Fig.4.10 show the trend of the objective function and the gradient calculated during training, respectively.

From the confusion matrix of Fig.4.11 the effectiveness of the method based on the neural network compared to the one based on the correlation coefficient can be appreciated. As can be seen, in fact, each sample of the test set is correctly associated to the damage label to which it belongs: the percentage of the elements in the diagonal of the confusion matrix is total, as symbol that the variation of noise has been smoothed, even in this case in which the index DI_{corr} was found to be less sensitive to the variation of the parameter.

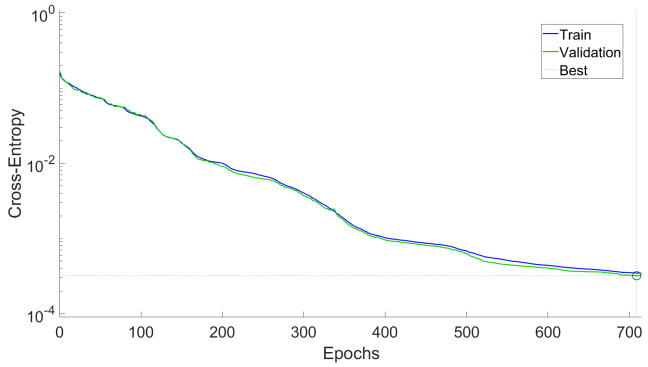

Figure 4.9. Crossentropy parameter evaluated as performance index in the training of network for quantification.

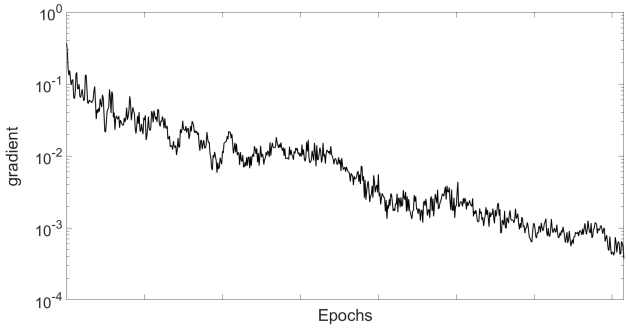

Figure 4.10. Trend of the gradient of the loss function during the training phase of the ANN used for quantification.

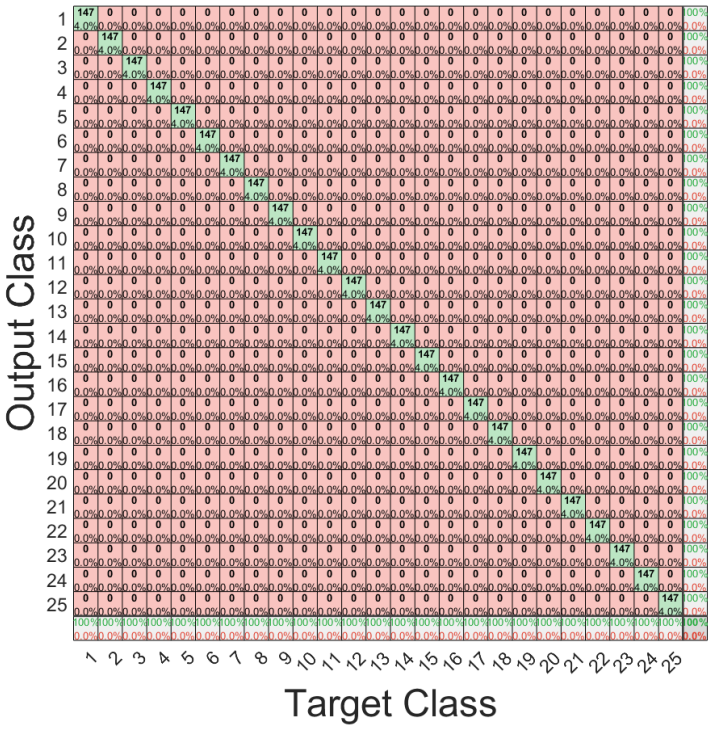

Figure 4.11. Confusion matrix evaluated for the damage quantification problem.

4.6 Experimental tests

The tests performed in the numerical case are repeated by processing the experimental data. In this case, the damage index DI_{corr} is calculated from the comparison between the subspace matrices of the damaged states simulated with the FE model and those of the experimentally produced case. The objective remains to locate the mass position and its magnitude.
Within the spirit of approaching the problem as on real structures, in this case only some of the simulated states have been experimentally produced, and for them the test set is composed of a limited amount of samples.

In particular, the cases reproduced for experimental validation of the

Table 4.7. Selected cases for experimental tests.

EXP. CASE	position	Mass
LOC1	p15	m10
LOC2	p17	m10
QNT1	p15	m10
QNT2	p15	m23

method are those listed in Tab.4.7, for the study of localization and quantification, respectively.

4.7 Experimental tests for damage localization

In this paragraph the results of the described procedure are shown. The cases selected for the experimental tests are the LOC1 case and the LOC2 case from Tab.4.7: the subspace matrices produced by the time-series data for these cases are compared with those obtained from the simulations with the calibrated FE model. For each of the 25 simulated scenarios, a population of $N_{test} = 200$ samples was considered, for a total of 5000 samples. Experimental data were acquired at a sampling frequency of 2000 Hz: an high-pass filter with a cutoff frequency of 70 Hz was applied during preprocessing, in order to clear low-frequency noises. The numerical data underwent the same treatment, in order to have uniformity between the data obtained with the two different procedures.

4.7.1 Damage localization using the subspace-based index

In the first test, the samples were compared with the experimentally recorded data using the 2D-correlation index between the subspace matrices.
Fig.4.12 shows the results of the application of the method for the LOC1 case to be identified. As can be seen, the trend of the index value resembles that obtained from the numerical tests reported in Fig.4.4: the influence of the symmetry perform an important role even in the experimental case.

The process of localization involves the steps of defining the mean values of the indices obtained for each of the attempt states, and then finding the minimum. As can be seen from Fig.4.13, performing this procedure the algorithm is able to recognize the correct position of the mass.

What interesting is that, in the correct position, the value of the index does not go to zero, but deviates from zero to a greater extent than in the numerical tests: the reason for this difference is to be found in the not-perfect correspondence between the real behavior and that simulated by the FE model. This difference was already highlighted in Ch.3 relative to the model updating, and it is present also in this case. Despite this, the

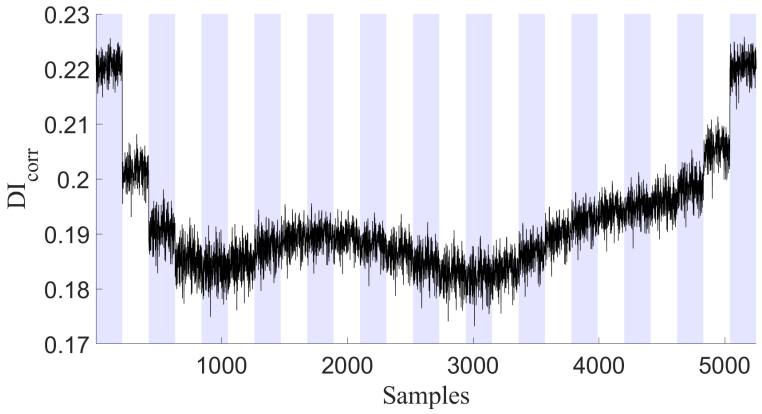

Figure 4.12. LOC1 case. Index trends for all simulated cases compared with the experimental damaged case with mass at position p15.

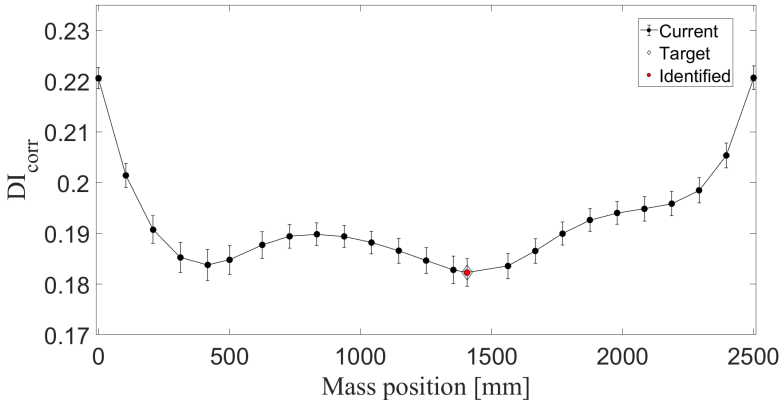

Figure 4.13. LOC1 case. Damage index trend as the position of the mass along the beam varies: average computed for the samples of each simulated case.

method manages to identify with precision the right position of the mass.

Differently happens instead in the LOC2 test, in which the mass is moved

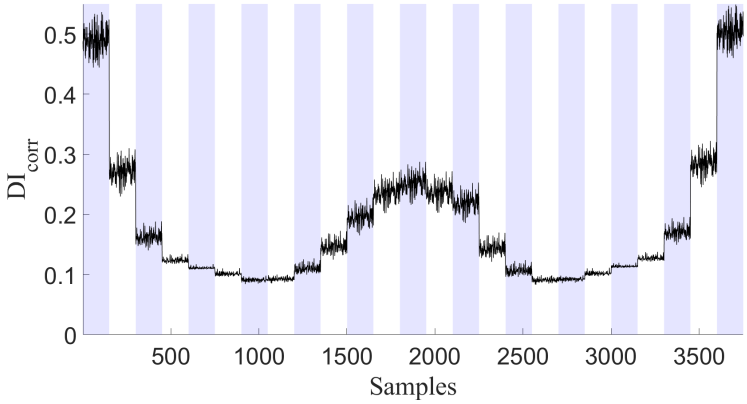

Figure 4.14. LOC2 case. Index trends for all simulated cases compared to the experimental damaged case with mass at position p17.

to the $p17$ position: following what reported in Fig.4.14, the index trend returns to reflect some symmetry with respect to the middle of the beam, making localization more difficult.

Looking at the trend of the mean values in Fig.4.15, it can be seen that this

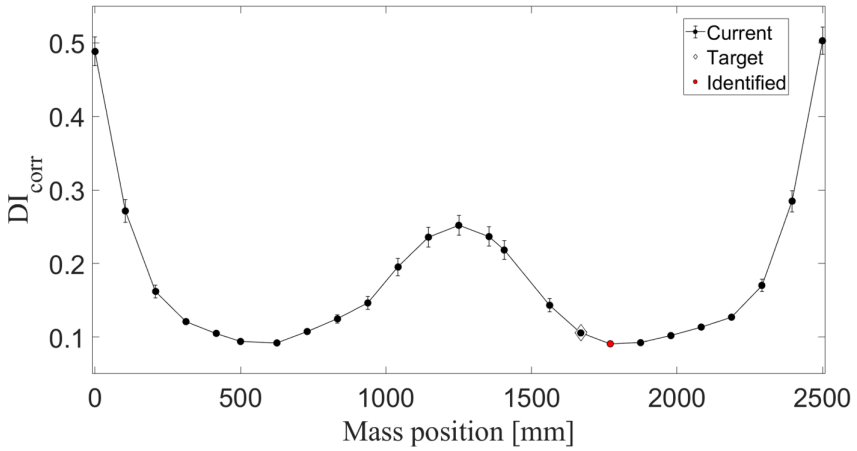

Figure 4.15. LOC2 case (mass in position p17). Damage index trend as the position of the mass along the beam varies: average calculated for the samples of each simulated case. The average values are represented with the respective standard deviations.

causes the identified position to deviate slightly from the target position. Despite this the right side with respect to the midpoint is recognized.

4.7.2 Damage localization tests using the ANN

The training and validation phases of the neural network were conducted considering a number of samples $N_{train} = 280$, of whom 75% for the actual training and the remaining 25% for the validation set. The testing phase was carried out with the experimental data.
The network training and classification algorithm for the purpose of damage localization consists of the following steps, similar to that described in Ch.4.4.2:

- Production of input data for the training: for each of the hypothesized damage scenarios, N_{train} subspace matrices H are produced from the FE model, varying the noise. Data are preprocessed before starting the training phase;

- Definition of the network architecture and subsequent training phase: in order for a network to be trained, it is necessary to define both the parameters directly related to the architecture, i.e. the number of layers constituting it and the number of nodes for each layer, and the nature of the functions that establish the relationships between the nodes. The network used for damage localization is a perceptron that needs one hidden layer, with a number of inner nodes equal to 20.
  The used activation function is the sigmoid - see Par.4.2.1. The loss function considered during the training is the cross-entropy loss function. Given the targets vector t and output vector y, the cross-entropy for each pair of output-target elements is calculated as:

$$(cross)_i = -t_i \cdot log(y_i)$$

  to which is added the regularization term as in the case of the SSE defined in Eq.4.5. The function has been preferred to SSE because it returns a value that heavily penalizes outputs that are extremely inaccurate (y near 1-t), with very little penalty for fairly correct classifications (y near t). The overall performance of the network is evaluated from the mean of the individual value;

- Classification of experimental data, coming from the test set: N_{test}

data coming from the experimental acquisition are preprocessed, then tested to be recognized by the network. The output layer of the network shows the values of the activation functions for each of the simulated attempt classes: the one with the higher value is the one predicted by the classifier. A check is made to find out if the predicted class coincides with the target one.

The training and classification results are shown in the following figures. Fig.4.16 shows the trend of the objective function during the training phase, while in Fig.4.17 is represented the gradient calculated in the various iterations: the low values of both functions symbolize the correct occurrence of the training.

As an outcome of the training of the network and subsequent classification

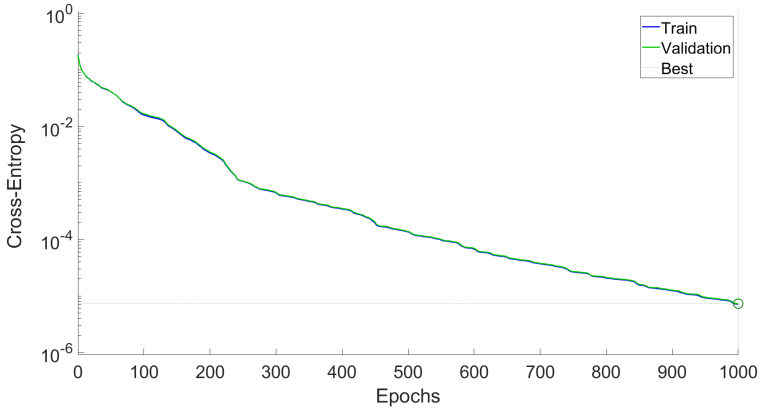

Figure 4.16. Crossentropy parameter evaluated as performance index in the training ofthe network for experimental damage localization.

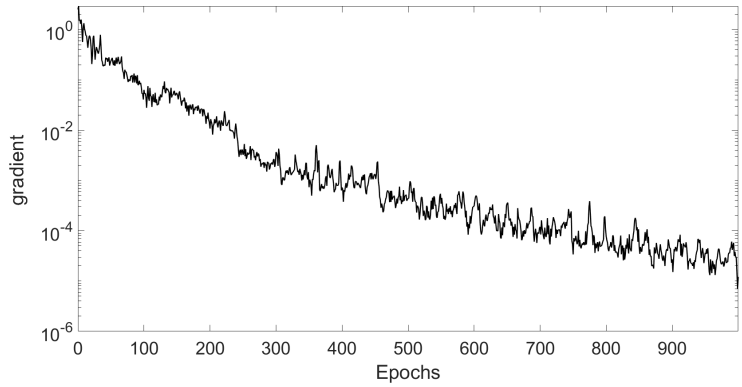

Figure 4.17. Trend of the gradient of the loss function during the training phase of the ANN used for experimental damage localization.

of the LOC1 and LOC2 damage states, the vector representing the values of the activation functions of the output layer is reported. Among the values contained in each of the vectors, the greatest value is the one related to the class predicted by the network.

$$h_{m_{10}p_{15}} = [\, 1.59 \cdot 10^{-06}\ 1.52 \cdot 10^{-07}\ 0.00216\ 0.0640\ 2.644 \cdot 10^{-06}$$
$$1.37 \cdot 10^{-07}\ 1.69 \cdot 10^{-11}\ 1.013 \cdot 10^{-08}\ 9.27 \cdot 10^{-09}\ 2.25 \cdot 10^{-06}$$
$$2.01 \cdot 10^{-07}\ 1.10 \cdot 10^{-06}\ 1.12 \cdot 10^{-04}\ 4.04 \cdot 10^{-04}\ \mathbf{0.931}$$
$$1.13 \cdot 10^{-05}\ 1.34 \cdot 10^{-06}\ 2.36 \cdot 10^{-05}\ 9.39 \cdot 10^{-08}\ 4.33 \cdot 10^{-06}$$
$$4.71 \cdot 10^{-06}\ 1.27 \cdot 10^{-06}\ 0.00198\ 2.29 \cdot 10^{-07}\ 2.55 \cdot 10^{-08}\,] \tag{4.9}$$

$$h_{m_{10}p_{17}} = [\, 6.63 \cdot 10^{-06}\ 2.36 \cdot 10^{-05}\ 2.93 \cdot 10^{-06}\ 1.10 \cdot 10^{-07}\ 6.53 \cdot 10^{-10}$$
$$1.49 \cdot 10^{-05}\ 0.00922\ 1.80 \cdot 10^{-05}\ 2.69 \cdot 10^{-04}\ 1.14 \cdot 10^{-04}$$
$$1.57 \cdot 10^{-}07\ 7.39 \cdot 10^{-09}\ 2.64 \cdot 10^{-06}\ 0.00199\ 1.42 \cdot 10^{-07}$$
$$3.14 \cdot 10^{-05}\ \mathbf{0.981}\ 0.00651\ 1.74 \cdot 10^{-06}\ 1.15 \cdot 10^{-04}$$
$$3.41 \cdot 10^{-05}\ 2.02 \cdot 10^{-08}\ 6.93 \cdot 10^{-07}\ 1.73 \cdot 10^{-07}\ 5.92 \cdot 10^{-07}\,] \tag{4.10}$$

As can be seen from Eq.4.9 and Eq.4.10, in LOC1 case, the largest component of the vector of activations is the one at position 15, corresponding to the target label p15. In the other case, the largest value is recorded for p17: in both cases, therefore, the network correctly classifies the experimentally produced damage states.

Note that the values contained in the two vectors are always in the range (0,1), since the sigmoid (Eq.4.2) was chosen as the activation function. On the other hand, the range of values would be (-1,1) if the hyperbolic tangent had been chosen, ref. Eq.4.3. The values contained in the output vectors are such that their sum is equal to unity: this characteristic makes them in a sense synonymous with the probability that the network classifies a certain class, either correct or wrong. Taking as an example the value of 0.931 of the first vector, the network classifies with almost absolute certainty that the class is the one corresponding to the component number 15 of the vector of labels, that is the class p15, precisely.

4.8 Experimental tests for damage quantification

What has been already described for the localization tests is also carried out for the damage quantification tests.

The cases selected for the experimental tests are the QNT1 case and the QNT2 case from Tab.4.7: the subspace matrices produced by the time-series data related to them are compared with those obtained from the simulations with the calibrated FE model. For each of the simulated scenarios, a population of $N_{test} = 200$ samples was considered, for a total of 5000 samples.

Experimental data were acquired at a sampling frequency of 2000 Hz and a low-pass filter with a cutoff frequency of 70 Hz was applied during pre-processing. The numerical data underwent the same treatment, in order to have uniformity between the data obtained with the two different procedures.

4.8.1 Damage quantification using the subspace-based index

In the first test, the samples were compared with the experimentally recorded data using the 2D-correlation index between the subspace matrices.

Fig.4.18 shows the results of applying the method having selected case QNT1 as the case to be identified. As can be seen from the figure, the

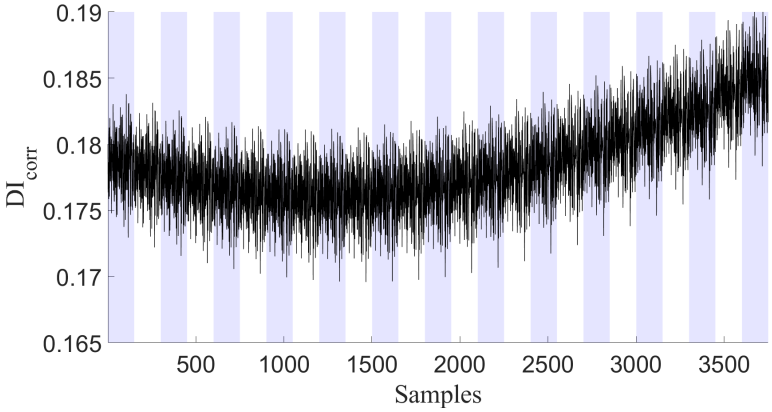

Figure 4.18. QNT1 case. Index trends for all simulated cases compared to the experimental damaged case with mass of magnitude m10.

uncertainty related to the process is more pronounced than that related

to the localization of the damage: within the different simulated cases, the index values oscillate much more. This is clearer if look at Fig.4.19 in which the mean values of the calculated indices are reported: as can be seen, the standard deviations produce much wider confidence intervals than in the localization case. Despite this, the proposed method manages to identify

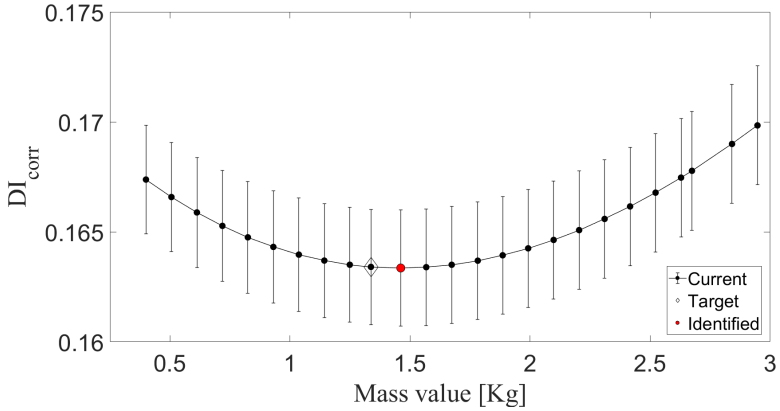

Figure 4.19. QNT1 case (target mass value to identify: m10). Damage index trend at the variation of the magnitude of the mass: mean calculated for the samples of each simulated case. The mean values are represented with the respective standard deviations.

the mass entity with a margin of error considered acceptable: referring to the values of Tab.4.2 the predicted class is $m11$ corresponding to a mass of 1.46 Kg, compared to 1.33 Kg of the target class, $m10$, with a difference of 9.7%.

The same results are obtained by analyzing the QNT2 case. Looking

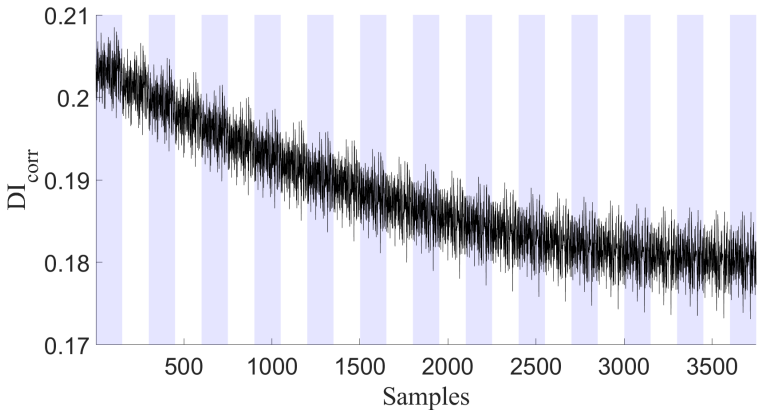

Figure 4.20. QNT1 case. Index trends for all simulated cases compared to the experimental damaged case with mass of magnitude m23.

directly at the trend of the average values of the index, it can be seen that,

also in this case, the value of the mass identified by the algorithm differs from the one actually applied on the beam. In this case, the value to be

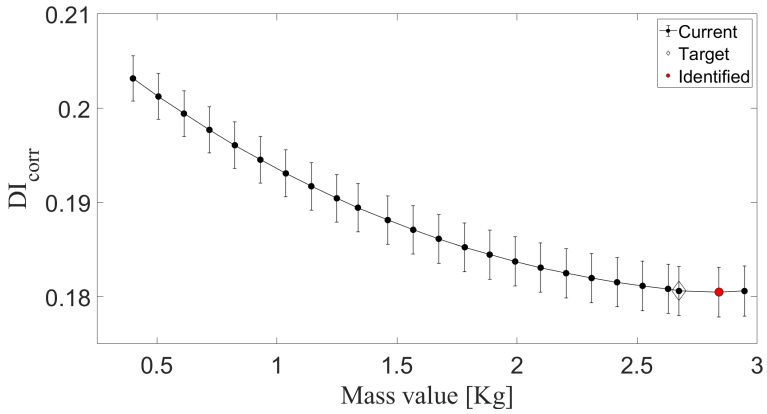

Figure 4.21. QNT1 case (target mass value to identify: m23). Damage index trend at the variation of the magnitude of the mass: mean calculated for the samples of each simulated case. The mean values are represented with the respective standard deviations.

identified is $m23$, corresponding to a mass of 2.67 Kg, while the identified one is 2.84 Kg, belonging to the class $m24$, with a difference of 6.4%.

4.8.2 Damage quantification tests using the ANN

The training and validation phases of the neural network were conducted considering a number of samples $N_{train} = 340$, of whom 75% for the actual training and the remaining 25% for the validation set. The testing phase was carried out with the experimental data.

The network training and classification algorithm for the purpose of damage quantification follow the steps described in ch.4.7.2.

Fig.4.22 shows the trend of the objective function during the training phase, while in Fig.4.23 is represented the gradient calculated in the various iterations: the low values of both functions symbolize the correct occurrence of the training.

As a result of the network training and subsequent classification of damage states QNT1 and QNT2, the vector representing the values of the output layer activation functions is reported. Among the values contained within each vector, the largest value is the one related to the class predicted by

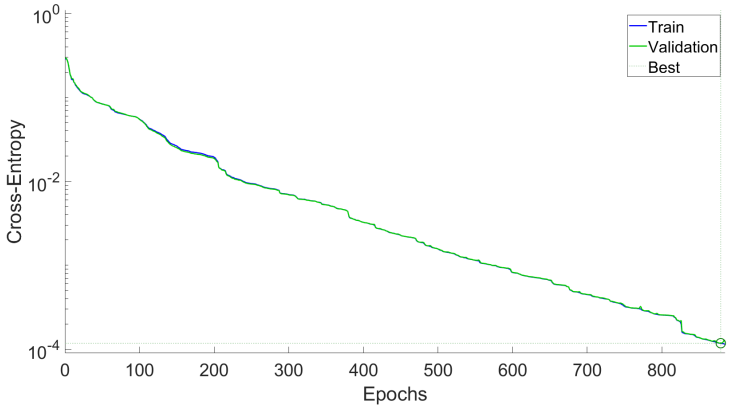

Figure 4.22. Crossentropy parameter evaluated as performance index in the training ofthe network for experimental damage localization.

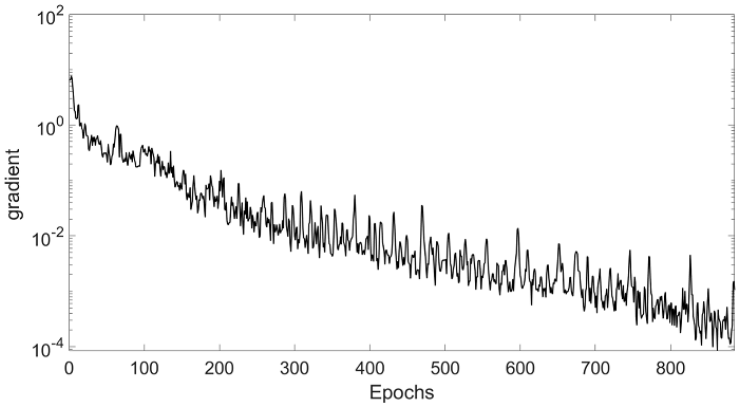

Figure 4.23. Trend of the gradient of the loss function during the training phase of the ANN used for experimental damage localization.

the network.

$$
\begin{aligned}
&h_{p_{15}m_{10}} = \\
&= [\, 5.01{\cdot}10^{-03} \;\; 1.08 \cdot 10^{-08} \;\; 0.000724 \;\; 9.24 \cdot 10^{-08} \;\; 1.72 \cdot 10^{-06} \\
&\quad 6.00 \cdot 10^{-04} \;\; 9.53 \cdot 10^{-04} \;\; 1.98 \cdot 10^{-04} \;\; 0.0018 \;\; 0.0012 \\
&\quad \mathbf{0.938} \;\; 1.14 \cdot 10^{-06} \;\; 6.21 \cdot 10^{-04} \;\; 0.022 \;\; 0.02279 \\
&\quad 1.20 \cdot 10^{-03} \;\; 3.105 \cdot 10^{-04} \;\; 1.68e-06 \;\; 0.00054 \;\; 0.0024 \\
&\quad 8.00 \cdot 10^{-04} \;\; 0.0003 \;\; 7.34 \cdot 10^{-04} \;\; 4.90 \cdot 10^{-06} \;\; 1.15 \cdot 10^{-08} \,]
\end{aligned}
\tag{4.11}
$$

$$
\begin{aligned}
&h_{p_{15}m_{23}} = \\
&= [\, 5.43{\cdot}10^{-11} \;\; 3.12 \cdot 10^{-07} \;\; 2.50 \cdot 10^{-04} \;\; 4.25 \cdot 10^{-03} \;\; 2.12 \cdot 10^{-03} \\
&\quad 3.51 \cdot 10^{-05} \;\; 6.73 \cdot 10^{-05} \;\; 1.07 \cdot 10^{-05} \;\; 5.01 \cdot 10^{-04} \;\; 5.51 \cdot 10^{-11} \\
&\quad 3.31 \cdot 10^{-07} \;\; 4.96 \cdot 10^{-04} \;\; 8.53 \cdot 10^{-04} \;\; 5.37 \cdot 10^{-06} \;\; 2.86 \cdot 10^{-06} \\
&\quad 9.93 \cdot 10^{-07} \;\; 2.48 \cdot 10^{-04} \;\; 2.76 \cdot 10^{-11} \;\; 1.75 \cdot 10^{-05} \;\; 1.35 \cdot 10^{-04} \\
&\quad 1.09 \cdot 10^{-10} \;\; 5.73 \cdot 10^{-06} \;\; 6.25 \cdot 10^{-07} \;\; \mathbf{0.991} \;\; 1.66 \cdot 10^{-07} \,]
\end{aligned}
\tag{4.12}
$$

As can be seen from the representations of each vector in Eq.4.11 and Eq.4.12, the activation functions with the largest value are those of the node 11 (m11, instead of the target value m10) and 24 (p24, instead of the target value m23), for the QNT1 and QNT2 test respectively. Tests performed by neural network training also suffer from a slight misclassification error.

It is estimated that this error can be therefore due to the not perfect calibration of the model regarding the real behavior: this difference, evidenced also from a value of the index not perfectly equal to zero, influences less in the problem of the localization of the damage than that of quantification, due to the lower sensitivity of the index to mass entity variations.

4.9 Experimental damage localization and quantification procedure

In the previous paragraphs, the localization and quantification cases were studied separately, with the aim of analyzing the peculiarities of each problem .

The purpose of the activities described in this section is to evaluate the effectiveness of the method in simultaneously identifying the location and magnitude of the applied mass.

Because of the amount of data necessary to the training of a neural net that includes all the cases to consider, inside the section only the method based on the calculation of the index DI_{corr} is applied.

Following what emerged in the previous paragraphs, the point of optimum is evaluated by calculating the mean value between the indices obtained for each attempted state, and then verifying if the minimum between them corresponds to the target state.

The tests performed are exclusively of experimental nature, and refer to the damage states already described in Tab.4.7: in this case, the number of simulated scenarios was increased by dividing the position and mass value ranges into 50 steps, for a total of 2500 simulated damage scenarios.

The results obtained are summarized in Fig.4.24 - 4.26. For every case

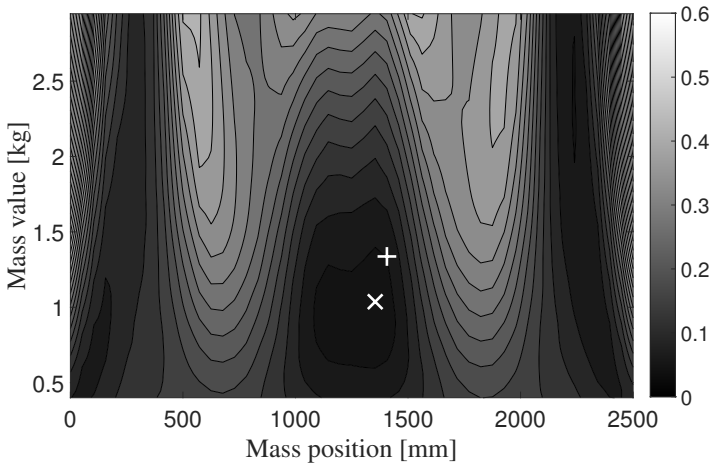

Figure 4.24. Case LOC1: variation of the objective function related to variations in the entity of the mass and of its position along the steel beam. The white cross indicates the identified minimum, the vertical cross the target point.

analyzed, the objective function is symmetrical with respect to the middle of the beam, whatever the mass value considered. Despite the symmetry problem, the value of the mean index is smaller in the side where the mass is actually situated, allowing its localization.

As can be seen from the figures and from Tab. 4.8, the minimum point identified by the algorithm is slightly different from the real values. It is noted that the algorithm succeeds in identifying the position of the mass

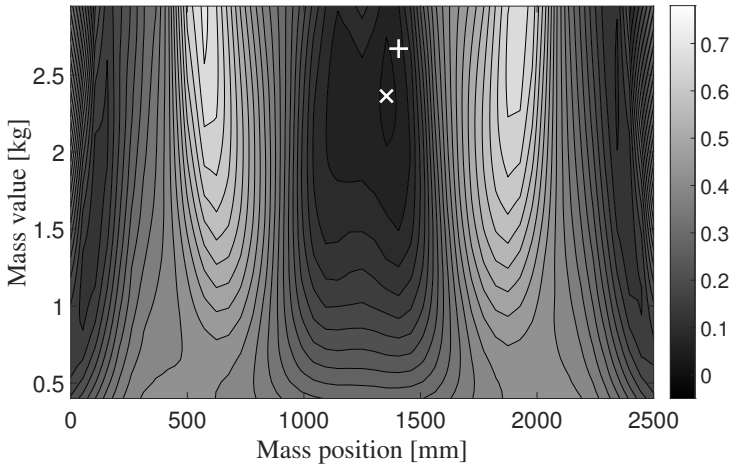

Figure 4.25. Case LOC2: variation of the objective function related to variations in the entity of the mass and of its position along the steel beam. The white cross indicates the identified minimum, the vertical cross the target point.

with a good precision, but shows more uncertainties in defining its magnitude.

Thus, what emerged confirms the evidence that the method is less sensi-

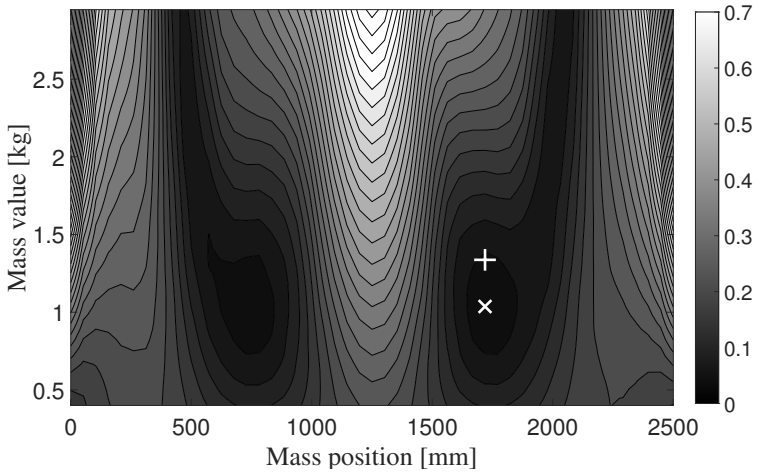

Figure 4.26. Case QNT2: variation of the objective function related to variations in the entity of the mass and of its position along the steel beam. The white cross indicates the identified minimum, the vertical cross the target point.

tive to variations in mass magnitude than to variations in mass position.

Table 4.8. Experimental damage detection tests: identified and target cases.

	Identified		Target		delta	
EXP. CASE	pos. (mm)	mass (kg)	pos. (mm)	mass (kg)	Δp (%)	Δm (%)
LOC1	p27 1355	m13 1.03	p28 1406	m19 1.33	-3.6%	-22.6%
LOC2	p34 1720	m13 1.03	p34 1720	m19 1.33	0.00%	-22.6%
QNT2	p27 1354	m38 2.36	p28 1406	m44 2.67	-3.6%	-11.6%

4.10 Conclusions

In this chapter, a damage localization and quantification algorithm based on subspace matrices was applied. Two methods have been adopted: the first is based on the use of a subspace based index as an objective function to be minimized in a discrete optimization algorithm, in order to find the maximum similarity between the produced damaged case and the attempt ones. In the second method, subspace matrices were directly adopted as features, and an artificial neural network was trained to classify the damage. Both methods were tested numerically and experimentally on a simple beam structure, producing damage by applying a point mass to the beam. The tests therefore investigated the effects of varying the position of the mass along the beam and varying the magnitude of the mass itself, leading back to the aforementioned problems of mass location and quantification. Due to the impossibility of damaging a real structure to reproduce all damaged scenarios, in all tests these latter have been simulated by means of an FE model. The FE model used is the one whose updating has been described in the previous chapter, in order to have the best possible match between the simulations and the behavior of the real structure.
In each test, several simulations have been done, varying the excitatory noise, in order to test the proposed methods in the best possible way.
A first data-driven approach has been carried out to study the value of the index as the position of the mass varies, comparing it with those from the undamaged state (with no applied mass): from this comparison, it appears that the only data-driven method is not sufficient to go beyond the anomaly detection (level 1 of Rytter's damage detection scale), confirming what already emerged in the literature: the index-function is not injective with respect to the variable-position.

The data-driven approach applied by varying the entity of the mass, fixed in the same position, has led to an interesting observation: the index, calculated as in the previous case, grows as the applied mass increases, in a monotonic way in the range considered. In order to estimate the extent of the damage (level 3 of Rytter's scale) it would be possible to do some data-driven reasoning evaluating the relative variation of the index from a initial state to the current one, to monitor the development of the damage. Applications to real problems could be, for example, the evaluation of the progress of degradation in an already localized area of a structure, or the fatigue damage in metal joints.

Simulations by means of the FE model are necessary, however, where a specified damage magnitude or position is actually to be classified in relation to others.

Numerical tests based on the calculation of the damage index DI_{corr} showed that this one is more sensitive to variation in the position of the mass, rather than to variation in its magnitude.

The mass localization problem on the structure-test has also highlighted the dependence of the results on the symmetry of the system: the confusion matrix related to the localization problem has in fact shown the presence of misclassified cases not only near the position to be identified (as is one would expect), but also in positions symmetrical with respect to the latter. The problem of identifying the mass entity is instead related to a lower sensitivity of the index itself towards the mass variation. In fact, the results have shown that the percentage of misclassified samples is higher than that found in the localization problem, and in some cases even exceeds that of true positives. The low accuracy problem was solved by averaging the indices obtained for each of the simulated cases, and then comparing them to estimate the minimum. The expectation is that the minimum of the averaged function-index would identify precisely the correct location or mass. Application of this method resulted in the correct classification of the totality of the hypothesized cases, for both location and quantification cases. The choice to delve into a method based on training a neural network stems in part from the desire to resolve any errors due to noise.

The neural network, through the training phase, stores information on the

inputs which results to be mainly independent from the generating noise. The network for the localization and quantification of the damage is a classifier, trained according to the methods of supervised learning: the parameters considered as input features are directly the subspace matrices, which during the training phase have been provided to the network, specifying the class label to which they belonged. Subsequently, the validity of the network in correctly classifying the various damage scenarios was assessed with a test set. The efficiency of the algorithm was assessed evaluating the confusion matrix. In each case, the network correctly recognizes the target cases to be identified.

The experimental tests followed what was done in the numerical ones: even in this case, the classification results were positive. However, both in the case of localization and identification of the mass entity, the proposed methods classified the damage class with a slight inaccuracy, which is however considered acceptable. It is believed that this inaccuracy is due to the fact that the FE model, although calibrated in the preliminary phase, does not perfectly match the behavior of the real structure.

The last test was carried out to simultaneously identify the magnitude of the mass and its position.

Tests confirmed the particularities already noted in previous cases: the damage index is less sensitive to the variation of the mass entity than of its position.

It is believed that this inaccuracy is due to the fact that the FE model, although calibrated in the preliminary phase, does not perfectly match the behavior of the real structure.

The proposed methods seem therefore to be promising in their application to damage detection problems: in the next chapters, the same methods will be applied to the anomaly detection of a real structure.

Santa Maria di Collemaggio in L'Aquila: introduction to the case study

Chapter abstract

The monitoring of real structures represents a challenge for the research, because it approaches structures having their own history and peculiarities. Among all kinds of structure, historical buildings take on even greater interest, given their cultural value. Often, the complexity of the monitored structure makes it difficult to reproduce its behavior through a numerical model. For this reason, the literature of recent years treated cases of monitoring and damage detection based on data-driven approaches. In this chapter the case study, the Basilica of Santa Maria di Collemaggio, in L'Aquila, is presented. Following the restoration interventions after the 2009 earthquake, a static and dynamic monitoring system has been installed in the Basilica: the chapter reports the results of the monitoring for a period of three years, from the date of its installation until 2020, with the aim of better understand the dynamic behavior of the structure. It has been noted that the dynamic behavior of the structure is strongly influenced by environmental effects, and there is the presence of a slow process of decay of natural frequencies.

This chapter represents a preliminary knowledge phase of the artifact: it introduces information on the dynamic behavior of the Basilica which is necessary for the anomaly detection procedure, described in the next chapter.

5.1 Introduction

Monitoring of historical structures has been the subject of research interest in the last decade. In this period, the study of these structures has brought out and tackles problems with substantial differences based on the case study structure.

Examples of such monitoring are the work by Ramos et al. (2010), which focuses on monitoring a cathedral, the works of Azzara et al. (2018); Saisi et al. (2015); Ubertini et al. (2017) who have studied the behavior of masonry towers; in Kita et al. (2019), the results of a monitoring campaign on a historic palace are reported, with the study of the influence of environmental parameters on the structural response. Focusing on churches, a few research groups, mainly concentrated in the Mediterranean area, dedicated their research efforts to this topic: Ramos et al. (2010) and Masciotta et al. (2017, 2016) monitored the Church of Monastery of Jeronimos. Elyamani et al. (2017) monitored the Mallorca cathedral (Mallorca Island, Spain) under ambient sources of vibration and seismic events. Gentile et al. (2019) reported on the long-term monitoring of the Milan cathedral.

Research activity by the University of L'Aquila regarding the Basilica of Santa Maria di Collemaggio began in the early nineties. From that period, numerous studies have been conducted, regarding phenomena affecting the Basilica in different disciplines, from historical (Lopardi (2002)), archaeological (Redi (2006)), architectural (Baiocchi et al. (2017); Brumana et al. (2018); Moretti (1972); Oreni et al. (2014)), structural (Aloisio et al. (2019a, 2020b, 2019b); Antonacci et al. (2020, 2001b, 2010); Crespi et al. (2016); Ranalli et al. (2004); Sfarra et al. (2015); Zucca et al. (2018)), geotechnical (Amoroso et al. (2018); Totani et al. (2016)) and even energetic (Aste et al. (2016)) perspectives. First studies on the dynamics of the Basilica appear in works by (Aloisio et al. (2020a); Antonacci and Beolchini (2005); Antonacci et al. (2001a); Galeota et al. (2019, 2015); Potenza et al. (2015)). Although the literature has therefore investigated the Basilica from every point of view, it should be noted that so far no study had addressed the issue of long-term monitoring.

After the 2009 earthquake in L'Aquila, the University of L'Aquila, the Uni-

versity La Sapienza in Rome and the Politecnico in Milan supported the design phase of the restoration, supervised by the *Soprintendenza ai Beni Architettonici e Paesaggistici per l'Abruzzo*.

The University of L'Aquila was further commissioned to conceive a monitoring system, which could operate during and after the rehabilitation. In the first working phase, the monitoring system provided the construction manager with a survey tool about structural interventions.

The significant number of accelerometers allows a refined resolution of the mode shapes and may give enough information to reliably estimate the evolution of the structural condition of the Basilica, especially after seismic events. Since its permanent installation in 2017, data coming from the monitoring system have been acquired with a frequency that has varied over the years, from the initial weekly acquisitions up to the daily cadence since 2020: from this amount of data were occasionally extracted and processed dates, in order to perform a sort of manual modal tracking.

In this chapter, the results deriving from the automatic processing of the acquisition data of the system installed in the Basilica are presented. The results for the period 2018/2019 are reported, in order to provide a knowledge base of the dynamic behavior of the structure, which was preparatory to the activities carried out subsequently and reported in the next chapter. Results evaluated from the static minitoring system are described in Alaggio et al. (2021).

5.2 Description of the Basilica

The Basilica of Santa Maria di Collemaggio is a large medieval church in L'Aquila, central Italy. The Basilica, built at the end of the 13th century, is linked to the history of San Pietro da Morrone and his election as Pope Celestino V (Giardini et al. (2006)), is one of the most important churches in L'Aquila. Placed on the top of a hill in the city, it has its main axis oriented in an east-west direction, with the apse in a dominant position with respect to the underlying Aterno valley. On the southern side of the church is the monastery, with a cloister and numerous additional bodies.

The elegant Romanesque façade has the appearance of a wall, with a central door, embellished in the 15th century, and two smaller flanking doors.

The Basilica consists of three naves, one central and two side. The central

(a) (b) (c)

Figure 5.1. (a) Facade, (b) interior, (c) Holy Door

nave has dimensions of 61 meters in length by 11.30 meters in width, with a maximum height of 20.40 meters. The two side ones, on the other hand, are about eight meters wide, with a maximum height of 15 meters.
The three naves are marked by 14 octagonal pillars that support pointed arches. The hall is separated from the transept by a triumphal arch grafted onto two large pillars, with a poly-lobed section with a diameter of 2.9 meters. Exposed wooden trusses cover both the hall and the transept.
Adjacent to the Basilica is the monastery with the cloister. A mighty octagonal tower is next to the facade. The church has been remodeled sev-

Figure 5.2. Collapse of the roof in the transept area following the 2009 earthquake.

eral times over the centuries mainly due to the damage caused by frequent earthquakes and presents a mixture of different architectural styles.
After the 2009 earthquake, the structure was seriously damaged: the subsequent consolidation and restoration works ended in 2017 and won the European Union cultural heritage award in 2020.

5.3 The Monitoring systems

The permanent monitoring system consists of nine crack measurement devices, 78 Force-balance accelerometers(FBA): 2 triaxial, 12 biaxial, and 48 monoaxial, and five temperature/humidity sensors.

The crack measurement devices are high precision triangulation lasers with a 25mm measuring range, 0.03mm linearity and 2.5μm reproducibility. FBA accelerometers are characterized by a 2.5V/g sensitivity.

Fig.5.3 illustrates the distribution of sensors within the Basilica. The

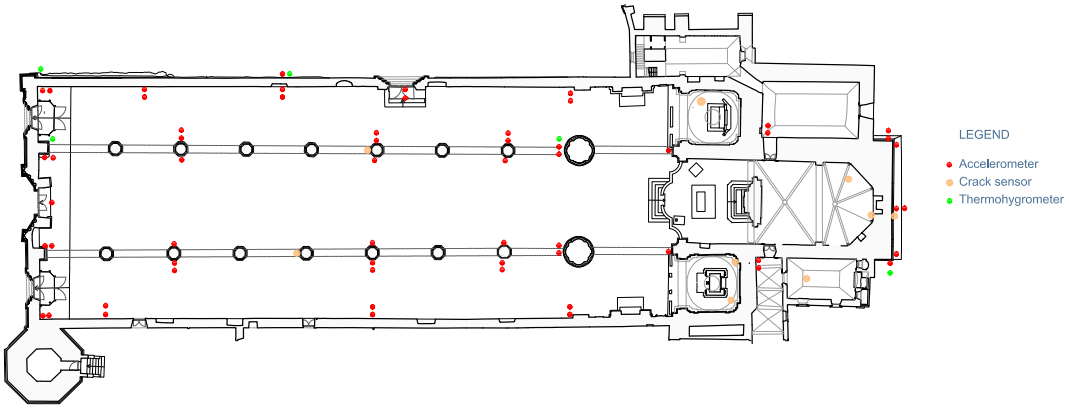

(a)

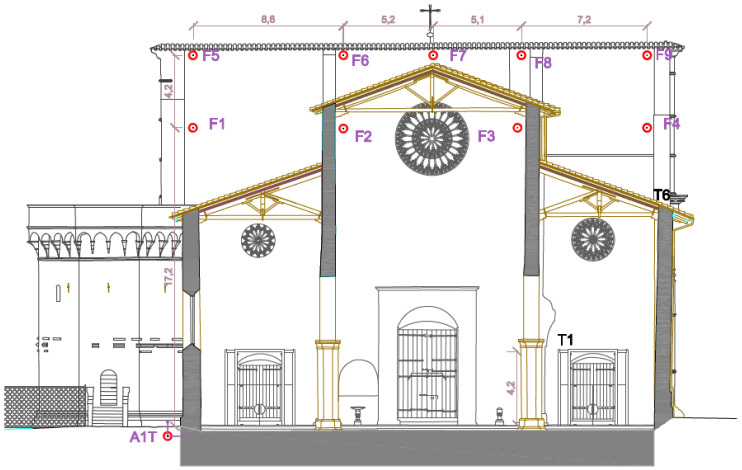

(b)

Figure 5.3. (a) Plan of the monitoring system; (b) layout of the facade FBA accelerometers.

accelerometers are connected to five control units devoted to the signals acquisition and digitalization. Each control unit gathers several accelerom-

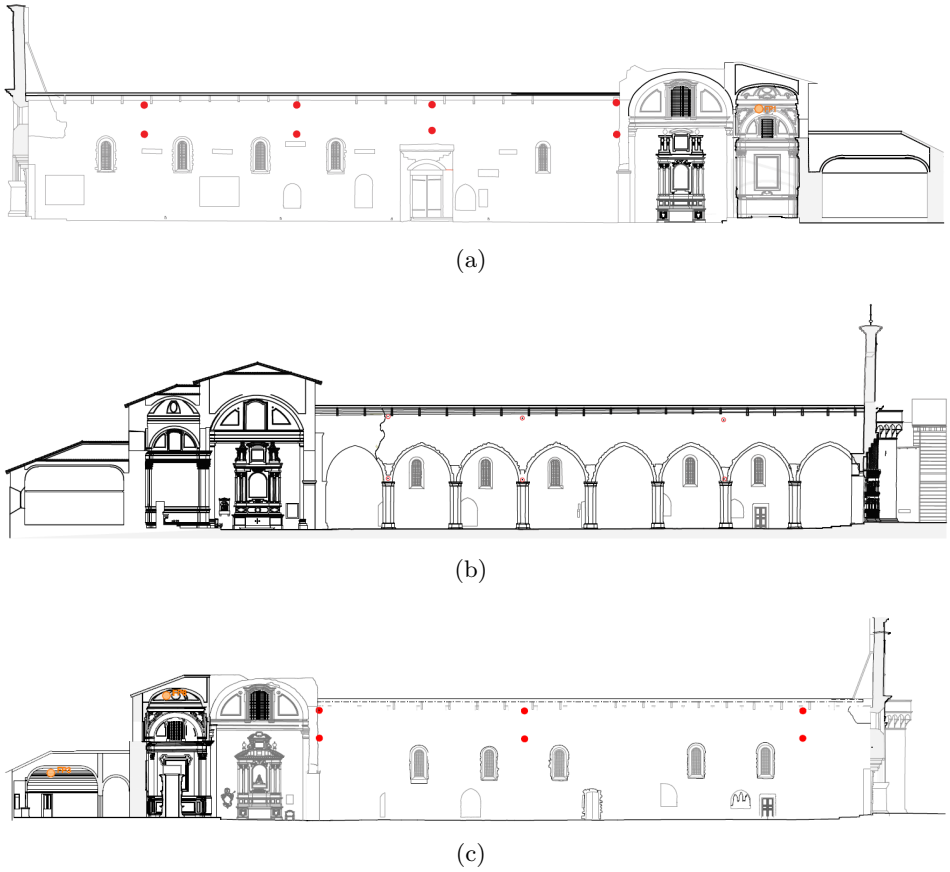

Figure 5.4. Prospect view of the layout of the FBA accelerometers on the Holy Door wall (a) and the adjacent nave walls (b)-(c).

eters sorted by installation areas, in order to minimize the length of the cables. Each control unit communicates via LAN to the data collection and processing computer (workstation) which is inside the sacristy. Each control unit interfaces with a GPS master clock which transmits every second a synchronization signal in the NMEA format via the RS422 interface; the string contains the absolute time data used to reference each recording. The data loggers autonomously ensure the synchronization with an accuracy higher than 40 parts per million (40 p.p.m.) in case of a transient interruption of the GPS signal. The system can record and report any interruptions in the GPS signal, which may last longer than a given threshold. The software Dymasoft drives the communication with the accelerometer acquisition units. The monitoring system, which acquires the signals streaming from the accelerometers, is set in the so-called event acquisition mode. In this mode, the system launches the acquisition when the signal triggers the alarm threshold and sends reports to users.

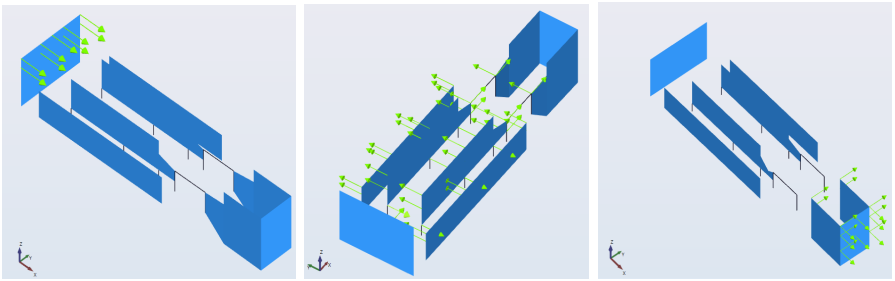

(a) (b) (c)

Figure 5.5. Position of the accelerometers on the facade (a), the nave walls (b) and the apse (c).

The current value of the alarm threshold is 0.05g. The threshold does not derive from a rigorous assessment regarding the relationship between the exceeding of given thresholds and the corresponding exceeding of safety levels. The installer initially set the low value of the threshold with the scope of gathering as many valuable recordings as possible. There are five leading software: (1) Solgeo Dymasoft for the management and configuration of the acquisitions, the setting of the recording thresholds, type of trigger, e.g.; (2) Solgeo Vibrosoft for the sole processing of the accelerometric signals; (3) the Vista Data Vision for the management and display of the data recorded by the alarm monitoring and management system; (4) Cyclops and (5) BeanScape for the acquisition of laser measurements and data from the thermo-hygrometers respectively. Hereafter follows a few technical details about the data loggers (Fig.5.6(e)): 24-bit digitalization per each channel, integrated digital antialiasing filter up to 48 channels, sampling rate selectable in the range 10Hz to 8kHz, bandwidth DC – 4 kHz, dynamic range higher than 134 dB, programmable gain filter antialiasing, cut-off frequency 0.4 of the sample rate.

Crack monitoring devices are placed over historically relevant cracks, by the apse, the chapel vaults and the nave arches. The crack monitoring devices are connected to the workstation directly via cable.

The thermo-hygrometers communicate directly with the workstation via Wi-Fi routers, which collect data from the sensors.

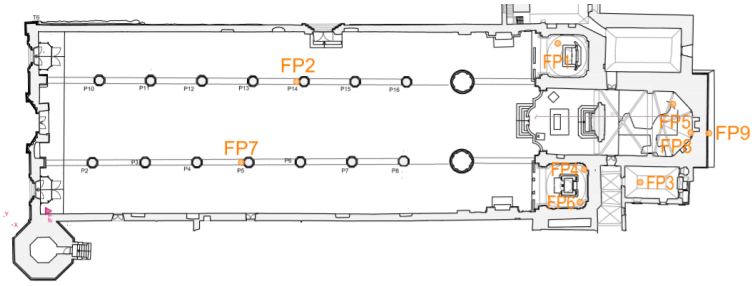

(a)

(b)

(c)

(d)

(e)

Figure 5.6. (a) Layout of the crack monitoring devices and (b) a crack monitoring device placed on a significant crack; (c) an FBA accelerometer, (d) a thermo-hygrometer, (e) data logger.

5.4 Dynamic monitoring

The following paragraph presents the results coming from the dynamic monitoring system, in the observation period. The data come from accelerometric chains arranged throughout the Basilica. Acquired data from the sensors placed in the apse were not considered: the apsidal body, being much more rigid than the remaining portion of the structure, seems insensitive to accelerations due only to environmental excitations.
The first part introduces the results of dynamic identification in terms of modal parameters. The following parts collect the natural frequencies and MAC (Modal Assurance Criterion) values identified from all time-series and relate them to the outdoor environmental parameters: temperature and relative humidity.

5.4.1 Modal identification

The implemented modal identification process involves the search for modal parameters based on the SSI method, already introducedin Ch.3.
The monitoring system acquires data at a sampling frequency of 250 Hz: following some preliminary tests, it was decided in the preprocessing phase to decimate the signal by a factor N_d=20. In this way, a higher quality of the signal was noticed in the frequency range of interest.
SSI identification technique needs some parameters to be defined: in particular, the time lag i and the model order n.
To clearly define the order of the system, it is good practice to build the stabilization diagram, which shows the poles identified as n increases: within the graph, physical modes appear stable as order increases. The built of the diagram requires the selection of a minimum and maximum order, n_{min} and n_{max} respectively.
Generally, the minimum order descends from a preliminary manual identification, roughly estimated as the double of the number of modes expected in the considered frequency interval.
The effort in identifying the weekly excited modes, which appear at higher orders, guides the choice of the maximum order. Still, higher orders could lead to the generation of spurious modes and other phenomena, i.e. modal

splitting: therefore, it must be kept as low as possible.

For the application presented, the value of the parameters has been chosen after some test to be pair to $i = 30$, $n_{min} = 40$, and $n_{max} = 150$.

The implemented modal identification algorithm is based on the one proposed by Cabboi et al. (2017), and extracts the parameters autonomously, allowing to quickly process the data of all the available dates.

The algorithm is a useful tool to evaluate the results of the stabilization diagram automatically: it selects the stable poles according to predetermined and self-calibrated criteria, and then generates clusters by collecting the poles with similar frequencies and mode shapes, as the order n increases. The clustering leads to the identification of the most stable modes.

The algorithm is set to discard damping ratios higher than 10% - which hardly occur in masonry buildings - in order to increase the efficiency of the identification. It verifies the stability of the poles as the order of the system increases. There is a cross-checking between each pole of the i-th model order and the previous one, according to the following criteria:

$$\left| \frac{f_i - f_{i-1}}{f_{i-1}} \right| \leq \delta_f \tag{5.1}$$

$$\left| \frac{\xi_i - \xi_{i-1}}{\xi_{i-1}} \right| \leq \delta_\xi \tag{5.2}$$

$$1 - \mathrm{MAC}\left(\phi_i, \phi_{i-1}\right) \leq \mathrm{MAC}_{thr.} \tag{5.3}$$

where f_i, ξ_i and ϕ_i are the natural frequency, damping and mode shape registered for each pole of the i-th order, $i = n_{min} + 1, ..., n_{max}$ from the i-th iteration; $\mathrm{MAC}_{thr} = 0.02$ is the threshold MAC value; $\delta_f = 0.01$ and $\delta_\xi = 0.01$ are the adopted tolerances for the natural frequencies and damping ratios.

Fig.5.7 shows the stabilization diagram obtained for a selected date, before and after the clustering.

Before proceedings with the identification for all the available dates, a date was selected: for it, the modal parameters identified by the algorithm were compared with those obtained from the ARTeMIS software. Results of the comparison presented in Tab.5.1 prove the validity of the implemented algorithm.

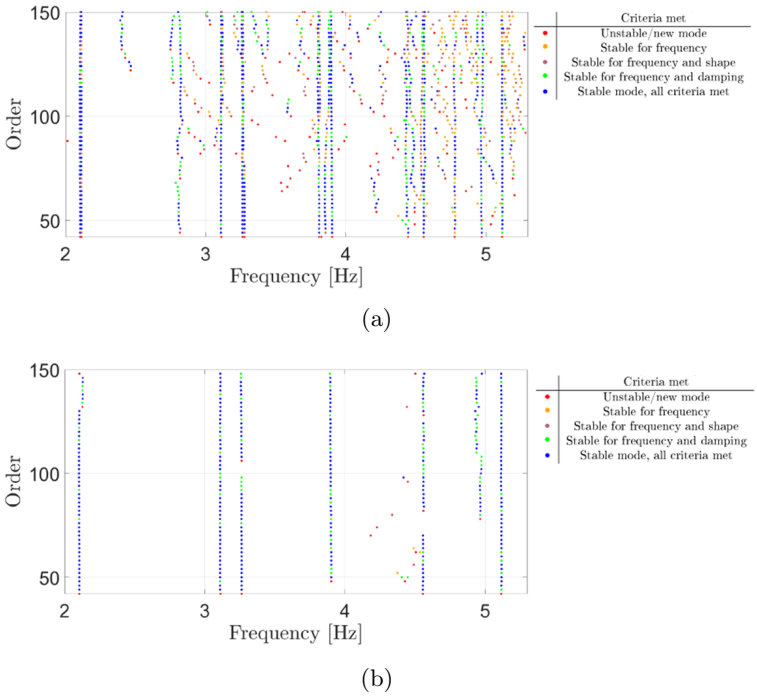

Figure 5.7. Example of stabilization diagrams obtained before (a) and after (b) the application of the identification and selection algorithm.

Table 5.1. Comparison between modal parameters identified with the automatic alghoritm and modal analysis.

	Automated procedure		Manual analysis	
Mode	F_{mean}	ξ_{median}	F_{mean}	ξ_{median}
1st	2.11	1.16	2.10	1.10
2nd	3.11	0.75	3.11	0.83
3rd	3.26	1.04	3.27	1.07
4th	3.83	0.94	3.80	0.68
5th	4.55	0.95	4.49	1.5
6th	4.95	0.87	4.97	0.9
7th	5.40	0.91	5.39	0.9

5.4.2 Modal tracking

Modal tracking phase is crucial for knowing the trend of modal parameters over time.
The tracking algorithm, also automatic, must take into account the variations to which the modal parameters may be subjected during the seasonal cycle, in such a way as to be able to discriminate physiological behaviors from anomalous ones.
The selection of the representative modes of the structure heads the assessment of their evolution over the year.
The following hypothesis is the basis of the implemented algorithm: if any anomaly occurs, the natural frequencies oscillate in a limited range around the reference frequency. In this tolerance range, the implemented algorithm selects the mode with the highest MAC among all.
Often, the tracking process generally requires a set of modal parameters to be chosen as reference for the subsequent iterations.
In most cases, there is a fixed reference compared to the modal parameters identified from the other recordings: as will be seen in the next paragraphs, it was possible to follow this approach in the case of the first four modes, which mainly affect the deformation of nave walls, by choosing the first available data of January 2018 as a fixed reference.
The upper modes were tracked applying a shifting reference: once completed the tracking procedure in the i-th iteration, the process updates the reference data set with the last one identified. This determination depends on the fact that fifth and seventh modes, mainly localized in the facade, show substantial variation over time both in frequency and shape. Consequently, the setting of a fixed reference data would not have allowed grasping these changes.

5.5 The dynamics of the nave walls

5.5.1 Modal identification

The first four identified modes can be reconducted to the dynamic of the nave walls.

The first mode at 2.09Hz (Fig.5.8(a)) interests the displacement of all measurement points in the same direction. The displacement is consistently low in the apse comparing to the nave walls motion: the apse is very rigid compared to other parts of the Basilica. The particular mode shape possibly originates from the Cross Laminated Timber (CLT) ceiling, behaving like a rigid diagram which imposes the same displacement to the nave walls summits. The higher modes affect the bending of the nave walls. The sec-

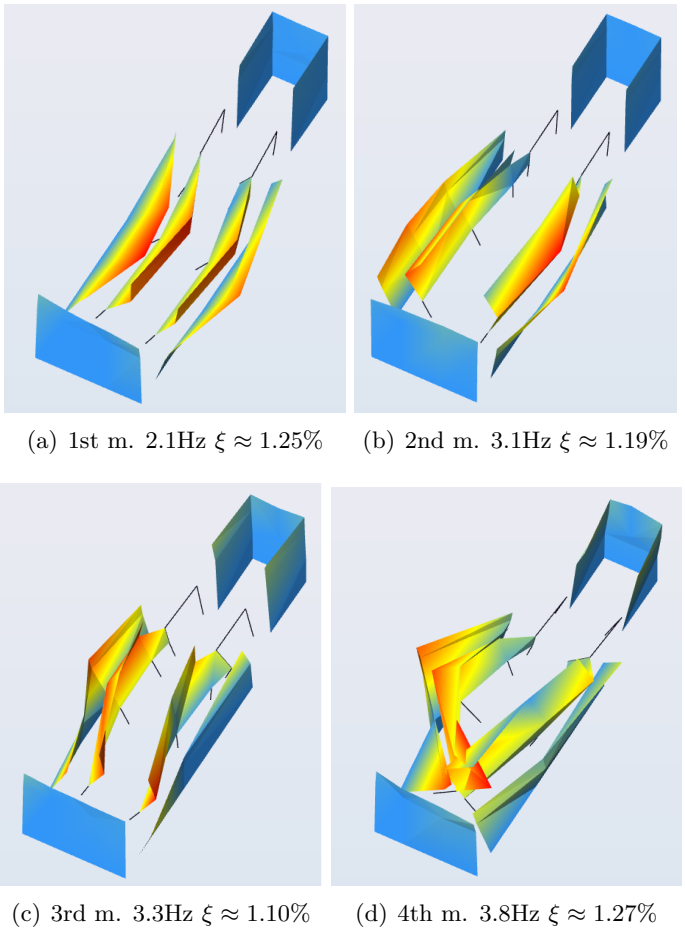

(a) 1st m. 2.1Hz $\xi \approx 1.25\%$ (b) 2nd m. 3.1Hz $\xi \approx 1.19\%$

(c) 3rd m. 3.3Hz $\xi \approx 1.10\%$ (d) 4th m. 3.8Hz $\xi \approx 1.27\%$

Figure 5.8. Illustration of the mode shapes of the nave walls, where m. stands for mode and ξ is the average modal damping.

ond mode at 3.11 Hz (Fig.5.8(b)) mainly regards the change of direction along the vertical: the measurement points by the top of the columns move oppositely to those by the CLT ceiling. Moreover, the phases of the two nave walls are opposite. The third mode at 3.27 Hz (Fig.5.8(c)) mainly concerns the change of direction of the measurement points along the longitudinal direction, like a second bending mode. The fourth mode at 3.82 Hz (Fig.5.8(d)) is quite twisted: it is a sort of third bending mode shape.

Tab.5.2 reports the cross MAC between the identified modes in Fig.5.8. The terms out of the main diagonal are shallow: the mode shapes are dissimilar between each other and distinctly identifiable.
The apse is quite massive, and participate to the identified mode shapes

Table 5.2. Cross MAC between the identified mode shapes.

	2.09	3.11	3.27	3.82
2.09	**1**	0.04	0.009	0.004
3.11	0.04	**1**	0.006	0.004
3.27	0.009	0.006	**1**	0.151
3.82	0.004	0.004	0.151	**1**

with much lower deformation than the other structural members due to its significant stiffness. The investigation of the apse dynamics requires dedicated efforts and will be the object of future studies. The dynamic

Table 5.3. Evolution of the natural frequencies, before and after the 2009 earthquake and, after the restoration.

	Before 2009 Antonacci et al. (2001a)	Since 2017
1st mode [Hz]	1.25	2.09
2nd mode [Hz]	1.72	3.11
3rd mode [Hz]	2.35	3.27
4th mode [Hz]	2.44	3.82

identification carried out before the restoration by Antonacci et al. (2001a) evidenced four modes (see Tab.5.3), resembling the ones in Fig.5.8 with the following natural frequencies: 1.25, 1.72, 2.35 and 2.44 Hz. The structural interventions following the 2009 earthquake produced meaningful differences on the corresponding natural frequencies, which have increased of 66.80%, 80.99%, 39.15% and 59.35% respectively; the average increment of the current four natural frequencies is approximately 60.82%, compared to the structural behaviour before the 2009 earthquake. The identification in operational condition, based on the current measurement set-up, marks a significant localization in the mode shapes, i.e. many mode shapes show significantly higher displacement in some parts rather than in others. As illustrated in Fig.5.8, the modes between the 1st and the 4th (2.1 – 3.8 Hz) affect almost exclusively nave walls. Although the Basilica can be considered as an elastic continuum, the localization of deformation produce the potential uncoupling of the macroelements responses, which are the facade and the nave walls.

5.5.2 Long-term monitoring

The natural frequencies identified from each set of time-series are concatenated and reported in Fig.5.9. Tab.5.4 evidences two concurring trends: the natural frequency oscillates between seasons; the natural frequencies are lightly decreasing in the entire period. The first observation is in full line with the findings by Azzara et al. (2018); Gentile and Saisi (2007); Masciotta et al. (2017); Ramos et al. (2010): the environmental parameters sensibly affect the natural frequencies. The second aspect does not occur in any case study, it is peculiar of the Basilica. Tab.5.5 shows the

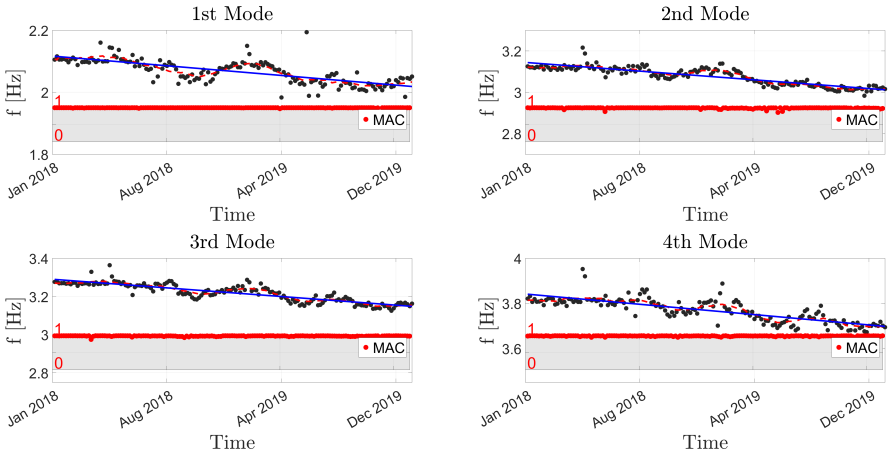

Figure 5.9. Variation of the natural frequencies and MAC of the detected modes during the investigated period. Red dashed line represents the moving mean of the samples, reflecting frequencies seasonal variation, blue straight interpolating line indicates its general decrease over time. The MAC values refer to a fixed set of modes corresponding to the recordings of 01/01/18.

maximum and minimum values of the linear correlation reported as a solid line in Fig.5.9. The natural frequencies of the nave walls exhibited a 0.1

Table 5.4. Statistical description of the frequency and MAC values.

Mode	Frequency [Hz]		MAC	
	Mean	Variance	Mean	Variance
1st	2.07	0.002	0.99	5.793×10^{-4}
2nd	3.08	0.002	0.99	4.408×10^{-4}
3rd	3.22	0.002	0.99	1.502×10^{-4}
4th	3.77	0.002	0.99	1.046×10^{-4}

Hz decrement. There are no detectable variations of the mode shapes: the MAC values, estimated to a reference set of mode shapes, stand approximately constant and close to 1, see Fig.5.9. The nave walls, which are bound together by the top CLT roof, are anchored to the nave walls and

Table 5.5. Decrease of the natural frequency according to the linear regressions in Fig.5.9.

Mode	$f_{in}[Hz]$	f_{fin} [Hz]	Δf
1st	2.12	2.02	-0.10
2nd	3.14	3.01	-0.13
3rd	3.29	3.15	-0.14
4th	3.84	3.69	-0.15

the facade by threaded steel bars.

The reason of this decrement may derive from the behaviour exhibited by the constituent materials over time. a more detailed description of this hypothesis can be found in Alaggio et al. (2021).

The natural frequencies are correlated to the outdoor temperature and the relative humidity, even if the latter does not yield significant correlations, see Fig.5.11. Conversely, the temperature values return good correlations, evidenced by the linear fitting in Fig.5.10. This negative dependence of the

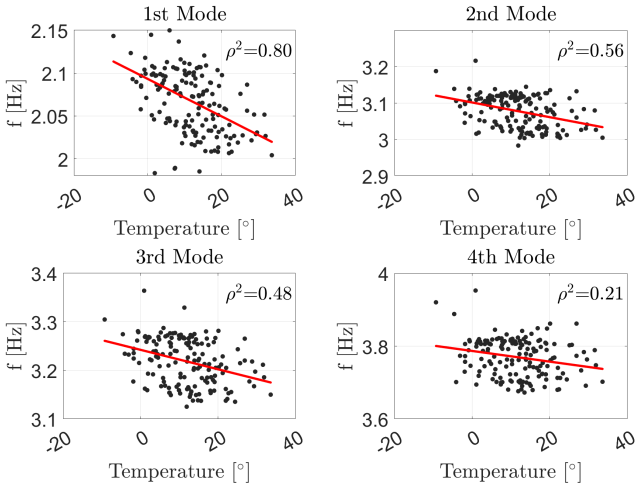

Figure 5.10. Correlation between the natural frequencies of the identified modes and the outdoor temperature (from 1/01/2018 to 31/12/2019).

natural frequencies to the outdoor temperature was observed in few cases: the Milan cathedral (Gentile et al. (2019)) and the Consoli Palace in Gubbio (Kita et al. (2019)). According to Gentile et al. (2019), the negative frequency-temperature correlation in the Milan Cathedral originates from the structural arrangement, consisting of double vault system constrained by an extended net of metallic tie-rods.

Kita et al. (2019) attributed the trend of the natural frequencies to an increase in global structural stiffness due to strengthening effects of metallic

reinforcements (tie rods shortening at lower temperatures) and the presence of a moderate structural damage state in the Palace.

In the current case, the trand may be due to the presence of the Cros-Laminated Timber roof and of its thermal properties.

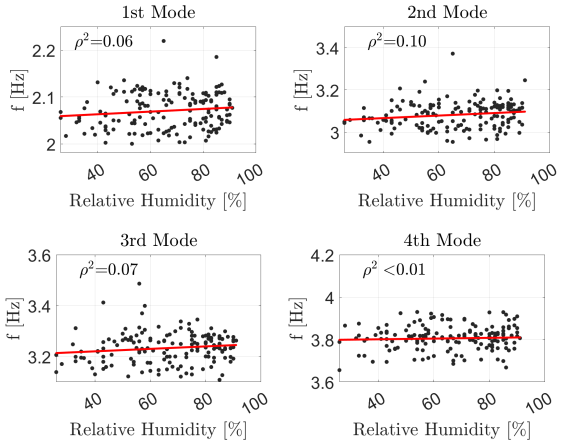

(a)

Figure 5.11. Correlation between the natural frequencies of the identified modes and the outdoor Relative Humidity (from 1/01/2018 to 31/12/2019).

5.6 The dynamics of the façade

5.6.1 Modal identification

The fifth, sixth and seventh modes mainly involve the façade, rather than the nave walls (Fig.5.12). They are all characterized by out-of-plane displacements most visible in the upper part, free, at their rear, from the nave walls constraints.

The fifth mode, at 4.5 Hz (Fig.5.12(a)), shows the bending of the façade by the rose window, while the modal components given by the sensors at the top edges have the same directions.

The sixth mode at 4.8Hz highlights the phase opposition of the displacement of the two upper edges of the façade and a deflection above the portal (Fig.5.12(b)).

The last identified mode is similar to the fifth. The main difference lies in a shallow deflection occurring by the middle of the façade.

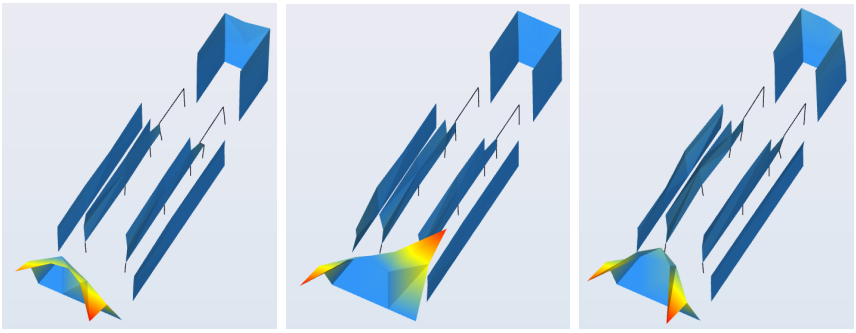

(a) 5th mode 4.5Hz $\xi \approx$ 1.5%

(b) 6th mode 4.8Hz $\xi \approx$ 0.9%

(c) 7th mode 5.2Hz $\xi \approx$ 0.9%

Figure 5.12. Illustration of the façade mode shapes, ξ is the averaged modal damping.

5.6.2 Long-term monitoring

Fig.5.13 presents the results of the modal tracking of the modes associated with the façade. The same trends of the previous modes cn be found: the seasonal fluctuations of frequencies and their slight decreasing over time. However, the seasonal fluctuations are more marked than those in the previous modes.

Tab.5.7 shows the maximum and minimum values of the linear correlation

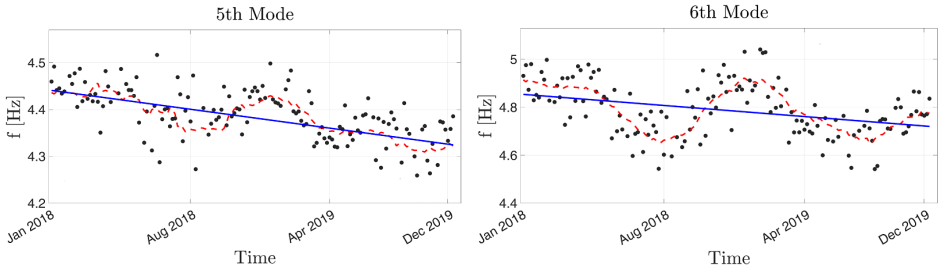

(a) 5th m. 4.5Hz $\xi \approx 1.5\%$

(b) 6th m. 4.8Hz $\xi \approx 0.9\%$

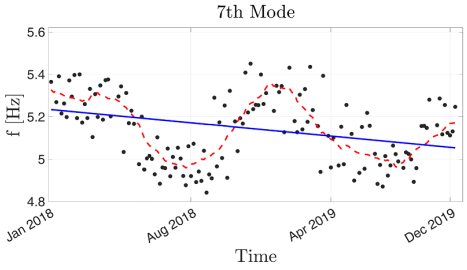

(c) 7th m. 5.2Hz $\xi \approx 0.9\%$

Figure 5.13. Variation of the natural frequencies during the year. The red dashed line represents the moving mean of the samples, the blue straight interpolating line indicates its general decrease over time.

Table 5.6. Statistical description of the frequency and MAC values.

Mode	Frequency [Hz]		MAC	
	Mean	Variance	Mean	Variance
5th	4.38	0.016	0.92	6.30×10^{-3}
6th	4.78	0.018	0.94	2.63×10^{-3}
7th	5.14	0.036	0.89	0.031

reported as a solid line in Fig.5.13.

An impressive phenomenon affects the fifth and seventh modes: not solely

Table 5.7. Decrease of the natural frequency according to the linear regressions in Fig.5.13.

Mode	$f_{in}[Hz]$	f_{fin} [Hz]	Δf
5th	4.44	4.32	-0.12
6th	3.14	3.01	-0.13
7th	3.29	3.15	-0.18

their natural frequencies decrease during the hot season, but their shape and the mutual distance between the frequencies do change during the year, almost cyclically in both the years under investigation.

In order to better understand what happens, dates belonging to two different seasons have been compared: as evidenced by Tab.5.8, the frequencies vary between 3% and 8% among January and September.

The MAC between modal shapes proves a similarity between the 5th mode

Table 5.8. The identified frequencies in January and September, 2019.

Mode	Jan	Sept	Δf (%)
5th	4.43	4.28	-3.3
6th	4.82	4.43	-8.0
7th	5.14	4.85	-5.6

of September and the 7th mode of January and vice versa (Tab.5.9). The sixth mode does not seem to be affected by changes in shape.

Fig.5.14 shows the one-year variations of the 5th and 7th natural frequencies, adimensionalized to the fifth mode, compared to the temperature values. The increase in temperature, typical of the summer season, leads the frequencies to approach each other.

The mode shapes change during the year: the two mode shapes mutate until reaching the maximum similarity in June, and then they exhibit the complete shape inversion between August and September, in which temperature attains the highest values.

Table 5.9. MAC evaluated between the modes of the façade identified in January and in September, 2019.

Mode	$5th_{Jan}$	$6th_{Jan}$	$7th_{Jan}$
$5th_{Sept}$	0.685	0.002	**0.901**
$6th_{Sept}$	0.130	**0.905**	0.150
$7th_{Sept}$	**0.689**	0.266	0.567

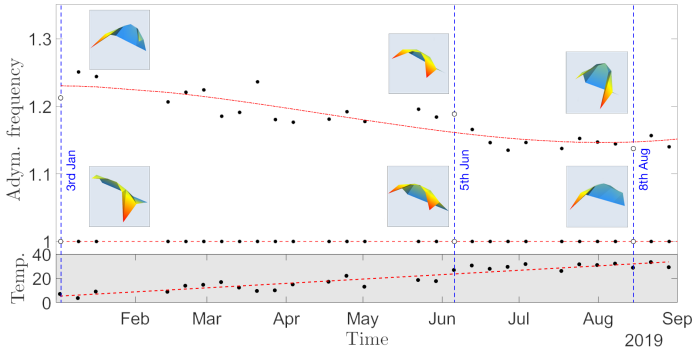

Figure 5.14. Evolution of the fifth and seventh natural frequency, adimensionalized to the fifth. The dash-dot line interpolates the data associated with the seventh mode. The pictures of the mode shapes correspond to the indicated dates. Below, the trend of temperatures in the same period. Data correspond to acquisitions recorded at the same hour (2 pm) between January and September, when temperature progressively rises.

Subsequently, the arrival of the cold season determines the reversed process: both the mode shapes return to their starting states.

The phenomenon is strongly related to temperature: the variation of the two mode shapes is synthetically described by introducing the R parameter, defined as

$$R = \frac{d_{F9}}{d_{F5}} \tag{5.4}$$

Referring to Fig.5.3, the parameter represents the ratio between the out-of-plane mode components in points $F9$, on the left top of the façade, and $F5$ on the opposite side. Fig.5.15 shows the value of the R parameter associated with the 5th and the 7th modes, which have opposite temperature correlations. The intersection of the two interpolating lines identifies a value of R approximately equal to one, meaning that the modal displacements of the two upper edges of the façade coincide, for both modes. The abscissa of the intersection point marks a temperature of about 20 degrees, attributable to that recorded in June.

The trend of frequencies of the 7th mode evidences a slight increase at the

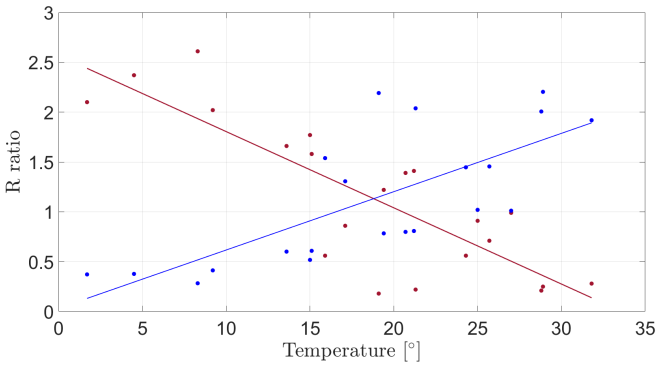

Figure 5.15. R Ratio evaluated for both the 5th mode (blue) and the 7th (red).

end of August, while the temperature still increases.

Although samples recorded in this month are too scarce to yield a sound validation, the overall phenomenon partially resembles that of mode interaction typical of frequency veering, well known in structural dynamics Benedettini et al. (2009).

This particular behaviour could be due to local effects related to the influence of temperature on the elastic parameters of the structure.

5.7 Conclusions

In this chapter, the case study was presented: the data of the monitoring system, both static and dynamic, highlight a complex behavior of the Basilica.

It has been noted that the behavior of the entire building can be essentially divided into that of three main macroelements: longitudinal and nave walls, rigidly connected by a CLT roof, the orthogonal façade and the apse area, which is extremely more rigid, if compared to the other two bodies.

This division will be examined in more detail in the following chapter, in which data belonging to a psudo-damaged state will be analyzed and threaten according to the the techniques of anomaly detection.

The apse, given its excessive rigidity, is almost insensitive to environmental excitement: it has therefore been neglected for the purposes of the analysis.

Both the nave walls and the façade, on the other hand, register a phenomenon that has already been verified in other investigated structures in

literature, namely the variation of the modal parameters as a function of seasonal temperature variations.

While for the naves the phenomenon translates only as a cyclic variation of the natural frequencies of the system, in the façade there is a phenomenon of cyclic inversion occurring between the fifth and seventh modal shapes, similar to a veering one.

The complexity of modal behavior emerged from the knowledge of the structure leads to reflect on the effectiveness of a parametric method for damage detection based on the modal parameters themselves. This method should in fact take into account not only the cyclical variations of the frequencies, but those of the modal forms. Although the former can be mitigated through the use of autoregressive models, among other things, the approach to solving the modal inversion problem represents an interesting challenge for future studies.

In the thesis work, the occurrence of this problem has made it preferable to approach anomaly detection through a non-parametric method, using damage indices already presented in the previous chapters.

Auto-associative neural networks for an anomaly detection procedure

Chapter abstract

Data-driven approaches become necessary when studying the problem of damage detection on particularly intricate structures. In fact, in some cases it is difficult to create a calibrated numerical model that allows to accurately simulate damage scenarios. In addition to this, there is the difficulty to estimate a priori which damage states may occur in the structure.

On the other side, data-driven approach only allows to reach the level of anomaly detection: in most cases, it is not possible to locate or quantify the damage.

In this chapter, the index proposed in the previous chapters is applied as a feature for the anomaly detection on the case study. In the spirit that accompanies the thesis work, for the same purpose a machine learning method is developed, which involves the training of an Auto-Associative Neural Network.

As seen in the previous chapter, the dynamic behavior of the Basilica is characterized by a marked seasonality and stabilization phenomena in progress: in light of this evidence, merits and demerits of the two methods are analyzed.

The analysis highlighted a greater potential for the method based on the Autoencoder, which succeeds in the attempt to mediate the effects caused by seasonality.

6.1 Introduction

In the previous paragraphs, it has been shown how the structural behavior of the Basilica is influenced by a seasonal variability, as well as by slow evolving phenomena.

The seasonal variations cause the modal parameters to oscillate cyclically during the year. This phenomenon concern all the macroelements investigated, but the façade above all. In this latter not only the natural frequencies, but also the modal shapes related to them vary seasonally.

From this observation it follows that parametric damage detection methods based on modal parameters could not be suitable for addressing the damage detection problem for the investigated structure, because they could lead to untruthful reporting of a damage (increasing the percentage of false positives).

In this chapter, a case classifiable as damage is introduced. This case derives from acceleration data recorded by the system on dates prior to an intervention made in the first month of 2018.

The intervention involved the insertion of connections between the façade and the remaining body of the church, through the use of metal anchoring bars. This choice was made to remedy the lack of clamping between the macro-element in question, the nave walls and the timber roof, lack evidenced by the relief of the crack pattern following the 2009 earthquake.

The objective of the chapter is therefore to compare the state of the Basilica before and after the intervention, operating in the spirit of anomaly detection.

The overall behavior of the structure was well described in the previous chapter: its complexities, already highlighted, lead to the choice in the direction of non-parametric methods: in the thesis work the parameters chosen as damage features are those derived from the subspace-based methods, as explained in the previous chapters.

The indices tested in laboratory and the implemented techniques are therefore applied for an anomaly detection problem on a real structure.

Contrary to what happened in Ch.3, in this case, given the complexity of the work, it is not possible to a priori suppose with certainty the dam-

age scenarios occurring in the structure: it seems very hard to predict and define the class labels necessary for the training of a classifier. Thus, the choice has benen that of operating with unsupervised learning methods.
Inside the chapter, the concept of AANN (Autoencoder) is first introduced, marking its particular features. Subsequently, the case study and the results of the application of the indices and of the anomaly detection techniques addressed are presented.

6.2 Auto-associative neural networks

In the introduction of the ANNs, it has always made reference to networks in which the training was supervised: during the training phase, both the data and the class labels to which these data belonged were provided.
An Auto-associative neural network (AANN), more commonly called autoencoder, is a network to which labels are not supplied (typical of the unsupervised learning). The objective of the training of a network of this type is to make it able to reconstruct the data that are provided in input. Given a training set $x^{(i)}$ consisting of i samples, $x^{(i)} \in \mathbb{R}^n$, target outputs $y^{(i)} = x^{(i)}$ are set to be equal to the input: the network in this case tries to learn a function $h_{W,b}(x) \approx x$.
The training process is still based on the optimization of a cost function. The cost function measures the error between the input x and its reconstruction at the output y. It has been shown (Olshausen and Field (1997)) and it is now affirmed that a network of this type works better when sparsity constraints are given.
To clarify the concept of sparsity, one must think about the way in which the transfer of information from one neuron to another in the various layers occurs: a neuron is considered to be "firing", if its output activation value is high. A low output activation value (i.e. zero, if the activation function is the sigmoid of Eq.4.2) means that the neuron in the hidden layer fires in response to a small number of the training examples. Define

$$\hat{\rho_j} = \frac{1}{m} \sum_{i=1}^{m} \left(z_j^h x^{(i)} \right) \tag{6.1}$$

as the average activation of hidden unit j (averaged over the trainig set); apex $(\cdot)^h$ stays for "hidden".
To apply sparsity means to impose the constraint that

$$\hat{\rho_j} = \rho$$

where ρ is called *sparsity parameter*, generally a value close to zero.
Adding a term to the cost function that constrains the values of $\hat{\rho}$ to be low encourages the autoencoder to learn a representation, where each neuron in the hidden layer fires to a small number of training examples. That is, each neuron specializes by responding to some feature that is only present in a small subset of the training examples. Sparsity is encouraged by inserting within the cost function another regularization term, which generally is the Kullback-Leibler divergence

$$\sum_{j=1}^{s_h} KL(\rho||\hat{\rho_j}) = \sum_{j=1}^{s_h} \left(\rho \log \frac{\rho}{\hat{\rho_j}} + (1-\rho) \log \frac{1-\rho}{1-\hat{\rho_j}} \right) \tag{6.2}$$

KL-divergence gives a measure of how different two distributions are: the term is zero if $\hat{\rho_j} = \rho$, otherwise it blows up to infinity if $\hat{\rho_j}$ tends to 0 or 1. By adding this term to the expression of the cost function given in Eq.4.5, which also takes into account the L_2 regularization term, the cost function to be minimized is defined:

$$\begin{aligned} J(W,b) = \left(\frac{1}{k} \sum_{i=1}^{k} J(W,b;x^i,y^i) \right) + \frac{\lambda}{2} \sum_{l=1}^{n_l-1} \sum_{i=1}^{s_l} \sum_{j=1}^{s_{l+1}} \left(w_{ij}^{(l)} \right)^2 + \\ + \beta \sum_{j=1}^{s_h} KL(\rho||\hat{\rho_j}) \end{aligned} \tag{6.3}$$

The term β is the sparsity regularization term.
The training of the autoencoder follows what described in Ch.4.2.2.

6.2.1 Damage indicator based on Autoencoders

The approach for anomaly detection sets up to train the AANN with the undamaged condition features. Train proceeds by presenting the network with many version of the features corresponding to the reference condition, corrupted by noise or other source of variability with the same features

prescribed as the output.

The damage index ID_{AE} is evaluated by calculating the Euclidean distance between the original vector v and the result of presenting it to the network, $\hat{v}$:

$$ID_{AE} = \|v - \hat{v}\| \tag{6.4}$$

If learning has been successful, then the difference of the previous equation is around zero if the feature vector v is representative of the reference state. In this way, the assumption is that the prediction error of the network will grow when the feature vector coming from a damaged condition is fed to the network itself.

As highlighted in Farrar and Worden (2012), there is no guarantee that the index will increase monotonically with the level of damage, this is why this form of novelty detection gives only a level 1 diagnostic in Rytter's term.

It is noted also that the universal approximation property of the neural network (for which it is referred to Bishop (1994)) means that the novelty detector can learn the properties of any normal condition distribution, it does not have to be Gaussian.

6.3 Application of anomaly detection procedure on the case study

In the following section, the damage indices proposed in Ch.3 and the developed techniques are applied to an anomaly detection problem.

The results obtained from the elaboration of these indices are compared with those obtained from the training of an AANN network (AutoEncoder), according to what reported in Par.6.2. The aim is to highlight strengths and weaknesses of one over the other.

As documented in Aloisio et al. (2021), during the end of the year 2017, the Basilica underwent a minor structural intervention: in particular, metal profiles were wall embedded to the masonry, to anchor the façade of the church to the remaining structure, as shown in Fig.6.1. In the work, it was seen how this type of intervention changed the dynamic behavior of the structure evaluating some subspace-based indicators.

The occurrence of this intervention has generated a case thanks to which

it is possible to test the indices and techniques developed for anomaly detection on a real case.

In order to implement the procedure, the accelerometric data of two conditions are compared: the first one, recorded before the CLT roof was connected to the façade, is assumed as damaged or actual state (although, chronologically, it happened before). The second data set, recorded after that the roof was connected to the façade, is assumed as reference or undamaged state.

The choice of assuming as damaged a state which occurred chronologically before the one assumed as reference, is dictated by the fact that much more data is available for the latter (from 2018 to 2021, date of writing). For this reason, it seems more logical in terms of anomaly detection to take this as reference, and highlight any changes in the other state, of which we have fewer samples.

For each of the two data sets, data from three different cases are processed:

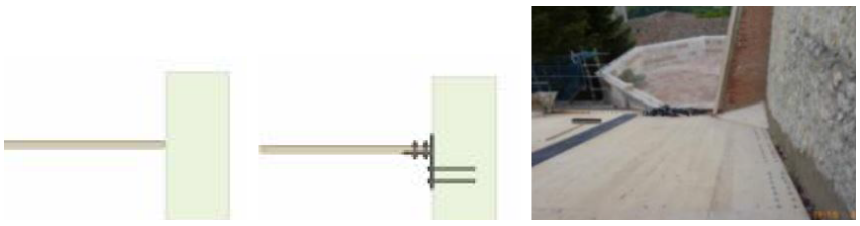

Figure 6.1. Detail of the connection between the façade and the CLT roof: schetch of the roof-façade interaction before and after the connection and a picture of the intervention.

the first case includes accelerometer data from all acquisition points, excluding the apsidal zone: in this way, an overview of the change in the global behavior of the structure pre and post-intervention is provided.

The other two cases focus on the two macro-elements most affected by the intervention, namely the façade and the nave walls: in a sort of attempt to localize the damage, it is highlighted which elements have been most affected by the change.

The following indices are evaluated for every case:

- ID_{corr} generated by evaluating the correlation between the covariance matrices, as in Ch.3.2. The evaluation of this index requires the choice of a reference date which to compare the others. Considering

the seasonal changes of the modal parameters, it has been considered explanatory to take as reference three particular dates, following what done in Ch.5.6;

- ID_{AE}: index evaluated from the results of the training of the autoencoder network, according to the procedure described in Par.6.2.

For each case, anomaly detection is done by setting a threshold at the 95% percentile of the samples relative to the reference state. The algorithm evaluate a case as belonging to the population of the reference state or as an anomaly on the basis of the exceeding of the threshold.

6.4 Anomaly detection performed with damage index ID_{corr}

As described in Ch.5.3, the permanent monitoring system consists of 78 Force-balance accelerometers (2 triaxial, 12 biaxial, and 48 monoaxial).
Following what was done in the modal identification phase, the accelerometric data, acquired with a sampling rate of 250 Hz, were decimated by a factor $N_d = 20$ before being processed. Subsequently, the covariance matrices were calculated considering a time delay $i = 30$.

6.4.1 Results from global setup

The indices ID_{corr} are evaluated by calculating the correlation coefficient between the matrix of the reference state and that of the current state to be evaluated. The first step is therefore to choose a date, among those acquired, to be used as a reference: as mentioned, given the seasonal variability of the phenomenon, we choose the three significant dates of 2019 corresponding to the maximum changes of the modal forms related to the fifth and seventh identified frequency (see Ch.5.6): 3rd of January, 5th of June, and 8th of August.
Once the reference dates are chosen, the index values are calculated for each available date in the period between the end of 2017 and the first half of 2021.

As can be seen from Fig.6.2-6.3-6.4, the trend of the index in the period

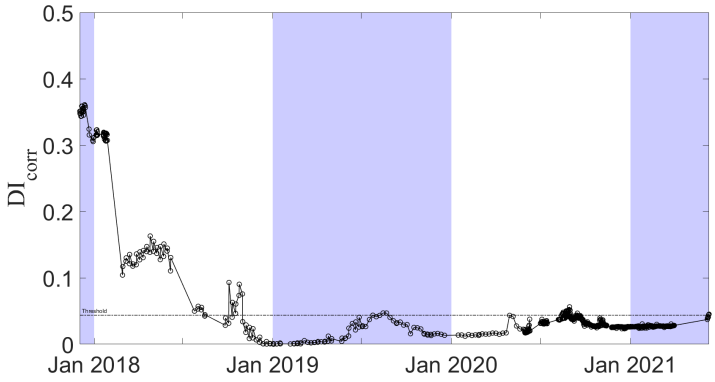

Figure 6.2. Variation of the damage index over time, considering the 01/01/2019 as reference date. The threshold value of the index is set at the 95% percentile of those obtained in the 2019/2020 period, considered as the undamaged state.

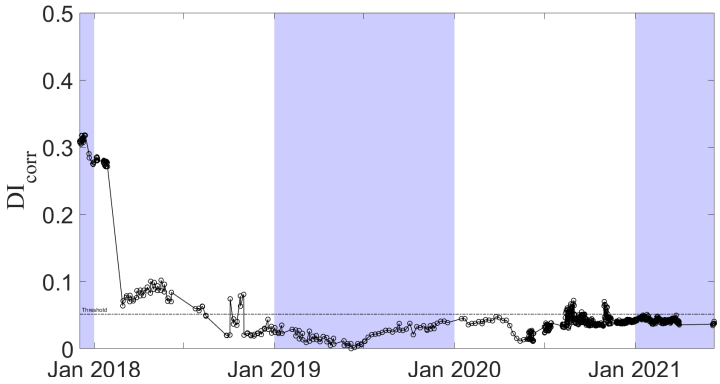

Figure 6.3. Variation of the damage index over time, considering the 05/06/2019 as reference date. The threshold value of the index is set at the 95% percentile of those obtained in the 2019/2020 period, considered as the undamaged state.

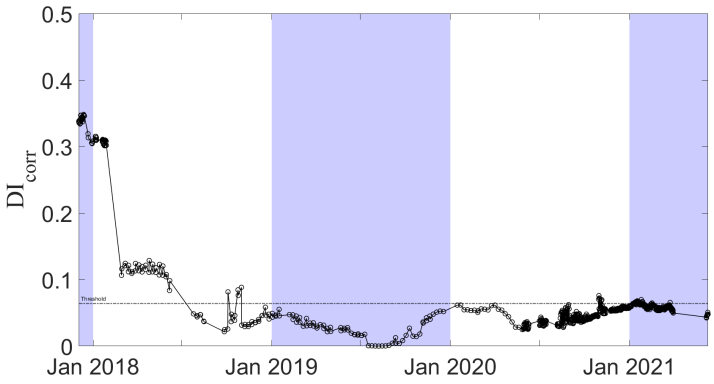

Figure 6.4. Variation of the damage index over time, considering the 08/08/2019 as reference date. The threshold value of the index is set at the 95% percentile of those obtained in the 2019/2020 period, considered as the undamaged state.

2019/2021 follows the periodic trend already seen in the modal tracking of frequencies in the previous chapter. Therefore, the index is not completely exempt from the environmental variations to which the structure is subject during the course of the year: although beeing in the undamaged state, the index tends to rise moving towards a season with a temperature which is different from that of the selected reference date.

From this observation derives the difference between the curves recorded in the three figures. Considering Fig.6.2, in which the reference date is January, it can be noticed that the index tends to be lower in the dates belonging to the cold seasons, to then rise in the warmer ones. The contrary happens instead if considering the reference in August, Fig.6.4.

Note also that the index tends to rise over time, as testimonial of the second phenomenon found in the modal tracking phase, related to frequency decay. All the index values exceeding the set threshold belong to the late 2020/2021: from this it can be seen that the phenomenon of frequency decay in this time span is still marked, making the reference state still unstable (it can be considered as a slow phenomenon).

What is most impressive, readable from all three figures, is what happens around the end of 2017/beginning of 2018, the period after the intervention described above: for these dates, whatever the date chosen as a reference, the index takes on a much higher value.

Drawing a threshold line encompassing 95% of the samples for the 2019/2021 reference state, we see that the 2017/early 2018 indices far exceed this threshold: the monitoring system, calibrated to this threshold, would therefore flag the anomaly.

What is also interesting, however, are the dates related to the hot season of 2018: although these dates are intended to belong to the reference state, being posterior to the connection intervention, the index is still high compared to later dates.

It is assumed that this difference can be due to two possibilities: another settling of the structure, or it can also be related to the decay of the frequencies, more pronounced in that year, the first after the intervention.

From the analysis of the dynamics of the structure made over the years, it results that is possible to split the behavior of the structure into that of its

main macroelements.

In a similar way to how the modal traking was carried out, the results of the analysis of the single macroelements, façade and nave walls, are now reported.

6.4.2 Results from sensor placed on the nave walls

The procedure for calculating damage indices is the same as that described in the previous paragraph.

Looking at Fig.6.5-6.6-6.7, results are different from those obtained considering all the sensors.

The first that strikes is the value of the index: it remains very low compared to that of the previous cases, indicating that the dynamic behavior of the naves has not changed too much after the intervention. In fact, the values of the damage index remain below the set threshold, even for the dates prior to the intervention of connection with the façade.

Attempting to localize the damage, we could say that the macroelement

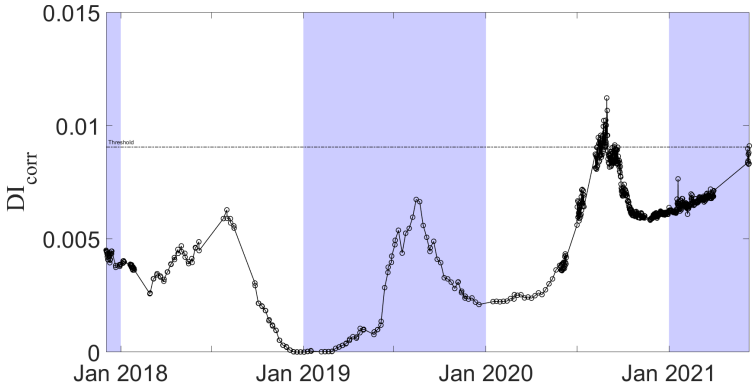

Figure 6.5. Variation of the damage index over time, considering the 01/01/2019 as reference date. The threshold value of the index is set at the 95% percentile of those obtained in the 2019/2020 period, considered as the undamaged state. Data coming from sensors placed on the nave walls.

in question does not seem to be affected by the phenomenon.

This could be linked to the extension of the naves in plan: in fact the variation of the dynamic behavior following the intervention, occurred in the part of the roof in contact with the façade, could not have been perceived by the sensors placed in the most distant points (for example, near the apse, see the building plan Fig.5.3). According to another hypothesis, the connection with the rigid roof represented a constrain more for the façade

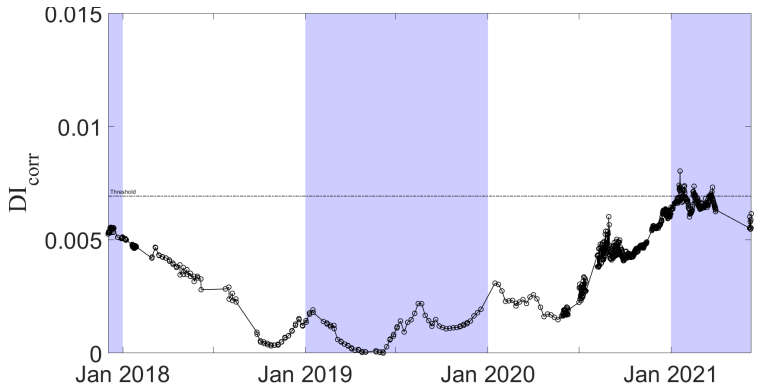

Figure 6.6. Variation of the damage index over time, considering the 05/06/2019 as reference date. The threshold value of the index is set at the 95% percentile of those obtained in the 2019/2020 period, considered as the undamaged state. Data coming from sensors placed on the nave walls.

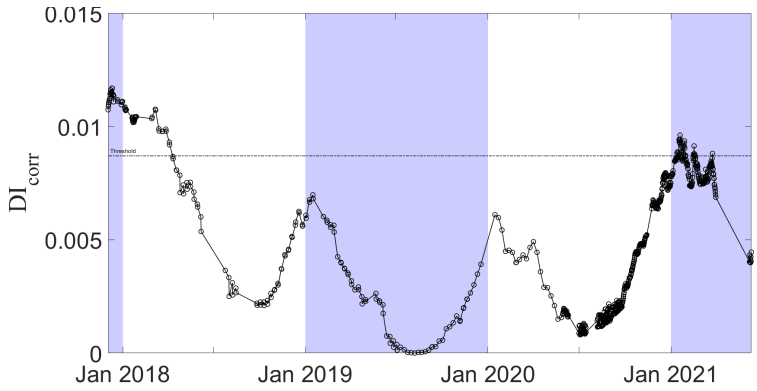

Figure 6.7. Variation of the damage index over time, considering the 08/08/2019 as reference date. The threshold value of the index is set at the 95% percentile of those obtained in the 2019/2020 period, considered as the undamaged state. Data coming from sensors placed on the nave walls.

than on the nave walls, which have already been made in solidarity with the roof by interventions prior to the one in question.

From the trend of the index in time, both the seasonal variability of the global dynamic behavior and the phenomenon related to the decay of the frequencies are recognizable.

6.4.3 Results from sensor placed on the façade

Data regarding the façade is taken from its 8 accelerometers (Fig. 5.3b). As can be noted in Fig.6.8-6.9-6.10, the trend of the index DI_{corr} in time is very jagged: however, it follows the trend found in the generic case. Unlike the latter, the value of the index in the 2017/18 dates is higher, and the difference with the period since 2019 is more pronounced (up to 15 times

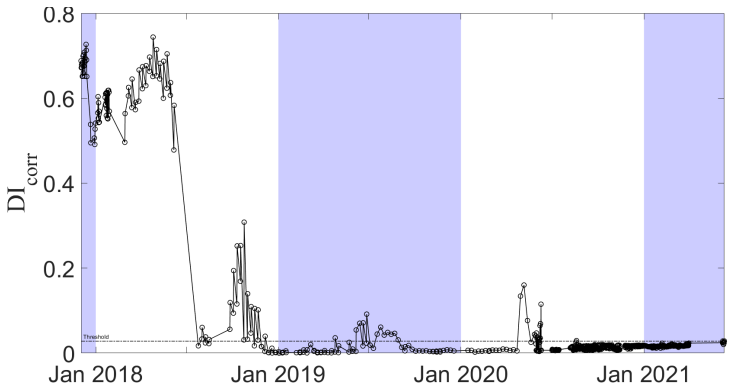

Figure 6.8. Variation of the damage index over time, considering the 01/01/2019 as reference date. The threshold value of the index is set at the 95% percentile of those obtained in the 2019/2020 period, considered as the undamaged state. Data coming from sensors placed on the façade.

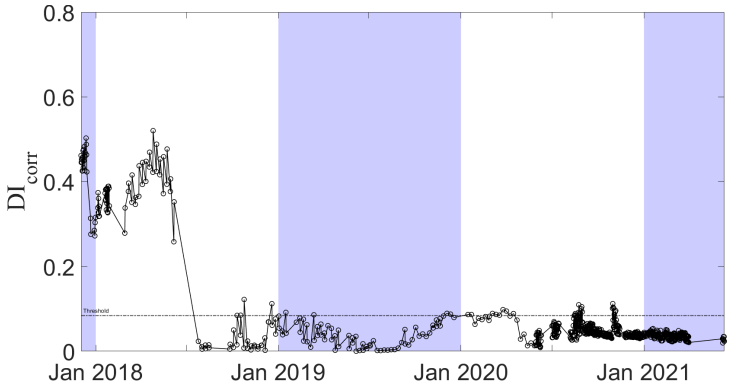

Figure 6.9. Variation of the damage index over time, considering the 05/06/2019 as reference date. The threshold value of the index is set at the 95% percentile of those obtained in the 2019/2020 period, considered as the undamaged state. Data coming from sensors placed on the façade.

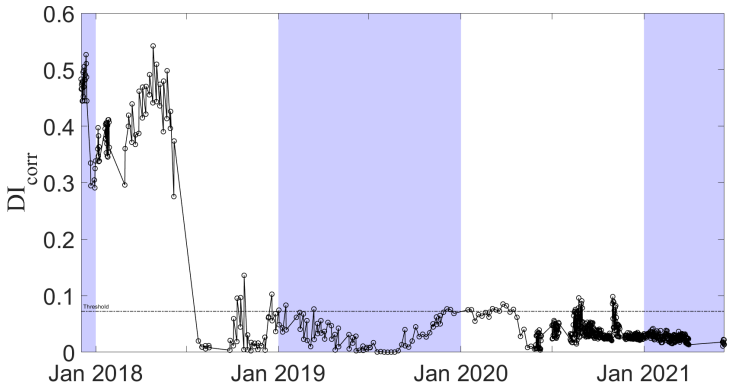

Figure 6.10. Variation of the damage index over time, considering the 08/08/2019 as reference date. The threshold value of the index is set at the 95% percentile of those obtained in the 2019/2020 period, considered as the undamaged state. Data coming from sensors placed on the façade.

higher than the threshold that includes 95% of cases from 2019 onward). From the reading of these values, it is easy to deduce how much the intervention has changed the behavior of the façade more than that of the walls of the nave.

6.5 Anomaly detection performed with Autoencoder

In the following paragraph, the process of anomaly detection is performed by means of the training of an Auto Associative Neural Network - or Autoencoder - as described in paragraph 6.2.

The choice of neural networks depends on the observation of the strong variability of the result depending on the date chosen as reference, that affects the evaluation of the system about the state of the structure. As can be seen from the Fig.6.8-6.10, monitoring system assessment outcomes for the 2020 date would change if we took the January date as the baseline (dates fall under the threshold) or the August 2019 (dates exceed the threshold).

Through the use of the autoencoder, the objective is to minimize as much as possible the influence of environmental effects, further demarcating the two phenomena attributable to the damage: post-intervention change and change related to the decay of frequencies over time.

As in the previous section, data from all sensors are first evaluated and then the contribution of individual macroelements is analyzed. For each case, training was conducted assuming as input the subspace matrices used to compute ID_{corr}, with dimensions varying for each case based on the number of sensors and the time lag, which was set to $i = 30$.

The Autoencoder was trained using one hidden layer, composed of $N_n = 10$ nodes.

The size of the hidden layer, smaller than the size of the input vectors, means that the network is forced to capture the information from reduced data sets: in the Encoding phase, it is said that the network creates a "bottleneck", through which the essential information for the description of the problem is captured.

In the next step, Decoding, the reduced matrix containing the weights W_{ij} associated with each node is used to reconstruct the original matrix.
The practical procedure therefore involves:

1. Choice of the range of dates to be used as the training set for the network: a two-year period, 2019/2020, was chosen in order for the net to recognize the presence of the seasonal trend in the training phase;

2. Matrix manipulation: before training, the input matrices $M_i \in \mathbb{R}^{N_e \times N_e}$, $i = 1, ..., N_c$ must be rearranged into column vectors $v_i \in \mathbb{R}^{N_e^2 \times 1}$. Next, the vectors are aligned to form the input matrix $M \in \mathbb{R}^{N_e \times N_c}$, where N_c is the number of samples considered in the training set;

3. Network Training Phase: the training is carried out following what described in Sec.6.2;

4. The result of the training is a network able to reconstruct any matrix given in input (of the same number of elements N_e) on the basis of the relationships that it has managed to capture in the training phase. According to what reported in Par.6.2, the damage index ID_{AE} is evaluated by calculating the Euclidean distance between the original vector v and the predicted vector $\hat{v}$:

$$ID_{AE} = \|v - \hat{v}\|$$

6.5.1 Results from global setup

The following section shows the results obtained by training an autoencoder with data from all available sensors. The number of channels is therefore 78, the time lag $i = 30$: each covariance matrix used for training has size 840×840. The available dates for 2019-2020 result in about 400 samples. Fig.6.11 reports the outcomes of the training: low values of the objective function and the gradient are synonymous that the training can be considered successful.

Fig.6.12 shows the trend of the damage index ID_{AE} over time: as for the index calculated from correlations, the difference between the values of the 2019/2020 reference state and those of 2017 is visible: the value recorded on

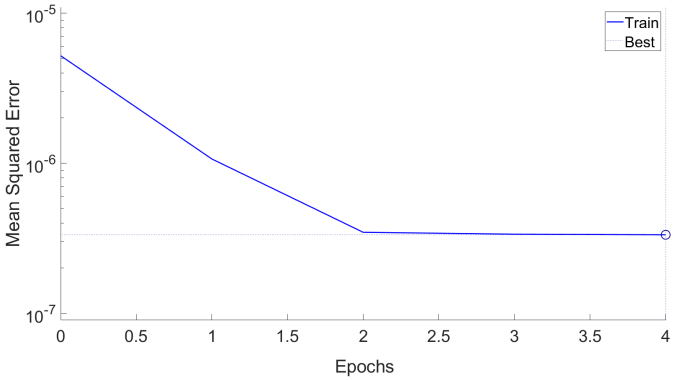

Figure 6.11. Trend of the loss function during the training of the netwoork.

the latter dates, $ID_{AE} = 0.75$, is about 4 times higher than the threshold value, again set at 95% of the values of the samples belonging to the 2019-2021 dates. Looking at the results, we still find a plateau in the summer

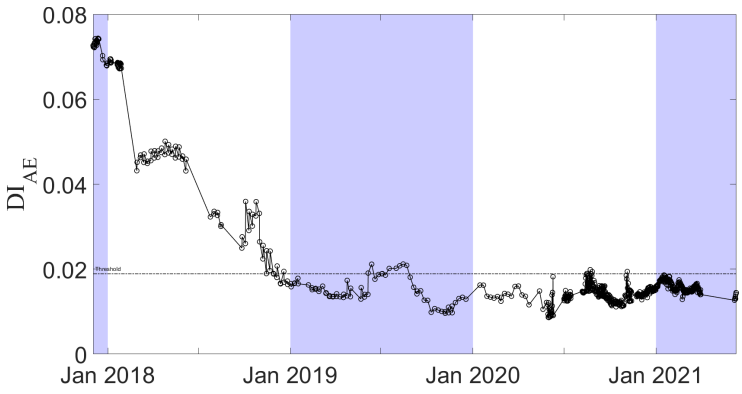

Figure 6.12. Variation of the damage index over time, considering the period 2019/2020 as training set for the AANN. The threshold value of the index is set at the 95% percentile of the samples regarding the reference period.

season of 2018: there is confidence that it cannot be due solely to seasonal variations.

The differences between the trends of DI_{AE} and DI_{corr} are the following:

- The DI_{AE} indices are all very close to the threshold line: this means that the autoencoder, trained over a two-year period, manages to mitigate the effects of cyclical phenomena even for dates in 2021;
- The indices never reach zero: it is assumed that this fact is due to the complexity of the variation of the dynamic behavior of the structure, remembering once again that it is subject to both seasonal phenomena and those of settling natural frequencies. This makes each sample different from the other: although the autoencoder manages

to mitigate in some ways the effects of temperature, it may not do so well with the latter.

6.5.2 Results from sensor placed on the nave walls and on the façade

Processing the nave wall data leads to substantially different results from those found with the DI_{corr} index. In fact, comparing Fig.6.13 with Fig.6.6, it can be seen that the values for 2017 and the first period of 2018 exceed the set threshold (the indices for 2107 are about twice the value of the same). In other words, with this metric, damage is also found in the nave wall data.

The index values relative to the remaining period show however a cyclic

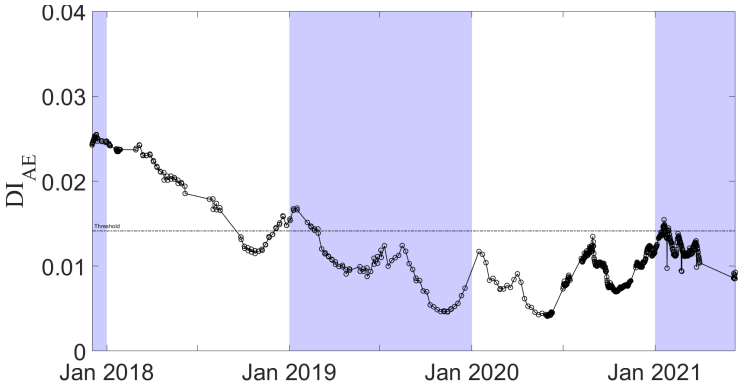

Figure 6.13. Variation of the damage index over time, considering the period 2019/2020 as training set for the AANN. The threshold value of the index is set at the 95% percentile of the samples regarding the reference period. Data coming from sensors placed on the nave walls.

trend, but with peaks different from the seasonal ones: this phenomenon is dictated by the training modality of the network which, trying to mediate between very different cases, obtains averaged results between the various seasons

Results from Fig.6.14, referred to the façade, confirm what was observed earlier: the index value for the 2017/2018 dates is more pronounced than those of the reference dates. In addition, although the index trend from 2019 seems more jagged, the seasonal trend seems to be lost, a symbol that the network has been more successful in its goal of mitigating thermal effects.

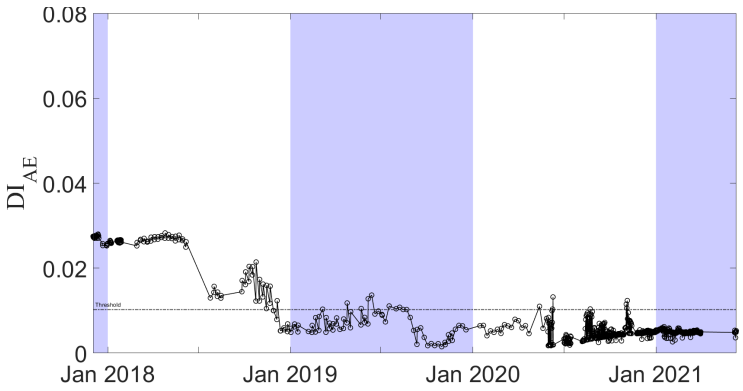

Figure 6.14. Variation of the damage index over time, considering the period 2019/2020 as training set for the AANN. The threshold value of the index is set at the 95% percentile of the samples regarding the reference period. Data coming from sensors placed on the façade.

6.6 Conclusions

In this chapter, the application of some anomaly detection techniques was presented. Both the presented techniques use the subspace matrices of the data as damage feature. The anomaly analysis is studied starting from the current state of the Basilica of Santa Maria di Collemaggio. This state, considered as undamaged, is compared with that recorded prior to a roofing intervention completed in early 2018. The intervention involved the connection of the façade to the Cross Laminated Timber roof behind it.

The anomaly detection phase is made by calculating two indices: the first one is based on the correlation index between the matrix of the reference state and that of the current state. The second one is based on the training of an Autoencoder network. From both indices, it was noted that the intervention had modified the dynamic behavior: the two indices evaluated for the dates in question exceeded a fixed threshold value.

It is possible to study the global behavior of the Basilica by dividing it into that of the macro-elements that compose it: analyzing them separately, it has been noticed that the index calculated for the nave walls tends to be lower than that calculated for the façade. This suggests that the façade wall has been more interested in the intervention than the naves (as it would be thought, given the type of intervention).

Testing the two indices, it was noted that, as it is formulated, the correlation-based index depends strongly on the date chosen as reference, while the

autoencoder-based index seems to succeed in mitigating environmental effects.

Despite this, the difficulty of determining the reference state remains, due to the presence of the phenomenon that causes the decrease in frequencies. The phenomenon is well highlighted using both indices proposed, and certainly deserves further study in the future.

Concluding remarks

Chapter abstract

In the thesis work, damage detection methods have been analyzed, based on the evaluation of the subspaces of dynamical systems.

Two approaches have been followed: in the first, a damage index derived from subspace matrices has been proposed. The second approach has been carried out considering the subspace matrices as damage features, and inserting the as input in the training of artificial neural networks.

Laboratory tests and the application to a case study have showed the effectiveness of the proposed methods for the damage detection procedure. The methods proved to be valid in both the anomaly detection phase, carried out through data-driven approach, and in the subsequent steps of the structural damage diagnosis, deepened following a model-driven approach.

This chapter contains the conclusions of the thesis work: therein, all the results obtained in the tests described in the previous chapters are critically analyzed.

Vibration-based damage testing has been increasingly successful in the Structural Health Monitoring field, as it allows to investigate the global behavior of a structure avoiding invasive and local testing.
Vibration-based damage detection studies are based on the observation that that the occurrence of structural damage leads to changes in the matrices that characterize the dynamic system. The occurrence of damage is investigated by evaluating the variation of some damage-sensitive parameters, called features, comparing the reference state of a structure with that of the current recording.
Parametric methods were the first approach to the problem, attempting to correlate the damage directly to the variation of the modal parameters.
Non-parametric techniques, developed later, process time series formulating features not directly correlated to physical quantities.
With the development of Artificial Intelligence algorithms, damage detection research has been influenced by methods from Machine Learning or, more recently, Deep Learning. This is due to the fact that through a neural network it is possible to create models in which relationships are established, even of a non-linear type. They seem to be well suited to interpret the often irregular trends over time of the damage features.
In the thesis work, the theme of damage detection was addressed, in particular the damage localization and quantification. These two problems are classified at level 2 and 3 in the scale of diagnostic levels proposed by Rytter and considered a reference in the literature. The features examined for damage detection have been the subspace-based damage indicators obtained from the analysis of the subspaces of the dynamics matrices: indices already present in the literature and of new conception were tested.
The process was initially conducted on a test structure represented by a suspended steel beam; damage was generated by introducing a point mass onto the system. During the tests, the magnitude of the mass and its location were varied in order to evaluate the effectiveness of the method.

The approach followed in the work has been of model-driven type, which means that numerical analyses have been carried out on an FE model, to simulate the damage scenarios to be compared with the one subsequently

produced experimentally.
The use of a model-driven procedure necessitated a preliminary calibration phase of the model itself. For this purpose, it has been evaluated the effectiveness of damage indicators as objective functions to be minimized in the optimization problem related to the model updating.
The proposed method gives promising results: the indicators seem to be more sensitive to the variation of dynamic system properties than techniques which uses objective functions based only on modal parameters

After calibrating the model, the damage detection has been performed following and comparing two methods:

- The first method is based on the calculation of an index derived from the 2D-correlation coefficient between two matrices, initially developed in the field of Image Processing. It involves the use of this proposed index as an objective function to be minimized in a discrete optimization algorithm, in order to find the maximum similarity between the produced damaged case and the attempt ones;

- The second method concern with the adoption of subspace matrices as features, and the training of an artificial neural network to classify the damage.

Both methods were tested numerically and experimentally on the steel beam structure. The tests therefore investigated the effects of varying the position of the mass along the beam and varying the magnitude of the mass itself.
A first data-driven test has been carried out, comparing vibrational data between the undamaged state (with no mass) and the damaged ones. From this comparison, it was confirmed that the only data-driven method is not sufficient to go beyond the level of anomaly detection. The attempts made for damage localization have shown that the selected features are not injective functions with respect to the variable-position: different positions lead to very similar function values.
Anomaly detection tests carried out varying the magnitude of the mass, fixed in the same position, have led to an interesting observation: the

subspace-based index grows as the applied mass increases, in a monotonic way within the range considered. It suggests that some data-driven reasoning could be done, in order to estimate the extent of the damage, after that the location of damage occurrence has been identified. Applications to real problems could be, for example, the evaluation of the progress of the degradation in a localized area of a structure, or the fatigue damage in metal joints.

Model-driven tests based on the calculation of the damage index DI_{corr} showed that it is more sensitive to variation in the position of the mass, rather than to variation in its magnitude.

The mass localization problem on the structure-test has also highlighted the dependence of the results on the symmetry of the system: the confusion matrix related to the localization problem has in fact shown the presence of misclassified cases not only near the position to be identified, but also in positions symmetrical with respect to the latter.

The problem of identifying the mass entity highlighted a lower sensitivity of the feature itself towards the mass variation. In fact, the results have shown that the percentage of misclassified samples is higher than that found in the localization problem, and in some cases even exceeds that of true positives.

The network used for the localization and quantification of the damage was a classifier: during the training phase, features have been provided to the network, specifying the class label to which they belonged. Subsequently, the validity of the network in correctly classifying the various damage scenarios was evaluated by giving it a test set and assessing the quality through the confusion matrix. In each case, the network correctly recognizes the target cases to be identified.

The choice of a method based on training a neural network stems in part from the desire to resolve any errors due to noise.

The neural network, through the training phase, stores information on the inputs which results to be mainly independent from the noise with which these are generated.

The numerical tests have shown how the training of the network leads to more accurate results than the method based on the index, being able to build relationships between the inputs and the labels associated to them.

However, it should be remembered that training an ANN can involve a greater computational burden, due to the number of samples to be supplied to the network during the training phase.
In the experimental tests, the classification results were also positive. However, both in the case of localization and identification of the mass entity, the proposed methods classify the damage type with a slight inaccuracy, which is however considered acceptable. It is believed that this inaccuracy is due to the fact that the FE model, although calibrated in the preliminary phase, does not perfectly match the behavior of the real structure.
The proposed methods seem therefore to be promising for application to damage detection problems in more complex structures.

The algorithms experimented in laboratory have been applied to study the behavior of a real structure. The case study, the Basilica of Santa Maria di Collemaggio in L'Aquila, represents the heart of the city, with its historical and cultural value.
The restoration work following the 2009 earthquake included the installation of a static and dynamic monitoring system. The system has been acquiring vibrational data for years, with sampling frequency ranging from weekly to daily. A preliminary phase of knowledge of the dynamic behavior of the structure has provided for the processing of data from the monitoring system, in the approximately four years since the system has been in operation. This study was only possible by implementing an automatic modal identification procedure, based on Stochastic Subspaced-based Identification technique, and subsequent tracking of the parameters in time. Through the processing of data from sensors, it was highlighted a highly intricate behavior, essentially due to the geometric complexity and heterogeneity of the present materials. From the analyzes it arose that the behavior of the Basilica is driven by two phenomena:

- The first phenomenon, already known in the literature, is the cyclic variation of the natural frequencies of the structure in the investigated range. This variation sees the frequencies increasing in cold seasons and vice versa in warm seasons. The correlation with temperature is even more marked if we examine separately the macro-elements

in which it is possible to divide the Basilica: analyzing the cyclic behavior of the façade, it can be seen that not only the frequencies change in time, but also an inversion of the modal forms of the fifth and seventh mode of vibration occurs.

- The second phenomenon in act is peculiar of the structure under examination, and sees a slight decay of the frequencies over the years: this phenomenon acts independently from the seasonal cyclicity. Some studies conducted have suggested that this decay may be due to the slow stabilization phenomena of the Cross-Laminated Timber roof. It is more pronounced in the period around the time of installation of the system, and is stabilizing over time.

These two phenomena make a precise definition of a reference state of the structure hard to perform: further studies have to be carried out in order to control these effects.

The complexity of the modal behavior emerged from the modal tracking led to reflect on the effectiveness of a parametric method based on the modal parameters themselves.
In the thesis work, the occurrence of this problem has made it preferable to approach anomaly detection through a non-parametric method, using damage indices already presented in the previous chapters.
The anomaly analysis has been carried out starting from the current state of the Basilica. This state, considered as undamaged, was compared with that of accelerometer data recorded prior to a roofing intervention completed in early 2018. The intervention in question regarded the connection, by means of steel bars, of the façade to the CLT roof behind it.
The anomaly detection phase has made by calculating two indices: the first one is based on the 2D-correlation index between the matrix of the reference state and that of the current state. The second one is based on the training of an Auto-associative neural network.
Evaluating both indices, it was noted that the intervention had significantly modified the structural behavior, with the result that the two indices calculated for the dates in question exceeded a set threshold value considered to be representative of the undamaged state.

It is possible to study the global behavior of the Basilica by dividing it into that of the macro-elements that compose it: analyzing the latter separately, it has been noticed that the index calculated for the nave walls tends to be lower than that calculated for the façade. This suggests that the façade wall has been more interested in the intervention than the nave walls.

Testing the two indices, it was noted that, as it is formulated, the correlation-based index depends strongly on the date chosen as reference, while the autoencoder-based index seems to succeed in mitigating environmental effects.

Despite this, the difficulty of determining the reference state remains, due to the presence of the phenomenon that causes the decrease of the natural frequencies.

[Blank page]

Bibliography

Abdeljaber, O., Avci, O., Kiranyaz, S., Gabbouj, M., and Inman, D. J. (2017). Real-time vibration-based structural damage detection using one-dimensional convolutional neural networks. *Journal of Sound and Vibration*, 388:154–170.

Adeli, H. and Yeh, C. (1989). Perceptron learning in engineering design. *Computer-Aided Civil and Infrastructure Engineering*, 4(4):247–256.

Alaggio, R., Aloisio, A., Antonacci, E., and Cirella, R. (2021). Two-years static and dynamic monitoring of the santa maria di collemaggio basilica. *Construction and Building Materials*, 268:121069.

Allahdadian, S., Döhler, M., Ventura, C., and Mevel, L. (2019). Towards robust statistical damage localization via model-based sensitivity clustering. *Mechanical Systems and Signal Processing*, 134:106341.

Aloisio, A., Alaggio, R., and Fragiacomo, M. (2019a). Dynamic identification of a masonry façade from seismic response data based on an elementary ordinary least squares approach. *Engineering Structures*, 197:109415.

Aloisio, A., Antonacci, E., Fragiacomo, M., and Alaggio, R. (2020a). The recorded seismic response of the santa maria di collemaggio basilica to low-intensity earthquakes. *International Journal of Architectural Heritage*.

Aloisio, A., Battista, L. D., Alaggio, R., Antonacci, E., and Fragiacomo, M. (2020b). Assessment of structural interventions using bayesian updating and subspace-based fault detection methods: the case study of s.

maria di collemaggio basilica, l'aquila, italy. *Structure and Infrastructure Engineering*, pages 1–15.

Aloisio, A., Battista, L. D., Alaggio, R., Antonacci, E., and Fragiacomo, M. (2021). Assessment of structural interventions using bayesian updating and subspace-based fault detection methods: The case study of s. maria di collemaggio basilica, l'aquila, italy. *Structure and infrastructure engineering*, 17(2):141–155.

Aloisio, A., Di Battista, L., Alaggio, R., and Fragiacomo, M. (2019b). Analysis of the forced dynamics of a masonry facade by means of input-output techniques and a linear regression model. In *COMPDYN, 2019, 7th International Conference on Computational Methods in Structural Dynamics and Earthquake Engineering.*

Alpaydin, E. (2020). *Introduction to machine learning.* MIT press.

Amoroso, S., Gaudiosi, I., Tallini, M., Di Giulio, G., and Milana, G. (2018). 2d site response analysis of a cultural heritage: the case study of the site of santa maria di collemaggio basilica (l'aquila, italy). *Bulletin of Earthquake Engineering*, 16(10):4443–4466.

Antonacci, E., Aloisio, A., Galeota, D., and Alaggio, R. (2020). The s. maria di collemaggio basilica: from vulnerability assessment to first results of shm. *Journal of Architectural Engineering*, In press.

Antonacci, E. and Beolchini, G. (2005). The dynamic behaviour of the façade of the basilica s. maria di collemaggio. *Structural analysis of historical constructions*, pages 469–476.

Antonacci, E., Beolchini, G., Di Fabio, F., and Gattulli, V. (2001a). The dynamic behaviour of the basilica s. maria di collemaggio. In *Proc. of 2nd Int. Congress on Studies in Ancient Structures, SAS2001.*

Antonacci, E., Beolchini, G., and Gattulli, F. D. F. V. (2001b). Retrofitting effects on the dynamic behaviour of s. maria di collemaggio. *WIT Transactions on Modelling and Simulation*, 30.

Antonacci, E., Gattulli, V., Martinelli, A., and Vestroni, F. (2010). Il crollo del transetto della basilica di collemaggio: analisi di vulnerabilita'e

meccanismo di collasso. In *Atti del workshop: Sicurezza e conservazione dei beni culturali colpiti da sisma: Strategie e tecniche di ricostruzione ad un anno dal terremoto abruzzese*, pages 8–9.

Aste, N., Della Torre, S., Adhikari, R. S., Buzzetti, M., Del Pero, C., Leonforte, F., and Manfren, M. (2016). Sustainable church heating: The basilica di collemaggio case-study. *Energy and Buildings*, 116:218–231.

Avci, O. and Abdeljaber, O. (2016). Self-organizing maps for structural damage detection: a novel unsupervised vibration-based algorithm. *Journal of Performance of Constructed Facilities*, 30(3):04015043.

Avci, O., Abdeljaber, O., Kiranyaz, S., Hussein, M., Gabbouj, M., and Inman, D. J. (2021). A review of vibration-based damage detection in civil structures: From traditional methods to machine learning and deep learning applications. *Mechanical systems and signal processing*, 147:107077.

Azzara, R. M., De Roeck, G., Girardi, M., Padovani, C., Pellegrini, D., and Reynders, E. (2018). The influence of environmental parameters on the dynamic behaviour of the san frediano bell tower in lucca. *Engineering Structures*, 156:175–187.

Baiocchi, V., Giammarresi, V., Ialongo, R., Piccaro, C., Allegra, M., and Dominici, D. (2017). The survey of the basilica di collemaggio in l'aquila with a system of terrestrial imaging and most proven techniques. *European Journal of Remote Sensing*, 50(1):237–253.

Bao, Y., Tang, Z., Li, H., and Zhang, Y. (2019). Computer vision and deep learning–based data anomaly detection method for structural health monitoring. *Structural Health Monitoring*, 18(2):401–421.

Basseville, M., Abdelghani, M., and Benveniste, A. (2000). Subspace-based fault detection algorithms for vibration monitoring. *Automatica*, 36(1):101–109.

Basseville, M., Mevel, L., and Goursat, M. (2004). Statistical model-based damage detection and localization: subspace-based residuals and

damage-to-noise sensitivity ratios. *Journal of sound and vibration*, 275(3-5):769–794.

Bathe, K.-J. and Wilson, E. L. (1976). *Numerical methods in finite element analysis*. Number BOOK. Prentice-Hall.

Benedettini, F., Zulli, D., and Alaggio, R. (2009). Frequency-veering and mode hybridization in arch bridges. In *Proceedings of the 27th International Modal Analysis Conference*.

Benveniste, A. and Mevel, L. (2007). Nonstationary consistency of subspace methods. *IEEE Transactions on Automatic Control*, 52(6):974–984.

Bhuyan, M. D. H., Viefhues, E., Döhler, M., Lecieux, Y., Mevel, L., Hille, F., and Schoefs, F. (2017). Output-only subspace and transfer matrix-based damage localization and quantification. In *IOMAC-7th International Operational Modal Analysis Conference*.

Bishop, C. M. (1994). Novelty detection and neural network validation. *IEE Proceedings-Vision, Image and Signal processing*, 141(4):217–222.

Brumana, R., Della Torre, S., Previtali, M., Barazzetti, L., Cantini, L., Oreni, D., and Banfi, F. (2018). Generative hbim modelling to embody complexity (lod, log, loa, loi): surveying, preservation, site intervention—the basilica di collemaggio (l'aquila). *Applied geomatics*, 10(4):545–567.

Cabboi, A., Magalhães, F., Gentile, C., and Cunha, Á. (2017). Automated modal identification and tracking: Application to an iron arch bridge. *Structural Control and Health Monitoring*, 24(1):e1854.

Carden, E. P. and Fanning, P. (2004). Vibration based condition monitoring: a review. *Structural health monitoring*, 3(4):355–377.

Catbas, F. N., Brown, D. L., and Aktan, A. E. (2006). Use of modal flexibility for damage detection and condition assessment: case studies and demonstrations on large structures. *Journal of Structural Engineering*, 132(11):1699–1712.

Cha, Y.-J., Choi, W., and Büyüköztürk, O. (2017). Deep learning-based crack damage detection using convolutional neural networks. *Computer-Aided Civil and Infrastructure Engineering*, 32(5):361–378.

Crespi, P., Franchi, A., Giordano, N., Scamardo, M., and Ronca, P. (2016). Structural analysis of stone masonry columns of the basilica s. maria di collemaggio. *Engineering structures*, 129:81–90.

Dackermann, U., Li, J., and Samali, B. (2013). Identification of member connectivity and mass changes on a two-storey framed structure using frequency response functions and artificial neural networks. *Journal of Sound and Vibration*, 332(16):3636–3653.

de Lautour, O. R. and Omenzetter, P. (2010). Damage classification and estimation in experimental structures using time series analysis and pattern recognition. *Mechanical Systems and Signal Processing*, 24(5):1556–1569.

Deraemaeker, A., Reynders, E., De Roeck, G., and Kullaa, J. (2008). Vibration-based structural health monitoring using output-only measurements under changing environment. *Mechanical systems and signal processing*, 22(1):34–56.

Dilena, M. and Morassi, A. (2011). Dynamic testing of a damaged bridge. *Mechanical Systems and Signal Processing*, 25(5):1485–1507.

Doebling, S. W., Farrar, C. R., Prime, M. B., et al. (1998). A summary review of vibration-based damage identification methods. *Shock and vibration digest*, 30(2):91–105.

Döhler, M. and Mevel, L. (2012). Modular subspace-based system identification from multi-setup measurements. *IEEE Transactions on Automatic Control*, 57(11):2951–2956.

Döhler, M., Mevel, L., and Hille, F. (2014). Subspace-based damage detection under changes in the ambient excitation statistics. *Mechanical Systems and Signal Processing*, 45(1):207–224.

Dwivedi, S. K., Vishwakarma, M., and Soni, A. (2018). Advances and researches on non destructive testing: A review. *Materials Today: Proceedings*, 5(2):3690–3698.

Elyamani, A., Caselles, O., Roca, P., and Clapes, J. (2017). Dynamic investigation of a large historical cathedral. *Structural Control and Health Monitoring*, 24(3):e1885.

Farrar, C. R. and Worden, K. (2007). An introduction to structural health monitoring. *Philosophical Transactions of the Royal Society A: Mathematical, Physical and Engineering Sciences*, 365(1851):303–315.

Farrar, C. R. and Worden, K. (2012). *Structural health monitoring: a machine learning perspective*. John Wiley & Sons.

Figueiredo, E., Park, G., Farrar, C. R., Worden, K., and Figueiras, J. (2011). Machine learning algorithms for damage detection under operational and environmental variability. *Structural Health Monitoring*, 10(6):559–572.

Galeota, D., Antonacci, E., Aloisio, A., and Alaggio, R. (2019). The s. maria di collemaggio basilica: from the vulnerability assessment to the first results of shm. In *Proceedings of the XVII National Conference ANIDIS, 13–17 September 2019, Ascoli Piceno, Italy*, volume 17. ANIDIS.

Galeota, D., Sforza, G., and Sbaraglia, L. (2015). Dynamic characterization of the basilica of s. maria di collemaggio after the earthquake of 2009 by means of operational modal analysis. *Computational Methods and Experimental Measurements XVII*, 59:357.

Gentile, C., Ruccolo, A., and Canali, F. (2019). Long-term monitoring for the condition-based structural maintenance of the milan cathedral. *Construction and Building Materials*, 228:117101.

Gentile, C. and Saisi, A. (2007). Ambient vibration testing of historic masonry towers for structural identification and damage assessment. *Construction and building materials*, 21(6):1311–1321.

Giardini, L., Pezzuti, M., and Redi, F. (2006). *Celestino V e la sua basilica*. Silvana.

Gres, S., Andersen, P., Johansen, R. J., Ulriksen, M. D., and Damkilde, L. (2017a). A comparison of damage detection methods applied to civil en-

gineering structures. In *International Conference on Experimental Vibration Analysis for Civil Engineering Structures*, pages 306–316. Springer.

Gres, S., Ulriksen, M. D., Döhler, M., Johansen, R. J., Andersen, P., Damkilde, L., and Nielsen, S. A. (2017b). Statistical methods for damage detection applied to civil structures. *Procedia engineering*, 199:1919–1924.

Haykin, S. and Lippmann, R. (1994). Neural networks, a comprehensive foundation. *International journal of neural systems*, 5(4):363–364.

Hou, R. and Xia, Y. (2021). Review on the new development of vibration-based damage identification for civil engineering structures: 2010–2019. *Journal of Sound and Vibration*, 491:115741.

Keesman, K. J. (2011). *System identification: an introduction*. Springer Science & Business Media.

Kita, A., Cavalagli, N., and Ubertini, F. (2019). Temperature effects on static and dynamic behavior of consoli palace in gubbio, italy. *Mechanical Systems and Signal Processing*, 120:180–202.

Kong, X., Cai, C.-S., and Hu, J. (2017). The state-of-the-art on framework of vibration-based structural damage identification for decision making. *Applied Sciences*, 7(5):497.

Le Cam, L. (1956). On the asymptotic theory of estimation and testing hypotheses, proseedings third berkeley simposium on math. stat. and probability.

Limongelli, M. (2010). Frequency response function interpolation for damage detection under changing environment. *Mechanical Systems and Signal Processing*, 24(8):2898–2913.

Ljung, L. (1986). *System Identification: Theory for the User*. Prentice-Hall, Inc., USA.

Lopardi, M. G. (2002). *I templari ed il colle magico di Celestino*. Idea libri.

Mahalanobis, P. C. (1936). On the generalized distance in statistics. National Institute of Science of India.

Masciotta, M.-G., Ramos, L. F., and Lourenço, P. B. (2017). The importance of structural monitoring as a diagnosis and control tool in the restoration process of heritage structures: a case study in portugal. *Journal of Cultural Heritage*, 27:36–47.

Masciotta, M.-G., Roque, J. C., Ramos, L. F., and Lourenço, P. B. (2016). A multidisciplinary approach to assess the health state of heritage structures: The case study of the church of monastery of jerónimos in lisbon. *Construction and Building Materials*, 116:169–187.

McCann, D. and Forde, M. (2001). Review of ndt methods in the assessment of concrete and masonry structures. *Ndt & E International*, 34(2):71–84.

McCulloch, W. S. and Pitts, W. (1943). A logical calculus of the ideas immanent in nervous activity. *The bulletin of mathematical biophysics*, 5(4):115–133.

Mehrjoo, M., Khaji, N., Moharrami, H., and Bahreininejad, A. (2008). Damage detection of truss bridge joints using artificial neural networks. *Expert systems with applications*, 35(3):1122–1131.

Moretti, M. (1972). *Collemaggio*. De Luca.

Olshausen, B. A. and Field, D. J. (1997). Sparse coding with an overcomplete basis set: A strategy employed by v1? *Vision research*, 37(23):3311–3325.

Oreni, D., Brumana, R., Della Torre, S., Banfi, F., and Previtali, M. (2014). Survey turned into hbim: the restoration and the work involved concerning the basilica di collemaggio after the earthquake (l'aquila). *ISPRS annals of the photogrammetry, remote sensing and spatial information sciences*, 2(5):267.

Pandey, A., Biswas, M., and Samman, M. (1991). Damage detection from changes in curvature mode shapes. *Journal of sound and vibration*, 145(2):321–332.

Park, G., Muntges, D. E., and Inman, D. J. (2001). Self-monitoring and self-healing jointed structures. In *Key Engineering Materials*, volume 204, pages 75–84. Trans Tech Publ.

Parloo, E., Guillaume, P., and Van Overmeire, M. (2003). Damage assessment using mode shape sensitivities. *Mechanical systems and signal Processing*, 17(3):499–518.

Pathirage, C. S. N., Li, J., Li, L., Hao, H., Liu, W., and Ni, P. (2018). Structural damage identification based on autoencoder neural networks and deep learning. *Engineering structures*, 172:13–28.

Pawar, P. M., Venkatesulu Reddy, K., and Ganguli, R. (2007). Damage detection in beams using spatial fourier analysis and neural networks. *Journal of Intelligent Material Systems and Structures*, 18(4):347–359.

Peeters, B. and De Roeck, G. (1999). Reference-based stochastic subspace identification for output-only modal analysis. *Mechanical systems and signal processing*, 13(6):855–878.

Potenza, F., Federici, F., Lepidi, M., Gattulli, V., Graziosi, F., and Colarieti, A. (2015). Long-term structural monitoring of the damaged basilica s. maria di collemaggio through a low-cost wireless sensor network. *Journal of Civil Structural Health Monitoring*, 5(5):655–676.

Rafiei, M. H. and Adeli, H. (2018). A novel unsupervised deep learning model for global and local health condition assessment of structures. *Engineering Structures*, 156:598–607.

Ramos, L. F., Marques, L., Lourenço, P. B., De Roeck, G., Campos-Costa, A., and Roque, J. (2010). Monitoring historical masonry structures with operational modal analysis: two case studies. *Mechanical systems and signal processing*, 24(5):1291–1305.

Ranalli, D., Scozzafava, M., and Tallini, M. (2004). Ground penetrating radar investigations for the restoration of historic buildings: the case study of the collemaggio basilica (l'aquila, italy). *Journal of cultural heritage*, 5(1):91–99.

Redi, F. (2006). Santa maria di collemaggio. archeologia di un monumento. *Celestino V e la sua Basilica*, pages 71–133.

Rens, K. L., Wipf, T. J., and Klaiber, F. W. (1997). Review of nondestructive evaluation techniques of civil infrastructure. *Journal of performance of constructed facilities*, 11(4):152–160.

Reynders, E., Pintelon, R., and De Roeck, G. (2008). Uncertainty bounds on modal parameters obtained from stochastic subspace identification. *Mechanical systems and signal processing*, 22(4):948–969.

Rytter, A. (1993). Vibrational based inspection of civil engineering structures.

Saisi, A., Gentile, C., and Guidobaldi, M. (2015). Post-earthquake continuous dynamic monitoring of the gabbia tower in mantua, italy. *Construction and Building Materials*, 81:101–112.

Schwarz, B. J. and Richardson, M. H. (1999). Introduction to operating deflection shapes. *CSI Reliability Week*, 10(538):121–126.

Sfarra, S., Bendada, A., Ibarra-Castanedo, C., Ambrosini, D., Paoletti, D., and Maldague, X. (2015). Santa maria di collemaggio church (l'aquila, italy): historical reconstruction by non-destructive testing techniques. *International Journal of Architectural Heritage*, 9(4):367–390.

Sohn, H., Farrar, C. R., Hemez, F. M., Shunk, D. D., Stinemates, D. W., Nadler, B. R., and Czarnecki, J. J. (2003). A review of structural health monitoring literature: 1996–2001. *Los Alamos National Laboratory, USA*, 1.

Stubbs, N., Kim, J.-T., and Farrar, C. R. (1995). Field verification of a nondestructive damage localization and severity estimation algorithm. In *Proceedings-SPIE the international society for optical engineering*, pages 210–210. SPIE International Society for Optical.

Toksoy, T. and Aktan, A. (1994). Bridge-condition assessment by modal flexibility. *Experimental Mechanics*, 34(3):271–278.

Totani, G., Monaco, P., Totani, F., Lanzo, G., Pagliaroli, A., Amoroso, S., and Marchetti, D. (2016). Site characterization and seismic response analysis in the area of collemaggio, l'aquila (italy). In *Proc., 5th International Conf on Geotechnical and Geophysical Site Characterization,*

Australian Geomechanics Society, Gold Coast, Australia, volume 2, pages 1051–1056.

Tran-Ngoc, H., Khatir, S., De Roeck, G., Bui-Tien, T., and Wahab, M. A. (2019). An efficient artificial neural network for damage detection in bridges and beam-like structures by improving training parameters using cuckoo search algorithm. *Engineering Structures*, 199:109637.

Ubertini, F., Comanducci, G., Cavalagli, N., Pisello, A. L., Materazzi, A. L., and Cotana, F. (2017). Environmental effects on natural frequencies of the san pietro bell tower in perugia, italy, and their removal for structural performance assessment. *Mechanical Systems and Signal Processing*, 82:307–322.

Van Overschee, P. and De Moor, B. (1996). Subspace identification for linear systems: Theory, implementation, applications.

Wahab, M. A. and De Roeck, G. (1999). Damage detection in bridges using modal curvatures: application to a real damage scenario. *Journal of Sound and vibration*, 226(2):217–235.

Worden, K., Farrar, C. R., Manson, G., and Park, G. (2007). The fundamental axioms of structural health monitoring. *Proceedings of the Royal Society A: Mathematical, Physical and Engineering Sciences*, 463(2082):1639–1664.

Yan, A.-M. and Golinval, J.-C. (2006). Null subspace-based damage detection of structures using vibration measurements. *Mechanical Systems and Signal Processing*, 20(3):611–626.

Yan, Y., Cheng, L., Wu, Z., and Yam, L. (2007). Development in vibration-based structural damage detection technique. *Mechanical systems and signal processing*, 21(5):2198–2211.

Ye, X., Jin, T., and Yun, C. (2019). A review on deep learning-based structural health monitoring of civil infrastructures. *Smart Struct. Syst*, 24(5):567–585.

Zucca, M., Franchi, A., Crespi, P., Longarini, N., and Ronca, P. (2018). The new foundation system for the transept reconstruction of the basilica di

collemaggio. In *10th IMC-Proceedings of the 10th International Masonry Conference*, pages 2441–2450.

List of Publications

Publications list

- R. Alaggio, A. Aloisio, E. Antonacci, R. Cirella, Two-years static and dynamic monitoring of the Santa Maria di Collemaggio Basilica, Construction and Buildings Materials (2020) 121069;
- R. Cirella, A. Aloisio, R. Alaggio, System identification of beam-like structures using residual indicators derived from stochastic subspace analysis, in EWSHM2020: European Workshop on Structural Health Monitoring, 2020;
- A.Aloisio, R.Cirella, E. Antonacci, R. Alaggio, Long term monitoring of the Santa Maria di Collemaggio Basilica, in COMPDYN2021: 8th ECCOMAS Thematic conference on computational Methods in Structural Dynamics and Earthquake Engineering, 28-30 June 2021;
- A.Aloisio, R.Cirella, E.Antonacci, R.Alaggio, Hypothesis on the decrement of the first natural frequencies of the Santa Maria di Collemaggio basilica from three years monitoring: the role of the CLT roof, International journal of architectural heritage (2021)